MRI evaluation of the anti-adhesion molecule antibody Natalizumab and the blood-brain barrier in Multiple Sclerosis

Derek Soon

Thesis submitted for the degree of doctor of philosophy to

University College London

NMR Research Unit

Institute of Neurology

Queen Square

London, UK

Date of Submission: July 2009

Table of Contents

Abstract

As Blood-brain barrier (BBB) breakdown is central to inflammatory lesion formation, it presents a potential target in the formulation of putative therapeutic agents in MS. The action of natalizumab, a monoclonal antibody acting at the BBB, is investigated through a phase III monotherapy trial (AFFIRM) and associated substudies.

Subtle BBB disruption from non-inflamed lesions, which could contribute to axonal damage through leakage of inflammatory cells and associated mediators into surrounding parenchyma, is also studied.

Introductory chapters (1-3) provide a brief overview of MS, clinical trials, magnetic resonance imaging (MRI), the BBB and natalizumab.

Chapter four describes MRI results of AFFIRM- a 2 year multi-centre trial involving 942 patients. Compared with placebo, natalizumab reduced number of gadolinium (Gd)-enhancing lesions by 92%, new/enlarging T_2-hyperintense lesions by 83%, and new T_1-hypointense lesions by 76%.

Chapter five describes a 57 patient AFFIRM trial substudy in which the influence of natalizumab on segmental atrophy was investigated. Atrophy was predominant in grey matter (GM) and was independent of lesion load. Fluctuations in white matter (WM) volume followed changes in inflammatory lesion load. Atrophy was not influenced by natalizumab

The effect of natalizumab on subtle BBB disruption (inferred by measuring the post-Gd %change in T_1 weighted signal intensity) is studied in chapter 6. This AFFIRM substudy involved 40 patients (27 on natalizumab, 13 on placebo.) Although subtle BBB leakage was consistently detected in non-visibly enhancing lesions, natalizumab did not influence the degree of leakage.

Chapter 7 describes a cross-sectional study which utilised post-Gd change in R_1 ($1/T_1$) as a marker BBB leakage. 19 patients (10 RRMS, 9 SPMS) were involved in this study. The subtle leakage observed from non-visibly enhancing lesions was distinct from leakage from visibly enhancing lesions. This was sustained over 60 minutes, greater in smaller lesions and in size-adjusted T_1 hypointense lesions.

List of Abbreviations

ABN	Association of British Neurologists
ABH	Acute Black Holes
AFFIRM	Natalizumab Safety and Efficacy in Relapsing Remitting Multiple Sclerosis
ANOVA	Analysis of variance
APP	Amyloid Precursor Protein
BBB	Blood-brain barrier
BP	Brain Parenchyma
BPF	Brain Parenchymal Fraction
BW	Bandwidth
CI	Confidence interval
CIS	Clinically Isolated Syndrome
CNS	Central Nervous System
CoV	Coefficient of Variation
CSA	Cross Sectional Area
CSE	Conventional Spin Echo
CSF	Cerebrospinal Fluid
DSS	Disability Status Scale
EAE	Extrinsic Allergic Encephalomyelitis
EDSS	Expanded Disability Status Scale
ETL	Echo Train Length
FID	Free Induction Decay
FOV	Field of View
FSE	Fast Spin Echo
FSPGR	Fast Spoiled Gradient Recall

Gd	Gadolinium
GE	Gradient echo
GM	Grey Matter
GMF	Grey Matter Fraction
ICAM-1	Inter-cellular adhesion molecule 1
IFNβ	Interferon β
IR	Interquartile Range
K^{trans}	Transfer Coefficient
LFA-1	Lymphocyte function associated antigen 1
LOCF	Last Observation Carried Forward
LVR	Lesion Volume Ratio
MCP-1	Monocyte Chemoattractant Protein 1
MRI	Magnetic Resonance Imaging
MS	Multiple Sclerosis
MSFC	Multiple Sclerosis Functional Composite
NAA	N-Acetyl Aspartate
NABT	Normal Appearing Brain Tissue
NAWM	Normal Appearing White Matter
NEX	Number of Excitations
N_p	Number of phase encoding gradients
PBH	Persistent Black Holes
PECAM-1	Platelet Endothelial Cell Adhesion Molecule
PML	Progressive Multifocal Leukoencephalopathy
PPMS	Primary Progressive Multiple Sclerosis
R_1	Longitudinal Relaxation Rate

RCT	Randomised Controlled Trial
RF	Radiofrequency
ROI	Region of Interest
RRMS	Relapsing Remitting Multiple Sclerosis
SE	Spin Echo
SI	Signal Intensity
SNR	Signal to Noise Ratio
SPM	Statistical Parametric Mapping
SPMS	Secondary Progressive Multiple Sclerosis
TE	Echo Time
TI	Inversion Time
TR	Repetition Time
VCAM-1	Vascular Cell Adhesion Molecule 1
v_e	Lesion leakage space
VEGF	Vascular Endothelial Growth Factor
VLA-4	Very Late Antigen-4
WM	White Matter
WMF	White Matter Fraction

List of Tables

List of Figures

Publications arising from this work

Miller DH, Soon D, Fernando KT, MacManus DG, Barker GJ, Yousry TA, Fisher E, O'Connor PW, Phillips JT, Polman CH, Kappos L, Hutchinson M, Havrdova E, Lublin FD, Giovannoni G, Wajgt A, Rudick R, Lynn F, Panzara MA, Sandrock AW; AFFIRM Investigators. MRI outcomes in a placebo-controlled trial of natalizumab in relapsing MS. Neurology. 2007; **68**: 1390-401

Soon D, Altmann DR, Fernando KT, Giovannoni G, Barkhof F, Polman CH, O'Connor P, Gray B, Panzara M, Miller DH. A study of subtle blood brain barrier disruption in a placebo-controlled trial of natalizumab in relapsing remitting multiple sclerosis. J Neurol. 2007; **254**:306-314

Soon D, Tozer DJ, Altmann DR, Tofts PS, Miller DH. Quantification of subtle blood-brain barrier disruption in non-enhancing lesions in multiple sclerosis: a study of disease and lesion subtypes. Mult Scler. 2007;**13**:884-894

Soon D, Miller DH. Measurement of Blood Brain Barrier Permeability in Multiple Sclerosis. In Filippi M, Comi G, Rovaris M eds. *Normal Appearing White and Grey Matter Damage in Multiple Sclerosis*: Springer-Verlag; 2004:9-22

Acknowledgements

This thesis would not have been possible without the help and support of a large number of people. Firstly, I would like to thank Professor DH Miller for being an excellent supervisor, whose insight and inspiration have been central to my growth as a scientist and clinician.

I would also like to thank Professor PS Tofts for his constructive and pertinent input, particularly in the development and testing of MRI protocols. Dr Daniel Altmann for providing balanced statistical advice and his help in the development of elegant and robust statistical analyses.

I am grateful to Ms Lesley Hearsum, Ms Sally Zalita and Mr Kelvin Hunter for their help in the organisation and monitoring of the receipt of the AFFIRM study data. My role in the analysis of the AFFIRM data included the identification and marking of lesions on the hard copies, and quality assurance of rated scans. I am grateful to Dr Kryshani Fernando (KF), who, as second rater, shared a significant proportion of the workload with me. Hard copy marking was checked by Professor Tarek Yousry (TY), who performed his task with patience and care, despite his other multiple commitments. The lesion volume quantification for the AFFIRM study was performed by a group of dedicated raters, notably Andrew John, Teresa Alfaro-Vidal, Kabir-Wilder Ahmed, Teresa Solano, Astra Rajkumar, Helen Procter and Virginia Santana, who were very ably supervised by Mr David MacManus. Dr Frances Lynn oversaw the statistical analysis of the data for the AFFIRM study.

I would like to thank my sponsors for funding my research (Biogen-IDEC funded the analyses of AFFIRM and related substudies and the MS Society of Great Britain and Northern Ireland supports the NMR Research Unit in which the BBB permeability study was undertaken)

I would like to thank Ikumi and my family for their continued and unfailing support and belief, and finally God, who has been my source of strength and inspiration through the years

CHAPTER 1

Multiple Sclerosis and Treatment Trials

1.1 Introduction

Multiple sclerosis (MS) is a chronic demyelinating disease of the central nervous system (CNS). The hallmark of the disease is the temporal and anatomical dissemination of multiple lesions in the brain and spinal cord. Initially, such lesions in the white matter (WM) are associated with inflammation - perivascular lymphocyte infiltration and blood-brain barrier (BBB) breakdown (Adams *et al.,* 1985). The resolution of inflammation is frequently accompanied by axonal loss (Trapp *et al.,* 1998; van Waesberghe *et al.,* 1999) and associated gliosis and induration, the most visible macroscopic pathological manifestation of the disease, earning it its name (Compston *et al.,* 2006a). Nonetheless, the pathology of MS is not solely confined to lesions in the WM. Demyelinated plaques are widespread in grey matter (GM) (Pirko *et al.,* 2007; Kidd *et al.,* 1999) and represent a population of lesions which are histologically distinct from their WM counterparts (Peterson *et al.,* 2001; Bo *et al.,* 2003). Normal appearing white matter (NAWM) also bears evidence of axonal damage and additional pathological features such as astrocyte proliferation and microglial activation (Trapp *et al.,* 1998; Allen *et al.,* 2001).

Possibly the first clearly described case of MS was that of Augustus d'Este, the illegitimate grandson of George III. Augustus d'Este kept a diary recording his symptoms from the start of his illness in 1822 to his death in 1848 (Firth, 1941). In it accounts of such symptoms as leg weakness, ataxia, bladder disturbance and erectile dysfunction are given. The earliest descriptive accounts of MS pathology were documented by 2 people, Robert Carswell, and Leon Jean Baptiste Cruveilhier, working independently of each other. Both individuals published pathological descriptions of MS lesions within a short period of time over 1838 and 1841. (Compston, 1988)

J.M. Charcot's contribution to the disease in the 1860's was not just in describing the clinical and pathological features, including demyelination and gliosis, but in recognising that these constituted a separate disease in itself, which he termed *la sclerose en plaques disseminées.* In addition, following the death of his housekeeper, he was able to correlate observed clinical features with the pathology of the disease. (Cook, 1998).

An estimated 2.5 million people globally suffer from MS. In the UK, it is the most common chronic neurological disease that results in locomotor disability in young adults. The incidence in England and Wales has been estimated as between 3.5 and 6.6 per 100000, with a prevalence of 100-120 per 100000 (Compston and Confavreux, 2006b; NCC-CC, 2004). The cost of MS has been estimated at roughly £17000 per year per patient, which translates to a national burden of £1.34 billion per year (NCC-CC, 2004).

The age of onset of the disease in any particular individual can sometimes be difficult to pinpoint, as early sensory relapses may often be ignored as innocuous or forgotten entirely. However, MS begins typically early in life, with a peak age of onset roughly around the age of 30. (Confavreux and Compston, 2006) The majority of patients experience their first symptoms between 20 and 40 years of age. A small proportion, roughly 5%, report symptoms before the age of 16 (Compston and Coles, 2002; Bauer *et al.,* 1990). The female to male ratio of the disease is roughly 2:1. Patients with primary progressive MS (who represent 15% of all MS cases) tend to have a higher mean age of onset (~38 years) and a much more equal female to male ratio. (Cottrell *et al.,* 1999; Thompson *et al.,* 2000).

1.2 Aetiology

The aetiology of MS is as yet poorly understood. An interplay of genetic and environmental factors are thought to be involved (Compston *et al.,* 2006c).

1.2.1 Environmental Factors

The monozygotic twin concordance in MS is 35%, indicating major environmental determinants in MS risk. Additional support for this comes from the striking geographical variation in the prevalence of the disease. The worldwide distribution of the disease is divided into 3 zones of MS risk (Kurtzke, 1975; Kurtzke, 2000).

1. High risk areas such as North America, Northern Europe, New Zealand with prevalence rates >30 per 100000
2. Intermediate risk areas such as Australia, Southern United States and parts of Russia, with prevalence rates of between 5 and 30 per 100000
3. Low risk areas such as equatorial Africa and much of Asia, with prevalence rates less

than 5 per 100000.

Moreover, within relatively racially homogenous countries, a consistent finding in epidemiological studies is an increase in prevalence with distance from the equator (Kurtzke *et al.,* 1979; Skegg *et al.,* 1987; Hammond *et al.,* 1988)

Migration studies from England (high prevalence) to South Africa (lower prevalence) have suggested that the risk of developing MS is determined by the environment to which the migrant is exposed before the age of 15. (Dean and Kurtzke, 1971; Dean *et al.,* 1997). No such cut-off age was found in migrant studies of previous residents of the UK and Ireland into Australia (Hammond *et al.,* 2000). Subjects in this study adopted the reduced risk of MS associated with living in Australia, regardless of age at immigration.

Taken together, the above studies suggest that exposure to certain environmental factors, probably early in life, could influence one's risk for developing MS. To date, speculation on an environmental trigger has ranged from an infective agent (Martyn, 1997; Sundstrom *et al.,* 2004), to diet (Lauer, 1997; Munger *et al.,* 2004) and exposure to sunlight (van der Mei *et al.,* 2003). However, no definite link with any environmental factor has thus far been demonstrated.

1.2.2 Ethnic Variation

Susceptibility to MS varies from race to race. MS is low amongst Sami, Maoris and Blacks and high amongst people of European origin. (the prevalence in North

Americans of African origin is about half that found in those of northern European origin),(Rosati, 2001). Studies on US servicemen indicate a higher risk of developing MS amongst those with a northern European ancestry (Page *et al.,* 1993). In addition, the prevalence of MS differs in racially distinct populations situated close to each other, for instance in Malta (4.2 per 100000) compared with neighbouring Sicily (53.3 per 100000). (Dean *et al.,* 1979; Vassallo *et al.,* 1979).

1.2.3 Genetic factors

Whereas the lifetime risk of developing MS in the general population in the United Kingdom is about 1:600 to 1:800 (~0.1%), close relatives of MS patients bear an increased risk of developing the disease. Age adjusted risk for developing MS is 3% for siblings and 2% for parents and children of subjects with MS. The risk of developing MS in the offspring of conjugal pairs is 20%, and the monozygotic twin concordance rate is 35% compared with a dizygotic twin rate of 3-5% (Compston and Coles, 2002). The risk for MS in non-biological adopted siblings is no higher than the population risk, confirming that familial increase in risk is due to genetic rather than environmental factors.

MS does not follow any mendelian pattern of inheritance, and the disease appears to be genuinely polygenic (Compston, 1999), probably with a number of genes each having a limited effect on susceptibility. More recently, a genome-wide association study identified a number of single nucleotide polymorphisms (including 2 within the gene for the interleukin-2 receptor α, 1 within the gene for the interleukin-7 receptor α and several within the HLA-DRA locus) which were associated with an increased risk of

MS (International Multiple Sclerosis Genetic Consortium *et al.,* 2007).

The common Caucasian MHC class II HLA-DR2 (DRB1*1501) haplotype appears to be linked with relapsing disease in northern European populations (Olerup and Hillert, 1991; Compston and Sadovnick, 1992) HLA-DR2 also appears more common in the typical forms of relapsing MS in the Japanese population (Kira, 2003), which has seen an increase in prevalence in the disease in the last 3 decades (Compston and Confavreux, 2006b). Progressive forms of MS have also been linked with HLA DR4 (Kantarci *et al.,* 2002) but a consistent gene association with disease course and prognosis has not emerged. Somewhat different HLA associations have emerged with MS in Sardinia (Marrosu *et al.,* 1997). Known carriers of the apolipoprotein E4 allele appeared in one study to have an earlier onset and more aggressive course of the disease (Enzinger *et al.,* 2004), however this was not confirmed by other investigators.

1.3 Pathology

The pathological hallmark of MS is the presence of demyelinating plaques of varying age distributed in space and time within the CNS. Because of better contrast and detectability on conventional magnetic resonance imaging (MRI) and histological methods, lesions within the WM have to date been the focus of much of the study of MS. It is hoped that the advent of high field MRI will facilitate the further study of GM lesions in the future. The main pathological features of MS plaques are 1) demyelination which is complete in many chronic lesions, 2) relative preservation of axons and glia (although axonal loss can be profound in some lesions especially when chronic), 3) perivenule location and 4) variable amounts of gliosis, inflammation and remyelination which may partly depend on lesion age but also on other factors that are not well understood.

Lesions in the WM have a predilection for certain brain regions, particular around the ventricles, periaqueductal sites and optic nerves. Cord lesions are frequently subpial in location. The mechanism(s) for preferential periventricular distribution of MS lesions remain unclear. Possible explanations include: 1) Slower bloodflow in postcapillary venules, facilitating leucocyte adhesion in such areas, 2) regional variation in microglia or capillary pericytes and 3) the local effects of toxins or cytokines in the CSF.

1.3.1 The Active lesion

The classic acute WM lesion of MS displays perivascular inflammation, with BBB breakdown and active demyelination. The precise triggers are unclear but the following sequence of events may be relevant. A rise in circulating cytokines such as TNFα and IFNγ (Beck J *et al.,* 1998; Dettke *et al.,* 1997) may precede lesion formation. This stimulates endothelial cells in the postcapillary venules to express adhesion molecules and MHC class II molecules, facilitating the adhesion of circulating leucocytes. These inflammatory cells infiltrate the parenchyma, release cytokines and chemokines (Balashov *et al.,* 1999) and express costimulatory molecules which further enhance T-cell proliferation and activation (Prat *et al.,* 2000). A pro-inflammatory loop is initiated (Compston and Coles, 2002) in which CD8+ T cells dominate in a Th1 type immune response. Inflammatory mediators stimulate disruption of the BBB (Minagar and Alexander, 2003) and the resultant perivascular cuff consists of local oedema and a lymphocytic infiltrate (Adams *et al.,* 1985). Myelin and oligodendrocytes, which form myelin sheaths around neighbouring axons, are opsonised and phagocytosed by macrophages and activated microglia. Oligodendrocyte loss correlates significantly with the number of macrophages in histological studies (Lucchinetti *et al.,* 1999).

1.3.2 Mechanisms of axonal loss

Although the most visible features of MS lesions are myelin sheath damage and oligodendrocyte death/dysfunction, axonal damage has been well described (Trapp *et al.,* 1998; Bjartmar and Trapp, 2001). The degree of axonal loss varies between patients and lesions (Bitsch *et al.,* 2000). Amyloid precursor protein (APP), a marker of acute axonal damage, is expressed in high levels in active lesions (Ferguson *et al.,* 1997; Kuhlmann *et al.,* 2002) and is also present in the active edges of chronic lesions. Local concentrations of APP correlate with severity of inflammation as measured by numbers of microglia and CD8 T-cells (Bitsch *et al.,* 2000). Axonal loss is at its most severe early on in inflammation. The degree of axonal damage has been correlated with disability in Extrinsic Allergic Encephalomyelitis (EAE), the animal model of MS, (Wujek*et al.,* 2002) and with spectroscopic markers of axonal integrity such as N-Acetyl Aspartate (NAA) in MS patients (Davie *et al.,* 1995; De Stefano *et al.,* 1998). Postulated mechanisms of injury include direct attack by immune cells, either cytotoxic T-cells (Neumann *et al.,* 2002; Medana *et al.,* 2001) or through NO mediated pathways (Smith KJ *et al.,* 2001). The lack of a myelin sheath with its attendant provision of trophic factors and protection from the inflammatory milieu has also been cited as a possible contributor to axonal loss. Disturbances to the local vasculature through oedema and vessel wall inflammation could also contribute to axonal damage.

Thrombotic occlusion of microvessels have been observed in MS (Lassmann, 2003), suggesting, in some cases, an ischaemic mechanism for axonal death.

1.3.3 Pathological Heterogeneity in lesions

Histological study of active lesions taken from biopsies and autopsies of MS patients has demonstrated heterogeneity in the phenotype of MS lesions. Acute lesions have been categorised into 4 distinct pathological patterns (table 1.1), according to the degree of T-cell involvement, oligodendroglial dysfunction and complement activation. (Lucchinetti *et al.,* 2000)

Patterns of lesion pathology (Lucchinetti *et al*., 2000)

Table 1.1Patterns of lesion pathology (Lucchinetti *et al.*, 2000)

Subtype	Immunology	Oligodendrocytes	Border
I 18%	CD8 T cells and macrophage mediated demyelination	Survival of oligodendrocytes with rapid remyelination	Sharp Centred around Venules
II 56%	As in I, plus antibody & complement deposition	Survival of oligodendrocytes with rapid remyelination	Sharp
III 24%	Microglial activation	Oligodendrocyte destruction Distal oligo-opathy and dystrophy. Early myelin loss Axonal damage	Indistinct Not centred around Venule
IV 2%	Macrophages and T cells. Only seen in PPMS	Primary oligodendrocyte degeneration. Axonal damage	Sharp, perivenous

An inflammatory infiltrate is present in all 4 lesion patterns. Patterns I and II are marked by an intense perivenous immune reaction with a sharply demarcated area of inflammation and demyelination and the attendant damage of axons, oligodendroglia and astrocytes, with pattern II having the additional association of complement activation and IgG deposition. Types III and IV appear to be the result of primary oligodendroglial dysfunction and apoptosis with subsequent demyelination.

Patterns I and II are seen in all disease subtypes, whereas pattern III has been observed largely in cases with disease duration less than 2 months. Pattern IV, the rarest, has only been observed in primary progressive disease. It has been suggested that while lesion patterns vary between different patients, lesions found within an individual patient share the same pattern.

As the lesions examined in the Lucchinetti study have been obtained through biopsy or autopsy, a selection bias may exist within the study toward larger, more severe, lesions, and as such, the lesions studied may not reflect active lesions in general. Nonetheless the findings of the study point strongly toward a pathological heterogeneity within the disease of MS and is consistent with the observations of diversity in disease course, presentation and response to treatment. Such heterogeneity has prompted speculation that MS may represent a collection of neuroinflammatory diseases rather than a single entity (Compston and Sadovnick, 2002)

1.3.4 Chronic Lesions

The inflammatory cellular infiltrate associated with demyelination decreases over time (Kuhlmann *et al.,* 2002). A glial scar develops amidst a residue of occasional inflammatory cells and damaged and demyelinated axons. Although oligodendrocyte precursors are present, the presence of viable oligodendrocytes and remyelination is variable. Ongoing inflammation and neuronal damage can still occur at the lesion edge

(Bitsch *et al.,* 2000).

1.3.5 Remyelination

Between 13-42% of lesions show evidence of remyelination (Barkhof *et al.,* 2003; Schmierer *et al.,* 2004). Remyelination can occur early in lesion genesis and appears to be most successful in lesions in which there are a large number of macrophages, and oligodendrocytes (Bruck *et al.,* 2003). Remyelinated plaques are frequently described as 'shadow plaques' (Prineas *et al.,* 1993). Such plaques display minimal axonal loss (Kornek *et al.,* 2000) and preservation of function. The factors that regulate remyelination are still poorly understood, but are thought to include the presence of signalling factors in the local environment, the proximity of viable oligodendrocytes or oligodendrocyte precursor cells capable of effecting remyelination and the degree of gliosis in the lesion, which may provide a mechanical barrier to remyelination. (Bruck *et al.,* 2003).

1.3.6 Grey Matter involvement

Demyelinating lesions also occur in the cortical GM. (Kidd *et al.,* 1999, Peterson *et al.,* 2001). They can be contiguous with subcortical lesions (type 1), confined to within the cortex (type 2) or can involve the pial surface (type 3) (Peterson *et al.,* 2001). They are associated with fewer inflammatory cells than WM lesions with 13 times fewer T cells and 6 times fewer macrophages and microglia (Peterson *et al.,* 2001). GM lesions may exhibit significant amounts of axonal loss and have significantly more apoptotic neurons than surrounding GM.

1.4 Clinical manifestations of multiple sclerosis

1.4.1 Symptoms and signs

Clinically, MS is characterised by symptoms reflective of lesions separated in time and space. Symptoms arise from the interruption of pathways, either through failure of saltatory conduction from demyelination, or by interruption or transection of axons. Demyelinated axons are more vulnerable to changes in the environment. For instance, an increase in temperature can exacerbate existing symptoms (Uhthoff phenomenon), as can the application of mechanical pressure (Lhermitte phenomeonon). Concurrent infection can also worsen pre-existing or re-awaken old neurological symptoms, either through changes in temperature or possibly – an effect of cytokines on nerve conduction (Moreau *et al.,* 1996).

Certain symptoms reflect specific locations of lesions. For instance myelopathic symptoms are likely to arise from spinal cord lesions, and dysdiadochokinesis and dysmetria from lesions in the cerebellum (including cerebellar peduncles). Given the predilection of lesions for certain anatomical locations within the CNS, specific symptoms and signs are encountered with greater frequency in MS. Table 1.2 gives a list of the most frequently encountered clinical findings in MS clinics at the Universities of British Columbia and Western Onatario, Canada, as provided by Paty and Ebers.

Table 1.2 Predominance of clinical findings in MS clinics in Canada (Paty and Ebers, 1997*)*

Symptom and signs	% Frequency
Increased deep tendon reflexes	90
Sensory loss (most commonly in legs and implicating the posterior columns of cord)	90
Leg weakness	90
Spasticity	90
Nystagmus	85
Bladder disturbance	80
Fatigue	80
Optic atrophy	77

Not all MS lesions give rise to symptoms. The clinical eloquence of a lesion depends on its location - lesions in the deep WM and not involving key pathways such as the corticospinal tract are less likely to cause acute symptoms when they appear. However, such lesions may contribute to cognitive impairment, especially with accumulation of multiple cerebral lesions. Cognitive deficits are detectable on formal testing, especially in attention, information processing and verbal memory (Piras *et al.,* 2003). Such changes are correlated with lesion load seen in the cerebral hemisphere in the WM on MRI (Hohol *et al.,* 1997). Fatigue is also common in MS patients, estimated at up to 80% MS sufferers (Bakshi, 2003), although its relationship with the underlying pathology is not well understood.

Acute lesions may also be asymptomatic if there is axonal preservation and rapid remyelination, whereas persistent deficits will be more likely if persistent demyelination results in substantial axonal loss.

1.4.2 Clinical course

MS is a diverse disease in terms of pathology, presentation and clinical course.

Following a survey of clinicians involved with MS, Lublin and Reingold put forward the following clinical classification of the disease (FIG 1.1) which now has widespread recognition. (Lublin and Reingold, 1996).

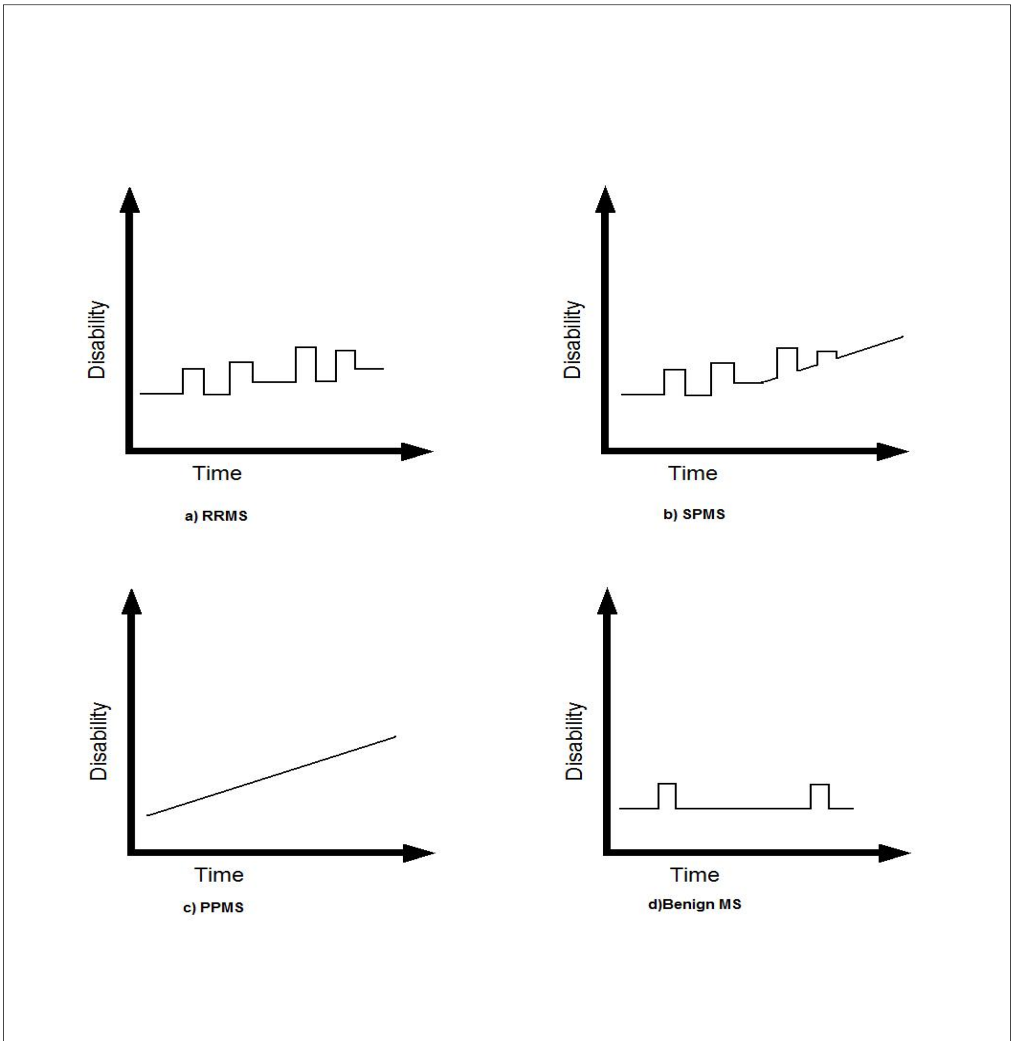

FIG 1.1 The disease course in 4 MS disease subtypes. a)RRMS; b)SPMS; c)PPMS; d) benign MS

Roughly 85% of MS patients present with relapsing remitting (RR)MS. This is associated with clearly defined relapses with or without full recovery, with no evidence of clinical progression between relapses. Average relapse rate varies between 0.1 and 1 per year (Weinshenker and Ebers, 1987) Good prognostic markers in RRMS include young age at onset, mainly sensory symptoms, symptoms implicating single site on onset, a long interval between the first and second relapse, and good recovery from initial relapse (Runmarker and Anderson, 1993)

Secondary Progressive (SP) MS is characterised by secondary progression, defined as gradually increasing disability progression for more than 6 months independent of relapses, following a period of relapsing remitting disease. A significant proportion of RRMS patients convert to SPMS, with a median time of onset of progression at 10 years from the start of the disease (Runmarker and Anderson, 1993; Confavreux *et al.,* 1980).

15% of MS patients develop the primary progressive (PP) form of the disease. (Cottrell *et al.,* 1999) This is characterised by progression of disability from onset with occasional plateaus and temporary (mild) improvements allowed. This clinical subgroup tends to have an onset later in life and 80-90% present with a progressive cord syndrome.

A minority of patients evolve to develop a benign MS course, which is defined as a relapsing remitting time course with minimal or no disability up to 15 years after onset. Other terms such as relapsing progressive and progressive relapsing have been less clearly defined and are not commonly used to define patients for inclusion treatment trials.

1.5 Diagnosis of multiple sclerosis

The diagnosis of MS rests primarily on evidence of lesions disseminated in space and time. Clinical evidence through carefully taken history and examination formed the cornerstone of the formalised set of diagnostic criteria set out in the 1960s (Schumacher *et al.,* 1965) (FIG 1.2) and every set of diagnostic criteria since. More recent revisions of the diagnostic criteria incorporate data from imaging, evoked responses and cerebrospinal fluid (CSF) electrophoresis (Poser *et al.,* 1983; McDonald *et al.,* 2001; Polman *et al.,* 2005) in recognition of the contribution of these investigations toward the diagnostic process.

Two successively proposed diagnostic criteria will be described in this section. Both are widely employed at present in clinical and academic settings. They are the Poser Committee Criteria (Poser *et al.,* 1983), devised to incorporate data from evoked responses and CSF electrophoresis, and the subsequent McDonald criteria (McDonald *et al.,* 2001), and its succesive revision (Polman *et al.,* 2005) devised to adapt to the increasing use of MRI as a sensitive and effective diagnostic tool.

1. Objective signs of dysfunction of the central nervous system; symptoms not acceptable
2. Evidence of damage to two or more sites
3. Predominantly damage to the white matter

4a. Two or more episodes of at least 24 h separated by at least 6 months

4b. Progression over 6 months

5. Age of onset 10–50 years

FIG 1.2 Schumacher Criteria for the diagnosis of MS

The Poser committee criteria were drawn up in 1983 as a result of a workshop on the diagnosis of MS attended by experts from the United States, Canada and the United Kingdom (Poser *et al.,* 1983) The criteria expanded on pre-existing Schumacher criteria to incorporate data from CSF electrophoresis and what was termed paraclinical evidence, described as "demonstration by means of various tests and procedures of the existence of a lesion in the CNS ... include the hot bath test, evoked response studies, imaging procedure and reliable, expert urological assessment". Diagnostic certainty was stratified into 3 levels: definite, probable and possible. In addition, the basis of the evidence (ie clinical vs laboratory supported) is described for each level. (Table 1.3)

Table 1.3 Poser Committee Criteria for diagnosis of MS (From Poser et al., 1983)

Category	Number of Relapses	Number of CNS sites involved		Paraclinical evidence	CSF Oligoclonal bands
Clinically	2	2			
Definite	2	1	and	1	
Clinically	2	1			
Probable	1	2			
Laboratory	2	1	or	1	+
Supported	1	2			+
Definite					
Laboratory	1	1	and	1	+
Supported	2				+
Probable					

Following a meeting of the international committee of MS diagnosis, a revised set of diagnostic criteria was proposed in 2001 which incorporates the use of MRI findings to allow for earlier and accurate diagnosis of MS (McDonald *et al.,* 2001). The levels of diagnostic certainty proposed by the Poser Committee were replaced with "MS", "not MS" and "possible MS" for cases with equivocal clinical and paraclinical findings. MRI criteria incorporated into the new set of diagnostic criteria were based on the findings of previous prospective studies on patients with single neurological episodes, the so called clinically isolated syndrome (CIS), (Barkhof *et al.,* 1997; Tintore *et al.,* 2000) and those with primary progressive MS (Thompson *et al.,* 2000) Criteria drawn up for MRI included evidence of dissemination in space, dissemination in time, and MRI evidence for primary progressive MS.

Criteria for Dissemination in Space

Three of the following[a]:

1. At least one gadolinium-enhancing lesion or nine T_2 hyperintense lesions if there is no gadolinium enhancing lesion

2. At least one infratentorial lesion

3. At least one juxtacortical lesion

4. At least three periventricular lesions

NOTE: A spinal cord lesion can be considered equivalent to a brain infratentorial lesion: an enhancing spinal cord lesion is considered to be equivalent to an enhancing brain lesion, and individual spinal cord lesions can contribute together with individual brain lesions to reach the required number of T_2 lesions

Criteria for Dissemination in Time

a. Detection of gadolinium enhancement at least 3 months after the onset of the initial clinical event, if not at the site corresponding to the initial event

or

b. Detection of a new T_2 lesion if it appears at any time compared with a reference scan done at least 30 days after the onset of the initial clinical event

MRI criteria for disease of insidious onset suggestive of PPMS

1. One year of disease progression (retrospectively or prospectively determined)

2. Plus two of the following:

a. Positive brain MRI (nine T_2 lesions or four or more T_2 lesions with positive VEP)

b. Positive spinal cord MRI (two focal T_2 lesions)

c. Positive CSF (isoelectric focusing evidence of oligoclonal IgG bands or increased IgG index, or both).

FIG 1.3 MRI criteria employed with McDonald Criteria for diagnosis of MS (McDonald et al 2001; Polman *et al.,* 2005)

The McDonald Criteria retains as its focus evidence of dissemination of MS lesions in time and space. Clinical evaluation remains critical and necessary for a diagnosis of MS. An advantage of the McDonald Criteria is that MS can now be made based on a history of a single relapse in which there was clinical confirmation of a CNS lesion. The application of the McDonald criteria to such patients revealed a specificity of 83-86% for the subsequent development of clinically definite MS by Poser criteria (Dalton *et al.,* 2002a; Tintore *et al.,* 2003).

Revisions to the McDonald Criteria have been published, allowing for a greater role in spinal cord lesions (Polman *et al.,* 2005) and a reduction in the interval between scans to determine a new lesion (Swanton *et al.,* 2006). Such revisions allow a greater sensitivity for the diagnosis of MS whilst retaining diagnostic accuracy and specificity (Swanton *et al.,* 2007). The latest accepted version of the McDonald Criteria is outlined in FIG 1.3.

1.6 Management of multiple sclerosis

Management of the MS patient encompasses both pharmacological and non-pharmacological approaches. Education about the disease and psychological support can be provided by MS specialist nurses and active support groups, either in terms of family members and loved ones, or in organised patient interest groups such as the MS Society. The provision of physiotherapy and occupational therapy, especially within an inpatient neuro-rehabilitation setting, has been shown to improve functional independence in disabled MS patients (Freeman *et al.,* 1997, Solari *et al.,* 1999).

Pharmacological therapy can be categorised into symptomatic treatment and disease modifying therapy. Several specific MS related symptoms are amenable to pharmacological therapy, including spasticity, bladder dysfunction, pain, fatigue and depression. The administration of high dose steroids in the event of an acute relapse has been shown to hasten recovery of function (Brusaferri *et al.,* 2000; Miller DM *et al.,* 2000). However, there is no evidence that steroids affect the long term outcome following a relapse.

Disease modifying therapies now available and licensed for use in MS include interferon β (IFNβ), glatiramer acetate, mitoxantrone and natalizumab. Amongst these, the most widely used are IFNβ in its various preparations and glatiramer acetate. IFNβ comes in two forms. IFNβ-1a (avonex and rebif) and IFNβ-1b (betaferon). IFNβ and glatiramer acetate reduce annualised relapse rate by 30% in patients with RRMS (IFNB MS Study Group, 1993; IFNB MS Study Group and University of British Columbia MS/MRI analysis Group, 1995; Johnson *et al.,* 1995; Jacobs *et al.,* 1996; PRISMS Study Group, 1998), with minimal effect on long term overall disability. While reducing relapse rate, Neither glatiramer acetate nor IFNβ exerts any significant effect on relapse-independent disability progression in SPMS and PPMS (Wolinsky *et al.,* 2007*;* European Study Group on interferon beta-1b in secondary progressive MS, 1998; Panitch *et al.,* 2004; Secondary Progressive Efficacy Clinical Trial of Recombinant Interferon-beta-1a in MS (SPECTRIMS), 2001; Leary *et al.,* 2003). Neither are therefore indicated for the treatment of PPMS. IFNβ−1b is used in SPMS only if concurrent relapses in these patients are significantly responsible for overall clinical dysfunction.

Evidence-based criteria dictating the prescription of IFNβ and glatiramer acetate in the United Kingdom have been drawn up by the Association of British Neurologists (ABN). In essence, treatment with IFNβ or glatiramer acetate is indicated in ambulant RRMS patients over the age of 18, with at least two relapses in two years. Prescription of these agents in the United Kingdom is coordinated and monitored through the Department of Health risk sharing scheme in which the long term efficacy and cost-effectiveness of these agents are investigated through annual assessments (Department of Health, 2002; Sudlow and Counsell, 2003).

1.7 Treatment trials

1.7.1 Definition and background

Treatment trials are planned experimental studies designed to evaluate the effect of putative treatments in humans. In general, they follow extensive pre-clinical studies using in-vitro and on animal models.

Preliminary treatment trials focus on safety and pharmacokinetics (absorption, metabolism and excretion). Further trials investigate efficacy by comparing against a control (standard treatment or placebo).

Prior to the 20th century, clinical trials took the form of uncontrolled empirical and observational studies, in which the putative agent is given to the patient, who is then observed for a therapeutic response. The identity of the treatment was known to both patient and observer (non-blinded). These trials were open to confounding by the placebo response (a response arising from the subject's or observer's expectations of the treatment, rather than from any specific therapeutic property of the treatment itself) and other sources of observer bias.

Double blinded Randomized Controlled Trials (RCT) compare the efficacy of an agent against that of a placebo, or existing treatment. In doing so, any response due to a placebo effect is allowed for by subtracting the response to placebo from the the response to the active agent. Treatment designation (ie whether one receives the agent or placebo) occurs in a randomized, systematic manner which minimizes the differences among groups by equally distributing people with particular characteristics among the different trial arms. Treatment designation is not revealed to the study subjects or investigators until the end of the trial, therefore removing observer bias.. Such trials have become increasingly used in the course of the 20th century and are the predominant design in phase III studies. Uncontrolled open-label studies, in which the study subjects and the investigators are aware of their treatment, are still used, particularly in long term and follow-up studies, although by virtue of their trial design and confounding placebo effect, the evidence provided by such trials is not as robust as RCTs.

1.7.2 Trial Design

The clinical development of a putative agent follows multiple stages, from phase 0 to phase IV studies.

Phase 0 studies involve administering a tiny dose of the agent (frequently one hundredth of a pharmacologically active dose) to healthy volunteers. Such studies serve as preliminary investigations into the safety of an agent, and the findings can influence the decision to proceed to phase 1 studies.

Phase I studies ascertain the safety and tolerability of the agent in healthy volunteers at doses approximating the pharmacologically active dose. Typically, subjects are observed through a period spanning several half-lives of the drug, allowing assessment of the agent's pharmacokinetics. Dose-ranging studies, where the medication is administered in ascending doses, determine the maximum tolerated dose.

Phase II studies serve as proof-of-concept efficacy assessments. They are intermediate in size and rarely involve more than a few hundred patients. Preliminary observations are made on efficacy and dose response, and a dosing regime is determined. Assessments on safety and pharmacokinetics started in phase I trials are extended. Surrogate outcome measures (which may be more sensitive than definitive clinical outcome measures) are often employed: MRI is used in this way in MS phase II trials.

Phase III trials are conducted after efficacy of treatment has been preliminarily demonstrated in phase II trials. These trials typically involve several hundreds of patients from multiple centres. They serve as definitive efficacy assessments on a large number of patients for whom the medication is intended. As such, these trials are designed as double-blinded RCT, with clearly defined inclusion criteria and outcome measures. The usual primary outcome measures in phase III MS trials are annualised relapse rate and changes in measured disability.

Phase IV trials extend the study of the drug in its post-licencing period. The trials are by necessity uncontrolled, open-labelled studies. They serve to provide continuing data on long term safety and, to a lesser extent, efficacy.

1.7.3 Outcome measures in MS trials

In MS drug trials, response to a drug is measured through changes in clinical and surrogate markers of disease activity and severity.

1.7.3.1 Clinical measures in MS

Clinical measures form the primary outcome measure in phase III MS trials. These are divided into those that reflect disease activity (relapse rate) and those that reflect the disability accrued as a result of the disease, such as the Expanded Disablity Status Scale (EDSS) and the Multiple Sclerosis Functional Composite (MSFC).

Relapses are the clinical expression of underlying disease activity. As such, despite variations in definition (Liu and Blumhardt, 1999), relapse frequency has been employed as a primary outcome measure in many pivotal MS treatment trials to date (IFNB MS study group, 1995; IFNB MS study group, 1993; PRISMS study group, 1998; Johnson *et al.,* 1995; Polman *et al.,* 2006). However, the relationship between relapses and long term disability is uncertain (Runmarker and Anderson, 1993). Moreover relapse frequency decreases over time as part of the natural history of MS (Weinshenker and Ebers, 1987). For these reasons, relapse frequency on its own provides an inadequate picture of the disease and other clinical markers are required in conjunction with relapse rate.

Disability scales are designed to provide objective measures of disability as a result of disease, and indirectly reflect disease progression and recovery. They are therefore useful and relevant in determining the efficacy of therapeutic intervention. The disability status scale (DSS) (Kurtzke, 1955) was developed to reflect and monitor MS-related disability within the context of a treatment trial involving isoniazid (Kurtzke, 2007). It incorporated functional scores from a set of clinical subsystems (pyramidal; brainstem; cerebellar; sensory; bowel and bladder; vision; cerebral; other) to provide a composite score on a graded scale, which encompassed a wide range of functional states extending from normality (DSS score 0) to death (DSS score 10). Refinements of the DSS led to the EDSS (Kurtzke, 1983), which provides greater differentiation of functional status, and is based on identifying neurological signs from a range of functional systems as well as evaluating ambulation. Like its predecessor, the EDSS is on an ordinal, albeit non-linear scale between 0 (normal neurological function) and 10 (death) with increments of 0.5. (FIG 1.4)

Kurtzke expanded disability status scale

0.0 = normal neurological examination

1.0 = no disability, minimal signs in one FS

1.5 = no disability, minimal signs in more than one FS

2.0 = minimal disability in one FS

2.5 = minimal disability in two FS

3.0 = moderate disability in one FS or mild disability in three of four FS though fully ambulatory

3.5 = fully ambulatory but with moderate disability in one FS and minimal disability in one or two FS; or moderate disability in 2 FS, or five FS with minimal disability

4.0 = fully ambulatory without aid, self-sufficient up and about some 12 hours a day despite relatively severe disability in one FS or combinations of lesser grades exceeding limits of previous steps; able to walk without aid or rest some 500 m

4.5 = fully ambulatory without aid, up and about much of the day, able to work a full day , may otherwise have some limitation of full activity or require minimal assistance, characterisd by relatively severe disability in one FS or combinations of lesser grades exceeding limits of previous steps; able to walk without aid or rest some 300 m

5.0 = ambulatory without aid or rest for about 200 m; disability severe enough to impair full daily activities (e.g. to work a full day without special provisions)

5.5 = ambulatory without aid or rest for about 100 m, disability severe enough to preclude full daily activities

6.0 = intermittent or unilateral constant assistance (cane, crutch, brace) required to walk about 100m with or without resting

6.5 = constant bilateral assistance (canes, crutches or braces) required to walk about 100 m with or without resting

7.0 = unable to walk beyond approximately five meters even with aid, essentially restricted to wheelchair; wheels self in standard wheelchair and transfers alone, up and about in wheelchair some 12 hours a day

7.5 = unable to take more than a few steps; restricted to wheelchair; may need aid in transfer, wheels self but cannot carry on in standard wheelchair a full day; may require motorised wheelchair

8.0 = essentially restricted to bed or chair or perambulated in wheelchair, but may be our of bed itself much of the day; retains many self care functions; generally has effective use of arms

8.5 = essentially restricted to bed much of the day; has some effective use of arm(s); retains some self care functions

9.0 = helpless bed patient; can communicate and eat

9.5 = totally helpless bed patient, unable to communicate effectively or eat/swallow

10.0 = death due to MS

FIG 1.4 The expanded disability status scale (Kurtzke, 1983)

The EDSS provides an objective framework with which to assess MS related disability in cross sectional and longitudinal studies. It is the single most widely used disability scale used to assess MS patients in clinical trials and natural history studies. The overriding advantages of the EDSS are its ease of administration and familiarity with investigating clinicians. However, it is not without its limitations (Willoughby and Paty, 1988; Sharrack and Hughes, 1996). Distinguishing between mild and moderate disability can be difficult, particularly within subsystems reflecting bowel and bladder, and cerebral function. Scores above 4.5 being heavily weighted towards ambulation, with less emphasis on upper limb and cognitive function.

To provide a better reflection of the latter two, the EDSS is frequently combined with the multiple sclerosis functional composite (MSFC) score (Rudick *et al.,* 1997; Fischer JS *et al.,* 1999). The MSFC combines assessments of ambulation (25 foot timed walk), upper limb function (nine hole peg test) and cognition (Paced Auditory Serial Addition test) to obtain a composite z-score reflective of disability. As such, it is not as weighted as the EDSS towards ambulation.

Limited sensitivity of clinical markers, coupled with a variability in disease course require that MS treatment trials be of sufficient size and duration to be adequately powered to demonstrate efficacy. Efforts have therefore been directed toward the identification of a suitable cost-effective and reproducible surrogate marker.

1.7.3.2 Surrogate markers in MS:

A surrogate marker is a non clinical measure that can be used in place of a clinical outcome index as a measure of disease activity and severity. It should accurately reflect disease severity and be sensitive in detecting clinically important change.

The following criteria have been suggested for the validation of surrogate markers for use in clinical trials (Prentice, 1989):

1. A given treatment should influence the clinical endpoint of interest and the surrogate in the same way.

2. The surrogate and clinical endpoints should be significantly correlated.

3. The effect of a given treatment on the clinical endpoint should be mediated through an effect on the surrogate endpoint .

To date, no single biomarker has satisfied all the above criteria for MS.

Nonetheless, as a potential surrogate marker of MS, MRI bears the following advantages:

1. Objectivity: MRI provides an objective picture of disease load and severity. Blinding of the observer is also easily maintained since analysis can be performed remote from the patient.

2. Sensitivity: Serial Gadolinium (Gd) enhanced monthly MR detects 5-10 new inflammatory lesions for every clinical relapse in both relapsing remitting and secondary progressive MS patients. Natural history studies have demonstrated frequent enhancing lesions occuring even during periods of clinical remission (Grossman *et al.,* 1986; Miller DH *et al.,* 1988; McFarland *et al.,* 1992). MRI thus provides a sensitive measure of inflammation by detecting many active but clinically silent lesions.

3. Archivability: MRI is easily archivable and retrievable, allowing future re-analysis

and audit.

4. Cost-effectiveness: MRI provides a reproducible and objective measure of severity and activity of the disease, Moreover, the use of MRI markers significantly improves the power of trials, allowing study populations in phase II clinical trials to be kept low (Tubridy *et al.,*1998a).

The reproducibility and objectivity of MRI variables make their use as surrogate markers an attractive possibility. However, for such a role to exist requires demonstration of correlation between the MR parameter and clinical outcome with a robust prediction of clinical effect on the MR outcome studied. Unfortunately, although MRI outcome variables correlate moderately with clinical outcome in early disease, the correlation with long term outcomes is weaker. For this reason, existing MRI measures are not regarded as fully adequate or validated surrogate measures (McFarland *et al.,* 2002). Their use is therefore limited to primary outcome measures in phase II proof of concept trials, and as supplementary outcome measures in phase III trials.

The principles of MRI and its use in the investigation of MS will be the focus of the next chapter

CHAPTER 2

Magnetic Resonance Imaging

MRI is a non-invasive method of obtaining high resolution images of internal structures within the body. Unlike X-rays, no ionizing radiation is involved in the acquisition procedure, making MRI relatively safe.

2.1 Basic Principles of MRI

2.1.1 Nuclear induction and the behaviour of protons in a magnetic field

Felix Bloch first described the phenomenon of nuclear induction, the main principle on which MRI is based (Block, 1946). Nuclear induction is the creation of a local magnetic field by the spinning of a charged particle (that is with an odd number of nucleons: protons and neutrons combined).

Hydrogen is present in abundance in biological structures as a constituent of water, fat and protein. MRI techniques manipulate hydrogen nuclei (protons) as their primary charged particle to generate images of biological structures.

Protons spin in their natural state, each one generating a local magnetic field (a magnetic dipole moment) aligned along its axis. In the absence of an external magnetic field, the axes of all protons face different directions and no net magnetic field is exerted. The application of an external magnetic field (B_0) causes an alignment of the axes of protons, either in the direction of the magnetic field (parallel) or opposite to it (antiparallel). As more parallel than non-parallel protons exist, a net magnetic moment aligned along the axis B_0 results. (FIG 2.1)

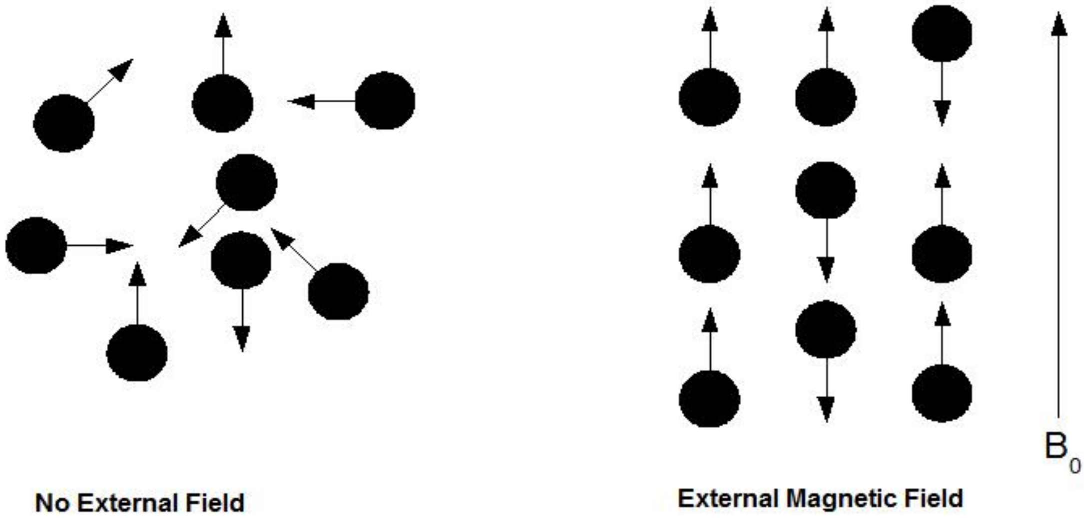

FIG 2.1 Random alignment of protons in the absence of an external magnetic field. The introduction of the external magnetic field (B_0) causes alignment of the protons in relation to the field, with a net magnetic moment in the direction of B_0.

Precession is the gyration of protons about the axis of the prevalent magnetic field, somewhat similar to the movement of a spinning top. This takes place in addition to the spinning movement of the proton about its axis (FIG 2.2). The frequency at which a proton precesses is given in the Larmor equation below:

$$\omega = \gamma B_0$$

ω = Precessional, or Larmor frequency (radians/sec or MHz),

γ = gyromagnetic ratio, constant for a given nucleus (in radians/secT or MHz/T)

B_0 = strength of the external magnetic field (T).

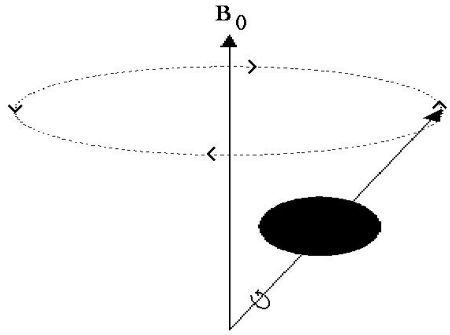

FIG 2.2 Precession of a spinning proton about the axis of the magnetic field B_o

In their natural state, the precessional position, or phase of protons varies between protons (FIG2.3)

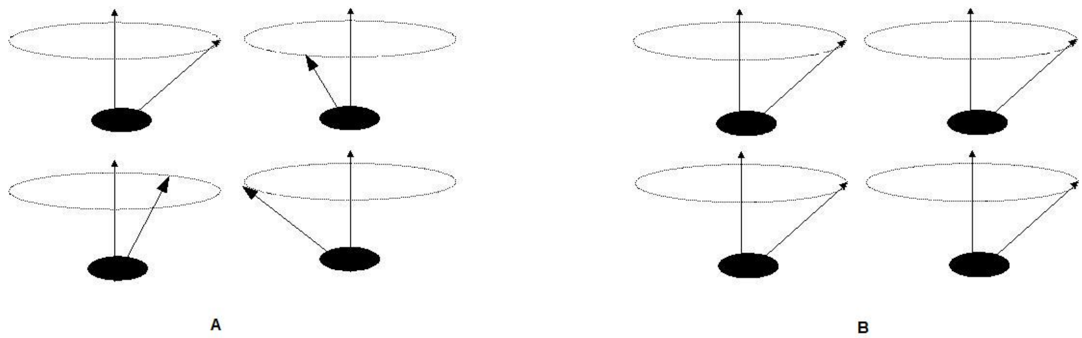

FIG 2.3 Protons precessing out of phase (A) and in phase (B) with each other

The introduction of a radiofrequency (RF) pulse at the precessional or Larmor frequency induces resonance, in which protons absorb the energy inherent in the RF pulse to attain a higher energy state. This results in (i) deviation of the net magnetic vector away from B_0 at a flip angle α; and (ii) attainment of phase coherence, in which the protons precess in phase with each other.

Therefore, a 90^o RF pulse will result in the 90^o deflection of the net magnetic vector from one aligned with B_o, (z axis), to one within the transverse (x-y) plane (FIG 2.4). The net rotating vector then induces an electrical voltage in a receiver coil or antenna orientated in the transverse plane, translating the spin into an oscillating electrical voltage, or signal, which can be read to construct an image.

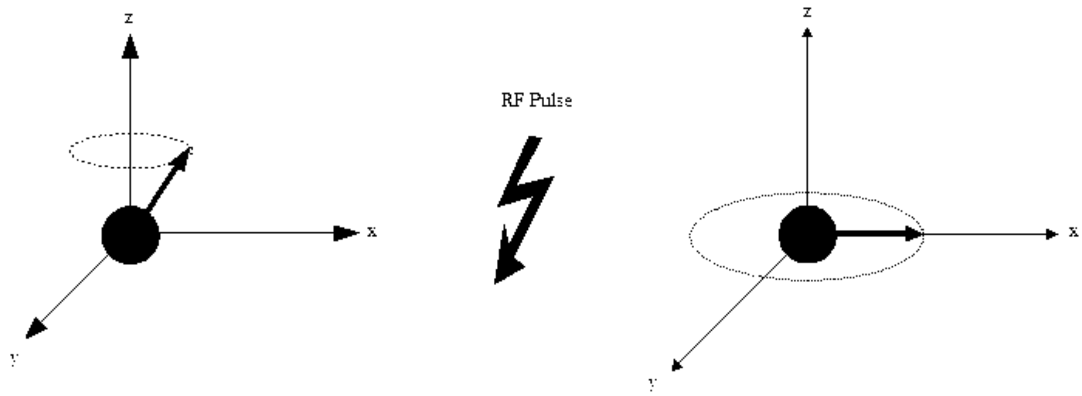

FIG 2.4 Re-orientation of net magnetisation into transverse (x-y) plane as a result of a 900 RF pulse

2.1.2 T_1, T_2* and T_2 relaxation

Following the cessation of the RF pulse, two principal processes take place:

1. Resumption of net longitudinal magnetization along B_0: T_1 relaxation

2. Loss of phase coherence, or dephasement, due to T_2 and T_2* relaxation. This results in a loss of transverse magnetisation.

T_1, T_2 and T_2* relaxation occur independently of each other.

T_2 and T_2* relaxation occurs at a higher rate than T_1 relaxation (roughly 10-fold quicker for various tissues at typical clinical field strengths). This results in a much quicker decay of transverse magnetisation than the recovery of longitudinal magnetisation.

T_1 relaxation, also known as spin-lattice relaxation, is the resumption of longitudinal magnetization along B_0. It results from the dissipation of extra energy absorbed from the RF pulse. This occurs once the RF pulse stops and results in a re-orientation of the axes of the protons to pre-pulse directions. T_1 relaxation is an exponential process governed by a recovery time constant T_1(FIG 2.5). T_1 is influenced by chemical lattice structure, and is shortest when efficient energy dissipation is facilitated.

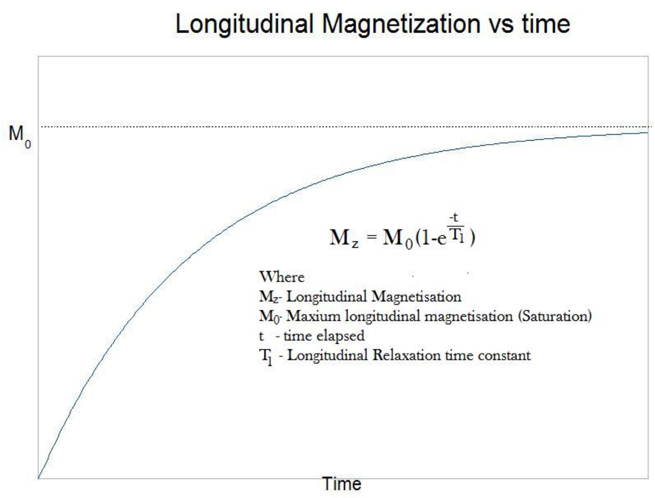

FIG 2.5 Resumption of net longitudinal magnetization: T_1 relaxation

Two processes drive the loss of phase coherence in protons following the cessation of the RF pulse. These are:

1. Spin interaction: Each spinning proton, by virtue of its magnetic dipole moment, causes minute variations in the local magnetic field of neighbouring protons. This results in subtle differences in precessional rate which in turn leads to dephasement. The decay is determined by the time constant T_2 and is called T_2 relaxation, or spin-spin

relaxation.

2. External magnetic field inhomogeneity: Local variations in magnetic field strength cause discrepancies in precessional frequency and dephasement over and above local spin-spin relaxation. This is called T_2* relaxation, the rate of which is governed by the time constant T_2*.

T_1 and T_2 vary with the chemical environment. For instance, fat has a short T_1 due to efficient dissipation of energy as facilitated by the structured molecular lattice. Conversely, T_1 is long in water, where the lack of such a lattice impedes the efficiency of energy transfer.

Tissues which are made of molecules with a large number of protons (for example lipids and proteins) have short T_2 due to the increased amount of spin-spin interactions within the molecule. In contrast T_2 is longer in water, where protons are more freely spaced apart and therefore subject to a relatively low number of spin interactions.

Differences in T_1 and T_2 in neighbouring structures can be exploited by MRI to generate contrast and delineate relevant tissue and pathology.

2.1.3 Repetition time (TR) and echo time (TE)

Repetition time (TR) and echo time (TE) are principal parameters within MRI. They can be manipulated to generate images which are weighted toward T_1, T_2 or proton density (PD) (Table 2.1).

In a spin echo sequence, signal intensity is given in the following equation:

$$SI \propto N(H)(1 - e^{\frac{-TR}{T_1}})(e^{\frac{-TE}{T_2}})$$

SI= Signal Intensity
N(H)= Proton Density
TR= Repetition Time
TE= Echo Time

TR is the time elapsed between subsequent applications of the same pulse sequence (FIG 2.6).

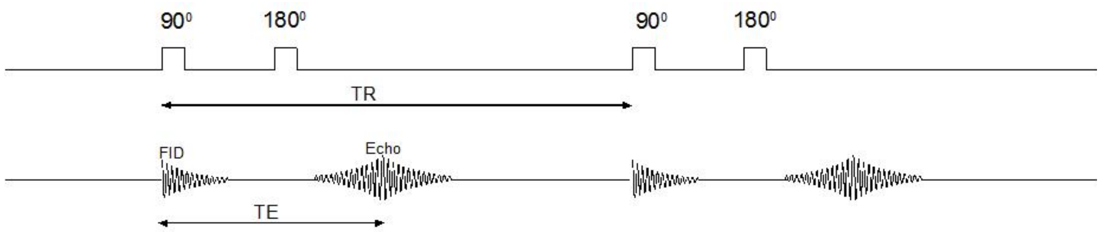

FIG 2.6 Pulse sequence diagram of a conventional spin echo (CSE) sequence. Net magnetization is reorientated into the X-Y plane as a result of the initial 900 RF pulse. This produces an oscillating signal which decays rapidly to T_2 and T_2* relaxation: free induction decay (FID). A subsequent 1800 pulse rephases the protons, forming an echo which is received through the coil. The process is repeated a set number of times, the time between subsequent 900 pulses is the TR, and the time between 900 pulse and echo is TE. In reality, TR is of much greater magnitude than TE (3000-4000ms for the former and <100ms for the latter)

Lengthening the TR minimizes T_1 weighting as follows:

From: $SI \propto N(H)(1 - e^{\frac{-TR}{T_1}})(e^{\frac{-TE}{T_2}})$

as $TR \to \infty$, $e^{\frac{-TR}{T_1}} \to 0$, therefore $SI \rightarrow N(H)e^{\frac{-TE}{T_2}}$

In other words, a sequence with a long TR will produce a signal intensity influenced preferentially by PD and T_2.

A long TR allows full T_1 relaxation of protons between 90^o pulses, and minimizes the effect of different T_1 properties of tissue. Conversely, a short TR maximizes differences between tissues with long (e.g. water) and short(e.g. fat) T_1 by only allowing full relaxation of protons with short T_1. Tissues with a short T_1 will appear bright and those with a long T_1 will appear dark on these so-called T_1 weighted images.

TE is the time elapsed between the 90^0 pulse and the reading of the signal formed from protons within the x-y plane, the so-called echo (FIG 2.6). Variation of TE influences the amount of T_2 weighting of an image, with a short TE minimising the T_2 weighting of the sequence as follows:

From: $SI \propto N(H)(1-e^{\frac{-TR}{T_1}})(e^{\frac{-TE}{T_2}})$

as $TE \rightarrow 0$, $e^{\frac{-TE}{T_2}} \rightarrow 1$

therefore $SI \rightarrow N(H)(1-e^{\frac{-TR}{T_1}})$

A sequence with a long TE accentuates the the differences in T_2 between tissues by allowing relatively more dephasement (and therefore signal decay) in tissues with short T_2 when the signal is received and read. In such a sequence, pixel intensity is positively related to T_2, where tissues with longer T_2 appear brighter than their counterparts.

Both T_1 and T_2 effects can be minimised by applying a sequence with a long TR and short TE. Such as sequence is known as a proton density (PD) weighted sequence. Pixel intensity in this case is then related to the local concentration of free protons.

Table 2.1 Manipulation of TR and TE to produce images of different weighting

	TR	TE
T_1 weighted Image	Short	Short
T_2 weighted image	Long	Long
PD weighted image	Long	Short

2.1.4 Signal intensity of normal and pathological tissue on MRI

CSF consists predominantly of free water and thus has a relatively long T_1 and T_2. Consequently, it appears dark on T_1 weighted images and bright on T_2 weighted images.

WM primarily contains closely packed axons and myelin sheaths- consisting largely of fat and macromolecules with relatively short T_1 and T_2. WM therefore appears brighter on T_1 weighted images, and less bright on T_2 weighted images compared with CSF.

GM consists largely of cell bodies which are a mixture of cytoplasm and macromolecules, resulting in an intermediate T_1 and T_2 (greater than WM and much less than CSF). This causes an intermediate signal intensity between the two on both T_1- and T_2-weighted sequences.

In relation to surrounding WM, MS lesions appear hyperintense on T_2 weighted images. This T_2 hyperintensity represents a heterogenous pathology (Barkhof *et al.,* 2003) including inflammation, gliosis, axonal loss and remyelination. MS lesions can appear isointense or hypointense on T_1 weighted MRI, the latter either representing a population of lesions in which active inflammation and oedema occurs- the "acute black holes" (ABH) (van Waesberghe *et al.,* 1998; Bagnato *et al.,* 2003) or more chronic lesions associated with gliosis and axonal loss- "persistent black holes" (PBH) (van Walderveen *et al.*, 1998; van Waesberghe *et al.*, 1999).

2.1.5 Spatial Encoding

The generation of anatomical images requires discernment of signal intensity at each location. This is performed through the imparting of spatial information into the received signal: so-called spatial encoding.

Spatial encoding is achieved through 3 orthogonal gradient coils corresponding to the x, y and z axes ($G_{x,}$, G_y and G_z respectively). These coils apply magnetic field gradients along their axes at predetermined times in the pulse sequence (FIG 2.7).

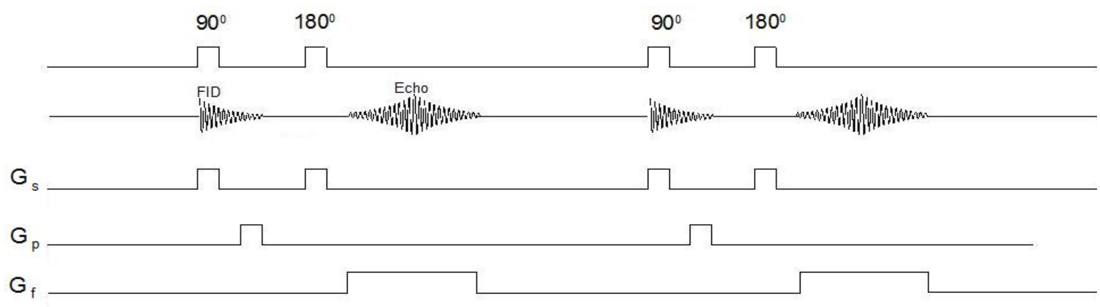

FIG 2.7 Pulse sequence diagram of CSE with orthogonal magnetic gradients G_s (slice select), G_p (phase encode) and G_f (frequency encode).

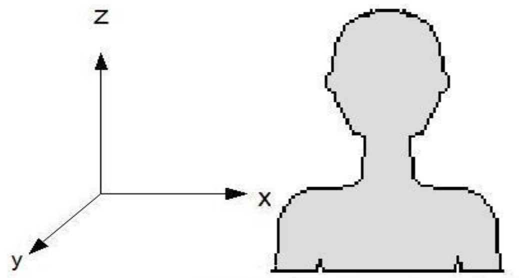

	Axial	Coronal	Saggital
Slice Select	G_z	G_y	G_x
Frequency Encode	G_x	G_x	G_y
Phase Encode	G_y	G_z	G_z

FIG 2.8 x,y and z axes in relation to the patient. The specific application of the orthogonal magnetic gradients as slice select, frequency encode or phase encode gradient is dependent on slice orientation

For axial slices, the slice select, phase encode and frequency encode gradients are along the z, y and x axes respectively. However, magnetic gradients can be used interchangeably depending on the slice orientation (FIG 2.8)

The slice select gradient is applied with the RF pulse (FIG 2.7) and causes a linear variation in precessional frequency along the z-axis. This allows selective excitation of the protons by the application of an RF pulse at the appropriate preceissional frequency, and therefore specific x-y slice selection.

The frequency encoding gradient is applied during the echo, causing a linear increase in precessional frequency along the x-axis, such that each successive column of pixels precesses at a greater rate.

The phase encode gradient is briefly applied between the 90^0 RF pulse and the echo. This transient gradient causes a brief variation in precessional frequency along the y axis, and when turned off, a linear variation in phase along the axis.

The phase encode gradient is re-applied with increasing magnitude at each repetition within a sequence, the number of phase encoding steps in the sequence equal to the number of rows of pixels in the image matrix (typically 256).

The result of the application of the above gradients is that the protons at each location within the selected slice will precess at their own unique phase and frequency depending on location within the x-y plane.

2.1.6 k-space

K-space is the data space in which the mathematically transformed signal is stored, and from which the image is constructed. Each slice has its own k-space.

In k-space, the received MR signal, or echo, is converted from the time domain to the frequency domain using a mathematical transformation called the fourier transform. Each transformed echo is then used to fill a row of k-space, the number of rows in k-space being equivalent to the number of rows within the image matrix (and the number of phase encodes in the sequence).

Echoes which fill rows in the centre of k-space have undergone the least dephasement and contain the highest signal. Rows further away from the centre are filled with echoes with increasing dephasement, such that rows at the edges of k-space contain the echoes which have undergone the largest phase encoding gradients. Thus, the centre of k-space contains most of the image signal, whereas the edges of k-space hold the finest anatomical detail.

As frequency and phase correspond to pixel position, image construction is possible using the data in k-space, which is in the frequency domain and organised in terms of degree of dephasement.

2.1.7 Image attributes

Image parameters can be manipulated to influence image attributes. An example of this is the manipulation of TR and TE to influence image weighting (2.1.3). The following section describes further image attributes of relevance to the MR sequences employed in this thesis

2.1.7.1 Field of View (FOV)

The field of view (FOV) is the size of the area studied (FIG 2.9).

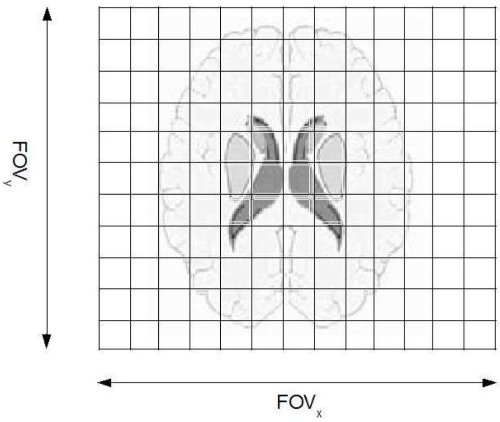

FIG 2.9 The image matrix consists of rows along the x axis and columns along the y axis. $FOV_x$and FOV_y are the dimensions of the image along the x-axis and y-axis respectively. Typical FOV for an axial brain scan is 240mm X 240mm

FOV of an axis is related to the magnetic gradient applied along it as follows:

$$FOV \propto \frac{BW}{G}$$

Where

FOV= Field of View (mm)
BW= Bandwidth (MHz)
G= magnitude of gradient (Mhz/mm)

The bandwidth is the range between the highest and lowest frequencies in the applied magnetic gradient. FOV increases with increasing bandwidth. FOV is inversely proportional to the magnitude, or steepness of the gradient applied. For a given bandwidth, a steeper gradient is associated with a smaller FOV.

A typical FOV of 240mm by 240mm provides adequate brain coverage.

2.1.7.2 Resolution

Image resolution determines the level of detail in an image. It describes the number of distinct points (generally black and white line pairs) that can be discerned over 1mm (lp/mm). Resolution is inversely related to pixel size.

Resolution is associated with the magnitude of the magnetic gradient, with steeper gradients resulting in higher resolution. A typical matrix along the phase and frequency encoding gradients is 256 columns and rows respectively (which approximates to an in-plane resolution of $1mm^{-1}$ using a standard 240 X 240mm field of view).

2.1.7.3 Signal to Noise Ratio (SNR)

Signal to noise ratio (SNR) is a measure of the signal strength relative to background noise. The higher the SNR, the more sensitive the sequence is at detecting subtle changes in tissue which may reflect early, subclinical pathological processes. SNR is given in the following formula:

$$SNR \propto (Voxel\ Volume)\sqrt{\frac{(N_p)(NEX)}{BW}}$$

where

SNR= Signal to Noise Ratio
N_p= Number of phase encoding steps
NEX= Number of excitations
BW= Bandwidth

SNR is proportional to voxel volume, in that larger voxels contain more protons, and therefore emit a proportionately higher amount of signal. Conversely, higher resolution (with smaller voxels) is associated with a lower SNR.

SNR can be improved by repeating the sequence and averaging the signal. The number of times this is done is called the number of excitations (NEX). A higher number of phase encoding steps (N_p) (and therefore increasing the number of repetitions in a sequence) also increases the SNR.

For a given voxel size and N_p, SNR is inversely proportional to the square root of the bandwidth of the phase and frequency encoding gradients.

2.1.7.4 Acquisition time

Acquisition time is the time required to undertake the MR scan. A short acquisition time is of relevance in the scanning of subjects with limited tolerance for lying within the scanner for extended periods. Acquisition time in a CSE sequence is given by the following formula:

$$T_A = TR.NEX.N_p$$

where

T_A= Acquisition time
TR= Repetition time
NEX= number of excitations
N_p= number of phase encodes

As shall be illustrated in the following sections, certain scan sequences can reduce acquisition time by alterations in the flip angle and in the manner in which k-space is filled.

2.2 Imaging Sequences

The following section will describe some of the sequences used in the ensuing chapters.

2.2.1 Conventional Spin Echo Sequence (FIG 2.6; FIG 2.7)

The CSE sequence is one of the most commonly used sequences in MRI studies of MS. Each repetition of the pulse sequence consists of an initial 90^0 RF pulse, followed shortly after by a 180^0 refocusing pulse

The initial 90^o RF pulse shifts the net magnetization vector into the transverse plane, creating an oscillating transverse magnetization which decays due to loss of phase coherence from T_2 and T_2* decay. This initial decaying signal is the Free induction decay (FID).

Loss of phase coherence from T_2* relaxation is recaptured by applying a subsequent 180^o (refocusing) pulse at time TE/2 after the 90^0 RF pulse. This pulse reverses the position of the magnetic vector and allows the protons spinning at different speeds due to external field inhomogeneities to regain phase coherence, generating a signal, or 'spin echo' which is received and stored in k-space.

In this thesis, CSE is employed in obtaining pre and post-contrast T_1 weighted sequences (4.2.4; 6.2.2).

2.2.2 Fast Spin Echo (FSE) Sequence

In CSE sequences, a single phase encode is performed at each TR, which is then repeated by the number of phase encodes per image, most often 128 or 256. In FSE, instead of a single 180^o refocusing pulse, a string of such pulses can be employed within each TR to generate multiple echoes and therefore multiple phase encodes. (FIG 2.10) The number of echoes per repetition is the echo train length (ETL).

Multiple echoes per TR gives rise to multiple TEs per TR, which could confound the T_2 weighting of the resultant image. This is addressed by applying weighting onto echoes closest to the desired, or effective TE. Such echoes undergo the lowest phase encoding gradients, with increasing gradients dephasing echoes further away from the effective TE. The result is that while all echoes contribute to the image, echoes approximating the effective TE will have the highest amplitude and contribute most to the image contrast. The resultant image has a contrast very similar to that of a CSE with the same (real) TE.

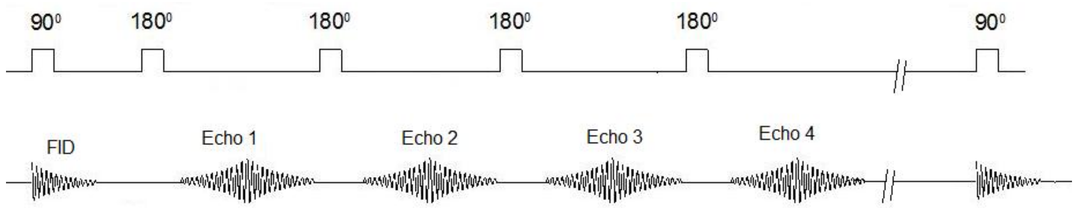

FIG 2.10 Multiple echoes per repetition in FSE sequence.

As each echo fills a line of k-space, a number of lines per TR is filled, equivalent to the ETL. Image acquisition time is therefore a fraction of that in conventional spin echo.

$$T_A = \frac{TR.NEX.N_p}{ETL}$$

where
T_A= Acquisition time
TR= Repetition time
NEX= Number of excitations
N_p= Number of phase encodes
ETL= Echo train length

The main advantage of FSE is that it allows the acquisition of high resolution images using a short acquisition time, with the attendant advantages discussed above, as well as potentially reducing motion artifact. Magnetic susceptibility artefacts from metallic objects are also reduced due to the multiple spins.

However, the greater number of echoes per repetition leaves a shorter inactive time period per repetition. This inactive time would normally be used in CSE to scan further slices. (FIG 2.11)

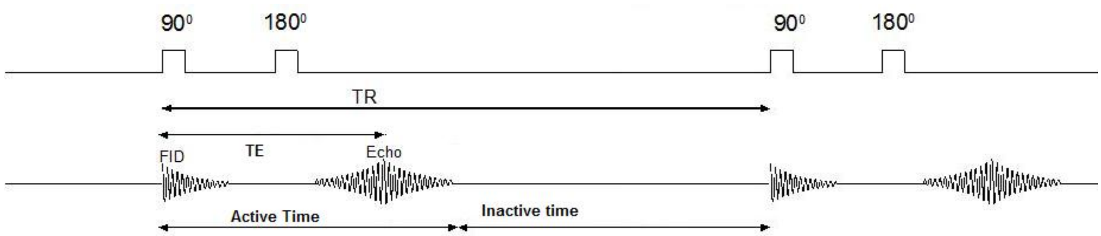

FIG 2.11 TE<< TR in most sequences. Therefore, in a significant proportion of TR, no further activity occurs. This is the inactive time. In CSE, further slices are scanned during this inactive time.

Therefore, slice coverage could potentially be compromised in FSE. In images where strong T_1 weighting is not required, inactive time and therefore slice coverage can be increased by lengthening the TR.

A further potential shortcoming of FSE is the deterioration of signal from echoes occuring later in the repetition. This is due to spin-spin interactions intrinsic within the imaged tissue (T_2 decay) and occurs independent of the refocusing pulses.

In this thesis, FSE is employed in the acquisition of PD weighted and T_2 weighted scans in a phase III treatment trial involving natalizumab (4.2.4), and further studies on BBB integrity. (6.2.2; 7.2.2.1)

2.2.3 Gradient Echo Sequences

Gradient echo (GE) sequences employ a smaller flip angle α. This results in a quicker restoration of longitudinal magnetization, allowing a shorter TR, and consequently a shorter acquisition time. No 180^0 refocusing pulse is employed, the application of which would result in an inversion of net magnetization along the z axis. This lack of refocusing pulse confers a greater magnetic susceptibility to the signal. The resultant echo undergoes T_2* as opposed to T_2 decay.

Image contrast is determined by α, TR and TE. Small values of α cause quicker restoration of longitudinal magnetization, minimizing the contrast between tissues of differing T_1 and reducing T_1 weighting. The converse is true with larger values of α.

In this thesis, GE sequences are employed in the acquisition of T_1 maps (7.2.2.1) and in the study of GM and WM atrophy (5.2.2)

2.2.3.1 High resolution three dimensional gradient echo imaging.

Three dimensional imaging employs an additional phase encoding gradient along the z (slice selection)-axis. This allows the acquisition of further data along the axis, and information is collected in three dimensional slabs, from which thin, contiguous slices are obtained. Small voxel size results in good spatial resolution, suitable for volumetric studies. Provided the voxels are isometric, slices can be reconstructed in any plane within the three dimesions.

In this thesis, a three dimensional inversion-recovery prepared fast spoiled gradient recall (FSPGR) sequence is employed to undertake volumetric measurements of the brain. In this sequence, an inversion pulse is added and the inversion time (TI), that is , the time between the inversion pulse and subsequent 90^0 pulse, can be varied to give further control over the degree of T_1 contrast. The multi-planar nature of the sequence with short TE and TR increases slice number and SNR in a rapid time period.

2.2.3.2 T_1 estimation

T_1 measurement is a potential method of detecting subtle parenchymal abnormality. Within the context of MS, T_1 has been found to be abnormally prolonged in lesions as well as NAWM (Stevenson *et al,* 2000; Parry *et al.,* 2002). The measurement of changes in T_1 after administration of Gd in dynamic contrast enhanced also provide a potential method of investigating perfusion and BBB leakage (Parker and Padhani, 2003)

There are a number of approaches which can be adopted to measure T_1. The gold standard utilises an inversion recovery sequence, in which a 180^0 pulse is employed to invert the net magnetization. A subsequent 90^0 pulse is then applied at inversion time TI, tipping the direction of magnetization onto the transverse plane and forming an FID, from whose amplitude the longitudinal magnetization can be measured. The process is repeated a number of times with varying TI. T_1 is then estimated by solving the following equation:

$$S(TI) = S_0(1 - 2e^{\frac{-TI}{T_1}})$$

Where

S(TI)= Signal measured at time TI
S_0= Signal that would be acquired if 90^0 pulse were applied without inversion pulse ie base magnetization
TI= inversion time

In order to obtain a T_1 map (as opposed to a single T_1 measure for the area imaged), the signal is phase and frequency encoded, and the sequence is repeated N_p times. To allow for adequate relaxation between inversion pulses, TR should be at least 5 times greater than T_1. Acquisition time, which is the product of N_p, number of inversions and TR, can sometimes become prohibitively long.

The ratio of SI from two images (in which TR or flip angle is varied) can be used to estimate T_1 using a look-up table. This so-called 2 point method offers the possibility of the construction of a T_1 map with a shorter acquisition time than the inversion recovery approach. Unfortunately, 2 point methods are more susceptible to artefact from nonuniformities in the RF pulse.

The method of obtaining T_1 maps in this thesis adopts a 2 point approach (using T_1 weighted and PD weighted GE sequences) which corrects for RF profile non-uniformity by employing a knowledge of the RF pulse profile and a map of the coil transmission B1 distribution. This method estimates T_1 to an accuracy of 1.4% and a precision of 3%. (Parker *et al.,* 2001)

<u>**2.3 The use of MRI in clinical trials**</u>

Trials based solely on existing clinical scales, such as EDSS and MSFC require large patient populations and need to be of sufficient duration to be adequately powered. The clinical scales employed, such as EDSS, although helpful, are frequently weighted towards locomotor function, and have poor reproducibility and sensitivity to change (Willoughby and Paty, 1988; Sharrack and Hughes, 1996). Even when combined with multi-domain clinical measures such as MSFC, such scales may lack the sensitivity to accurately reflect disease progress such as is seen in the complex and variable nature of MS. The advantage of MRI is in the provision of objective, reproducible measures, which are sensitive to pathological change.

MRI measures also provide the potential for reducing the size of population cohorts required in drug trials: Based on a protocol of monthly Gd enhanced imaging in a placebo controlled parallel group design over 6 months involving patients with either RRMS or SPMS, it was demonstrated that in order to detect a 70% reduction in disease activity, a trial of 2X30 RRMS or 2X50 SPMS patients will be sufficient. With the addition of pre-treatment scans, the trial size could be further reduced (2X20 and 2X30 for RRMS and SPMS patients respectively (Tubridy *et al.,* 1998a). The use of MRI as a surrogate marker therefore represents an attractive complement to existing clinical indices.

However, for such a role to exist, there needs to be a demonstration of correlation between the MR parameter and clinical outcome, with a robust prediction of clinical effect from the MR outcome studied. As previously discussed, MR parameters are presently used only as secondary endpoints in phase III studies, mainly because of the as yet limited relationship between clinical and MR markers of progression (McFarland *et al.,* 2002). With the increasing range of quantitative MRI parameters and improvements in sequence methodology, further evaluation of cohorts in systemic cross-sectional and longitudinal studies and in well defined population groups may improve correlations with clinical disability. Should MRI outcomes eventually gain acceptance as primary endpoints in phase III studies, a potential benefit would be to increase the statistical power of clinical trials and reduce the cohort sizes required. The following sections will describe some of the MRI based measures of disease activity and progression employed in this study.

2.3.1 Gadolinium enhanced MRI

Gadolinium (Gd) is a paramagnetic element, that is, in an externally applied magnetic field, it enhances the relaxation of surrounding protons, resulting in a high signal on T_1 weighted imaging. In its chelated form (Gd-DTPA) (Mitchell, 1997), it is used as a contrast agent in MRI. In a combined MRI-pathology study of EAE- an animal model for MS- Gd enhancement in lesions was correlated with histopathological evidence for BBB breakdown using the marker horseradish peroxidase (Hawkins CP *et al.,* 1990). Histo-MRI correlative studies show that Gd enhancing lesions exhibit local inflammatory features. (Katz *et al.,* 1993; Bruck *et al.,* 1997). Serial analysis studies indicate that Gd enhancement is a consistent feature of new lesions (Bastianello *et al.,* 1990; Lai *et al.,* 1996; Tortorella *et al.,* 1998). Gd enhancement lasts approximately 4-6 weeks in new lesions (Miller DH *et al.,* 1988; Barkhof *et al.,* 1992; Thompson *et al.*, 1992; McFarland *et al.,* 1992; Smith ME *et al*., 1993). Such lesions are also more commonly seen in relapses (Grossman *et al.,* 1986; Tubridy *et al.,* 1998b), although the majority of such lesions are clinically silent.(Harris JO *et al.,* 1991; Thompson *et al.,* 1992). Lesions are more likely to result in a relapse if they are located in a clinically eloquent place, such as the spinal cord (Thorpe *et al.,* 1996) and optic nerves (Youl *et al.,* 1991; Hickman *et al.,* 2004). A meta analysis of 9 studies showed that the relapse rate in a year was weakly related with the number of Gd lesions in the first 6 months (Kappos *et al.,* 1999). The number of Gd enhancing lesions correlate moderately with the number of Gd enhancing lesions in the ensuing 11 months (Molyneux *et al.,* 1998).

Serial Gd enhanced MRI has been used as a primary outcome measure in phase II trials of RRMS and SPMS (Paty and Li, 1993; Durelli *et al.,* 1994; Stone *et al.,* 1997; Jacobs *et al.,* 1996; Pozzilli *et al.,* 1996; Moreau *et al.,* 1994, Sipe *et al.,* 1994; Edan *et al.,* 1997; Karussis *et al.,* 1996; Mancardi *et al.,* 1998). The utility of Gd enhanced MRI is as a marker of inflammation, and indirectly, of the underlying processes which cause clinical relapses. This is supported by the generally concordant effect which exists of disease modifying therapy reducing both relapses and Gd enhancing lesions, although the magnitude of the effect on each may differ.

Although more enhancement is potentially picked up by increasing the frequency of the scans to once a week (Lai *et al.,* 1996), modifying the dosage of Gd (Fillipi *et al.,*1996), or employing the use of additional MT sequences (Silver *et al.,* 1997), such changes also introduce a proportionate increase in variability of activity between subjects, which counterbalances the greater number of Gd enhancing lesions picked up, conferring no net benefit in terms of sample size requirements for phase II trials. (Silver *et al.,* 2001a)

Gd enhancement as detected in monthly scans is therefore best regarded as a proof-of-concept marker for identifying agents that have the potential to reduce relapse rate in relapsing MS. The utility of Gd enhanced MRI in clinical trials is also tempered by the finding that the correlation of enhancement with clinical disability over the medium or longer term is poor or even absent (Kappos *et al.,* 1999).

2.3.2 Total T_2 lesion load

T_2 weighted MRI is sensitive in detecting focal MS lesions in the WM, and total T_2 lesion load is the most established MR surrogate. As serial studies on RRMS demonstrate that almost all new T_2 lesions start as Gd enhancing lesions, T_2 lesion load can be seen as a plausible marker of the total amount of inflammation to date. An exception to this would be in advanced disease and in progressive MS, where the association between new T_2 lesions and BBB breakdown is less strong (Thompson *et al.,* 1991).

Nonetheless, studies of early relapse-onset MS show that volume of T_2 lesions in the 1^{st}

14 years is at least partly related to concurrent and to disability at timepoints up to 20 years, with the greatest correlation between lesion load and disability occuring within the 1st 5 years of disease (Brex *et al.,* 2002; Fisniku *et al.,* 2008a).

Relapse rate in the early years has also been related to time to develop moderate disability (EDSS 4) but not more severe disability (Confavreux *et al.,* 2000; 2003).

Although Gd enhancement and T_2 lesions can be related to relapses, the relationship with long term disability is modest (Kappos *et al.,* 1999; Truyen *et al.,* 1996; Mammi *et al.,* 1996; Gawne-Caine *et al.,* 1998, Riahi *et al.,* 1998). The imperfect correlation with disability can be demonstrated in lesions in corticospinal tracts, indicating that lesions in such tracts alone are insufficient in accounting for all disability (Riahi *et al.,* 1998). Interestingly, there is little correlation between cord lesion volume and EDSS (Kidd *et al.,* 1993).

Reasons for the discrepancy between radiological findings and clinical indices include limitations of the EDSS previously alluded to in chapter 1. In addition, T_2 hyperintense lesions represent quite heterogeneous pathology, including variable amounts of acute inflammation, axonal loss and remyelination (Barkhof *et al.,* 2003). There is also growing evidence of pathology in the NAWM (Trapp *et al.,* 1988; *Werring et al.,* 1999; Stevenson *et al.,* 2000). Similarly, the contribution of cortical lesions to the total disease burden is being increasingly recognised (Pirko *et al.,* 2007*;* Kutzelnigg *et al.,* 2005), many such lesions being invisible on standard MRI sequences (Guerts *et al.,* ; Kidd *et al.,* 1999).

Taken together it would appear that focal inflammation inferred from the development of new/enhancing MRI lesions may only partially predict short and medium term relapses but less so later disability.

2.3.3 T_1 hypointense lesions

Roughly 20-30% of T_2 lesions appear hypointense to surrounding NAWM on T_1 weighted imaging. Such T_1 hypointense lesions are associated with a greater degree of demyelination and extracellular matrix disruption than their T_1 isointense counterparts. T_1 hypointense lesion load correlates well with T_2 lesion load (O'Riordan *et al.,* 1998). These lesions may be associated with oedema and lymphocytic infiltration (Bruck *et al.,* 1997) or with axonal damage and extracellular matrix disruption (van Walderveen *et al.,* 1998) depending on the stage of evolution of the lesion itself.

T_1 hypointense lesion volume has been shown to correlate more closely with disability and progression than more conventional MRI markers of disease such as T_2 lesion load (Truyen *et al.,* 1996; van Walderveen *et al.,* 2001). In-vivo spectroscopy studies of T_1 hypointense lesions reveal lower concentrations of the neuronal marker N-acetyl aspartate (van Walderveen *et al.,* 1999). Further evidence of axonal loss associated with such lesions is provided by the relation between T_1 hypointense lesions and atrophy (Sailer *et al.,* 2001). Magnetisation transfer ratio (MTR) is also significantly lower in T_1 hypointense lesions (Hiehle *et al.,* 1995), suggesting a greater degree of demyelination than lesions which are T_1 isointense. Histological studies show a greater degree of demyelination, axonal loss and extracellular matrix disruption in T_1-hypointense lesions (van Walderveen *et al.,* 1999; van Waesberghe *et al.,* 1999; Bruck *et al.,* 1997; Barkhof *et al.,* 2003), than in T_2 lesions which are T_1 isointense, wherein remyelination tends to be a more common feature (Barkhof *et al.,* 2003).

It may be useful to monitor conversion of individual Gd enhancing lesions into more persistent T_1 hypointense lesions as a surrogate marker for poor recovery from relapses. Glatiramer acetate (Filippi *et al.,* 2001) and Natalizumab (Dalton *et al.,* 2004a), but not IFNβ (Brex *et al.,* 2001) have been reported to reduce the conversion of Gd enhancement into permanent T_1 hypointense lesions

2.3.4 Volumetric measures

Sequential volumetric MRI measures of the brain provide a reproducible and often sensitive marker of brain tissue loss (atrophy), and have been used in the study of neurodegenerative diseases such as Alzheimer disease (Fox and Freeborough, 1997). In MS, this approach has facilitated in vivo studies of brain atrophy (Anderson *et al.,* 2006).

Axons and myelin constitute the largest volume in WM, with GM consisting mostly of neuronal cell bodies, axons and myelin. (Miller DH, 2004) It follows that volume loss in MS likely reflects loss of axons and neurones, a process which contributes to permanent disability progression. An important caveat is that within the setting of acute inflammation, the volume loss from such neuro-axonal degeneration may be masked by a concommitant increase in oedema, and latterly gliosis. Similarly, acute reduction in volume may reflect the resolution of oedema, rather than neuronal loss. For this reason, any therapeutic trial using brain atrophy as a measure has to take into account the effect of the agent on inflammation and the subsequent impact on volumetric measures.

In general, 3D sequences are more reliable than 2D sequences in volumetric measurements due to a lower dependence on slice re-orientation and easier segmentation (Sharma *et al.,* 2004). A number of measures have been adopted in the estimation of brain volume loss, including ventricular enlargement (Sharma *et al.,* 2004; Turner *et al.,* 2001) to brain width (Simon *et al.,* 1999) and corpus callosum cross sectional area (Paolillo *et al.,* 2000). Methods which adopt GM, WM and BP volume as measures have to overcome the problem of accurate segmentation of the brain from surrounding tissue and indeed the individual segments from each other. This is most efficiently achieved through semi or fully automated thresholding techniques (Rudick *et al.,* 1999; Smith SM *et al.,* 2002; Ashburner and Friston, 1997; Ashburner and Friston, 2000). Normalization to head size should be performed because small volume changes tend to be masked by the biological interindividual variability in absolute brain volumes. Normalization methods include standardizing to the scalp (Freeborough and Fox, 1997) or to a calculated total intracranial volume (Chard *et al.,* 2002a). Volume change can then be estimated by comparison of calculated normalized volumes in consecutive scans This is the method adopted in this thesis.

CIS patients who develop MS have significantly greater atrophy than their counterparts who do not develop MS (Brex *et al.,* 2000; Dalton *et al.,* 2002b, Filippi, 2004). The volume loss is predominantly in the GM (Dalton *et al.,* 2004b) and is associated with previous inflammatory lesion load (Paolillo *et al.,* 2004). Atrophy of about 10-15%, as measured by optic nerve cross sectional area reduction is also seen in patients with isolated optic neuritis (Hickman *et al.,* 2001).

Brain volumes in RRMS patients are consistently lower than their healthy counterparts (Chard *et al.,* 2002a; Bermel *et al.,* 2003; De Stefano *et al.,* 2003; Lin *et al.,* 2003a). In early MS, volume loss appears once more to be most pronounced in GM (Tiberio *et al.,* 2005).

A number of studies have indicated a greater degree of atrophy in progressive MS patients than those with RRMS (Stevenson *et al*., 1998; Kalkers *et al.,* 2001; Lin *et al*., 2003a; Dalton *et al*., 2006; Fisher *et al.,* 2008; Fisniku *et al.,* 2008b). Some studies indicate a correlation between atrophy in SPMS and disability (Kalkers *et al*., 2001; Lin *et al*., 2003b; Fisniku *et al.,* 2008b; Fisher *et al.,* 2008). Taken together, these studies point to a considerable correlation between GM atrophy and disease progression and disability. Longer follow up studies of 5 years also indicate ongoing atrophy in patients with primary progressive MS, as measured by ventricular enlargement and cord cross sectional area, which was correlated with ongoing EDSS progression (Ingle et al., 2003).

Thus, using a number of volumetric measures, atrophy is demonstrable in the earliest stages of MS. Such atrophy has a moderate relation with disability progression and is the preferred method at present for monitoring neurodegeneration. It is therefore frequently used as an outcome measure in therapeutic trials within MS.

In a IFNβ trial of RRMS patients, brain volume was analysed 6 months prior to and 24 months after starting IFNβ. Reduction in brain volume weakly correlated with Gd lesions on the 6 months pre-treatment monthly scans. A weak association was also detected between disability and atrophy (Gasperini *et al.,* 2002). However, there was no difference in volume change between treatment groups. The finding of an association between disability and atrophy was in agreement with those of previous studies (Losseff *et al.,* 1996; Paolillo *et al.,* 1999).

Another 2 year trial examined the effect of IFNβ on the brain parenchymal fraction (BPF), a derived measure of the total volume of the brain, divided by the total intracranial volume. BPF decrease was noted to be smaller in the IFNβ arm in year 2 (Rudick *et al.,* 1999) but there was little correlation with lesion measures. An 8 year follow up of this study found that those with greater atrophy in the 1st 2 years were more likely to develop severe disability in the long term (Fisher *et al.,* 2002).

A trial of glatiramer acetate on 239 patients showed over 9 months a 0.7-0.8% reduction in central cerebral volume with no patient group differences (Rovaris *et al.,* 2001).

Overall, there is little evidence to suggest that any of the existing anti-inflammatory agents to date have a robust effect on volume change.

2.3.5 Detection of low grade BBB leakage

2.3.5.1 Evidence for BBB leakage in MS lesions

BBB disruption is evident in active lesions from visible Gd enhancement. In chapters 6 and 7 of this thesis, changes following the administration of triple dose Gd are studied to infer low grade BBB leakage in non- visibly enhancing lesions.

Tryptan blue dye injected supravitally has provided evidence of detectable BBB disruption, mainly in acute lesions, but also to a lesser degree in chronic lesions (Broman, 1964). Histological studies in the 1980's demonstrated perivenular fibrinous exudates and lymphocytic infiltration in acute and to a lesser extent chronic lesions, providing histological evidence of both widespread BBB leakage and inflammation in MS lesions (Adams *et al.,* 1985). In addition, the detection of extravascular deposits of fibrin in chronic lesions further support the presence of low grade BBB leakage in such lesions (Kwon *et al.,* 1994; Claudio *et al.,* 1995). An as yet unproven hypothesis is that low grade BBB disruption in non-visibly lesions could lead to the leakage of pathogenic mediators of tissue damage (e.g. inflammatory cytokines) that contribute to demyelination and axonal loss, and hence disability. It is therefore of interest and relevance to study low grade leakage in such lesions.

The use of Gd enhanced MRI studies to detect focal BBB disruption in new or actively inflamed MS lesions has been described previously.

Quantitative investigations, where the Gd mediated change is measured, could facilitate the detection of more subtle, low grade BBB leakage. Such studies have been performed in the ischaemic rat brain (Harris NG *et al.,* 2002) and intracranial tumours (Zhu *et al.,* 2000). Using the proportional change of T_1 weighted signal intensity as a marker for BBB leakage, Gd-DTPA enhanced studies on MS lesions have demonstrated subtle leakage from visibly non-enhancing lesions up to 40 minutes following the administration of Gd-DTPA. (Silver *et al.,* 2001b). This method has been adopted in

Chapter 6 of this thesis in which the effect of natalizumab, a VLA4 antagonist, on low grade BBB leakage was determined.

2.3.5.2 Using $\Delta R_1/\Delta t$ as an index of BBB leakage

Longitudinal relaxation rate (R_1), is the inverse of T_1. The change in R_1 following Gd administration, or ΔR_1, is described in the following equation:

$$\Delta R_1 = \frac{1}{T_1} - \frac{1}{T_{1(0)}} = r_1 C_t(t)$$

where
$C_t(t)$= local concentration of Gd at time *t* following its administration (mM)
T_1 = T_1 at the time *t* following Gd administration (s)
T_{10} = T_1 before Gd administration, or native T_1 (s)
r_1 is the relaxivity of Gd, a constant ($s^{-1}mM^{-1}$)

From in-vitro studies, r_1 for Gd- DTPA is estimated as 4.5 $s^{-1}mM^{-1}$ (Tofts and Kermode, 1991; Tofts *et al.,* 1999).

The gradient of ΔR_1 over time elapsed ($\Delta R_1/\Delta t$) is proportional to the change in local Gd concentration over time and can serve as a quantitative marker for BBB leakage which is more sensitive and potentially more reproducible than measuring change in T_1 weighted signal intensity *per se*. The usage of this marker to measure low grade leakage in RRMS and SPMS will explored in chapter 7 of this thesis.

2.4 Methods employed in analysis

2.4.1 Region of interest analysis

A region of interest (ROI) is a subset of pixels within the image defined by manually or automatically applied boundaries, and selected for further analysis. ROIs may be used to delineate MS lesions or anatomical structures (for instance deep gray matter).

The total volume encompassed within ROIs applied to MRI visible lesions can be calculated to infer a total MS lesion load. In addition, to look for changes over time, ROIs applied to an initial image can be re-applied to spatially registered successive images.

A semi-automated method is adopted in the delineation of lesions in this thesis (Plummer, 1992). This employs a local thresholding technique based upon local environmental intensity within the lesion. The operator places the cursor at or near the edge of the object of interest, from which an outline of the object is provided by adopting an algorithm based on locating, in successive iterations, the "strongest edge point", that is, the points representing the greatest change in intensity from one pixel to another. This approach provides an intra-rater coefficient of variation (CoV) of 2.5 ± 2.1 and inter-rater CoV of 4.5 ± 1.6. (Grimaud *et al.,* 1996)

2.4.2 Spatial Registration

Registration is the process in which electronic images are aligned with each other. In doing so, common features overlap and differences between images are readily identifiable and measurable. Intrasubject registration in longitudinal studies can help to overcome small positioning errors and allows comparison of images taken across a time interval. Across-subject (inter-subject) registration allows pooling of images from different subjects, such that group comparisons can be made.

Registration transforms an image (target image) such that it is spatially aligned with its counterpart (source/reference image). This spatial transformation may preserve the distance between all points within the image, known as rigid body registration, in which the target image is translated and rotated to best fit the the source image. Alternatively, it may allow for a global change of scale and shear, known as affine or non-rigid transformation. This latter form of registration more closely approximates the behaviour of biological systems, and is the form of registration adopted in the studies described in this thesis.

2.4.3 Segmentation

Segmentation is the process of dividing an image into distinct tissue segments, ie the GM, WM and CSF in the brain. Together with ROI based analysis, it facilitates more detailed study of specific brain segments, including analysis of segmental atrophy.

Automated approaches toward segmentation are favoured because of a high degree of reproducibility and reduced operator bias.

Segmentation of the brain into GM, WM and CSF is achieved in this thesis using statistical parametric mapping (SPM) (Ashburner and Friston, 1997; 2000). This employs a general linear model with Gaussian field theory to make inferences about regional effects. Brain tissue types are identified by intensity thresholding, and intensities are then remodelled by a mixture of K Gaussian distributions, parameterised by means, variances and mixing proportions. Segmentation is assisted by overlying probability maps derived from segmented images of healthy subjects assumed to be representative (Montreal neurological institute brain template). It is a process which requires initial registration of the images to standard space.

However, this approach may be affected by partial volume error interfering with the Gaussian distribution. Mis-registration with the prior probability images, based entirely on relatively young and healthy brains rather than on subjects with neurological disease can be another source of error. The segmentation is at risk of failing if the contrast in the relevant image is poor. Misclassification of lesions can also occur, and indeed often does unless additional lesion-masking strategies are employed (Chard *et al.,* 2002b).

Based on these potential pitfalls, the sequences that lend themselves the most to automated segmentation are high resolution, high contrast volumetric data sets, such as three dimensional IR prepared FSPGR. When SPM segmentation has been applied to these sequences, scan-rescan volume CoVs of 0.5%, 0.7% and 1.1% for brain parenchymal, GM and WM segments respectively have been achieved (Chard *et al.,* 2002b).

2.5 Summary

MRI is a sensitive and objective measure of evolving MS pathology in vivo, with the potential to reduce the number of patients required to demonstrate a treatment effect in drug trials. However, its applicability as a primary outcome measure in phase III trials is limited by the imperfect correlation with disability. Gd enhancement and T_2 lesion load reflect relapses and history of relapses, especially in early disease. T_1 lesion load – or at least its persistent, non-reversible component - may to an extent reflect accumulated disability from relapses. Volumetric measurements (extent and rate of atrophy) provide inferential information on myelin and axonal loss that may occur in parallel with clinical disease progression, although the sensitivity of such measures may be affected by fluctuations in inflammation. Quantitative measures of Gd enhancement provide a potentially useful tool to detect subtle BBB disruption, the significance of which is as yet uncertain.

CHAPTER 3

The Blood-brain barrier, α4β1 integrin and Natalizumab

3.1 The blood-brain barrier

3.1.1 Introduction and History

The BBB is an anatomical and biochemical barrier of the brain microvasculature, situated at the level of the endothelium. It serves to regulate the exchange of substances between the blood and the brain, and in doing so performs a protective function by controlling the influx of neurotransmitters and potential toxins from the blood.

The concept of the BBB first emerged with the discovery by Paul Ehrlich that aniline dyes injected intravenously stained somatic organs, but not the brain (Ehrlich, 1885). Shortly after, Lewandowsky postulated the existence of the BBB, or *bluthirnschranke,* while studying potassium ferrocyanide penetration into the brain (Lewandowsky, 1900). Edwin Goldmann, a student of Ehrlich, demonstrated that tryptan blue dye injected intrathecally stained the brain but not the somatic organs, providing further evidence for a barrier between the blood and the brain which was impermeable to all but small molecules (Goldmann 1914). Electron microscopic studies in the late 1960's and early 1970's demonstrated that intrathecally injected horseradish peroxidase, a substance to which the BBB is impermeable, traversed the astrocytic foot processes without crossing the endothelium, locating the BBB principally at the level of the endothelium.

(Brightman and Reese, 1969)

Because of the low permeability to charged particles, trans-endothelial electrical resistance is much greater across the BBB than across endothelium in somatic capillaries (Crone and Christensen, 1981; Crone and Olesen, 1982). Electrical resistance studies have been useful in determining the integrity of the BBB in endothelia *in vitro* and have been employed to study the development of the BBB in neonatal rats (Butt *et al.,* 1990)

3.1.2 Anatomy

The BBB is present in more than 99% of the capillaries of the brain (de Vries *et al.,* 1997), covering an enormous surface area of roughly 100- 180cm^2/g of brain tissue. In certain areas, it is replaced by a blood-CSF barrier, which, although more permeable than the BBB, still prevents the entry of many blood borne compounds into the CSF and hence the brain. This occurs in areas which serve a neurosecretory function, such as the posterior pituitary gland, and in areas which perform a chemoreceptive function, such as the circumventricular organs.

3.1.3 Constituents of the blood-brain barrier

A typical capillary in the brain consists of an endothelial layer, which, together with abluminal pericytes, is enveloped by a basement membrane, the basal lamina. Astrocytes communicate with this unit by astrocytic foot processes (FIG 3.1)

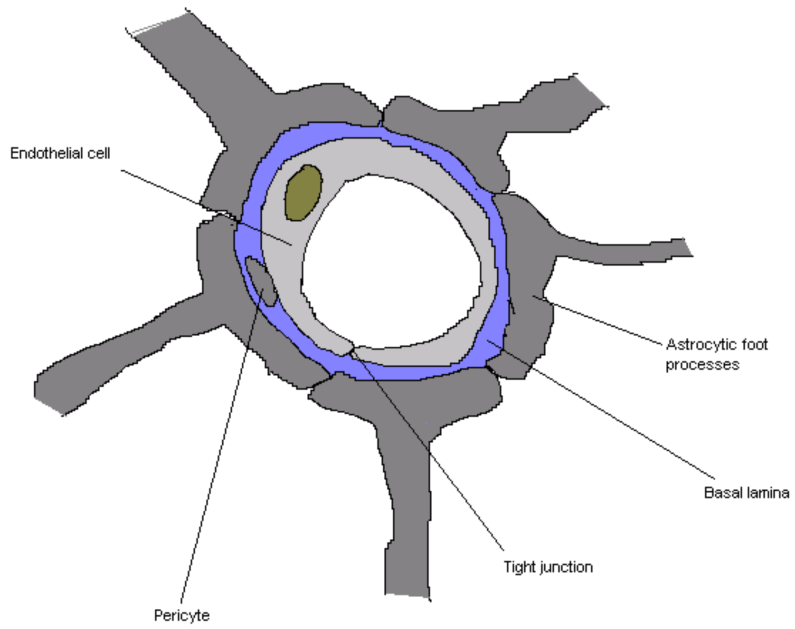

FIG 3.1 Schematic cross section of a brain capillary

3.1.3.1 Endothelium

The endothelium in a typical brain capillary differs from its somatic counterparts in a number of respects. They lack fenestrations (Fenstermacher *et al.,* 1988), which are trans-endothelial openings through which substances can flow. There is also a paucity of pinocytic vesicles (Coomber and Stewart, 1985; Sedlakova *et al.,* 1999), and a high concentration of mitochondria (Oldendorf and Brown, 1975; Oldendorf *et al.,* 1977), related to the large number of energy dependent transcapillary transport systems at the level of the BBB. The neutralisation of blood-borne substances which may interfere with normal brain function, such as catecholamines and other neurotransmitters, is carried out by the enzymatic barrier at the level of the endothelium (Minn *et al.,* 1991). The asymmetry in the luminal/abluminal distribution of the enzymes and channels such as Na/K ATPase results in the generation of a transendothelial polarity.

The most significant difference between endothelial cells in the brain and in the body is the abundance of transmembrane protein complexes which cause the adhesion of adjacent endothelial cells. These so-called junctional complexes were first described from electron microscopic studies on the rat and guinea pig (Farquhar and Palade, 1963). Junctional complexes form interconnected, intermembrane strands arranged as a series of multiple barriers to paracellular diffusion of molecules (Schneeberger and Karnovsky, 1976).

There are two main subtypes of junctional complexes: adherens junctions (zonula adherens) and tight junctions (zonula occludens).

Adherens junctions consist mainly of calcium dependent cell surface molecules known as cadherins. They are thought to play a role in the modulation of cell polarity, cell-cell interaction and paracellular permeability.

Tight junctions are the most abundant form of junctional complexes at the BBB, and together with the endothelial cell layer, form the anatomical basis of the BBB. *In vitro* studies on endothelial cell cultures demonstrated a reduction in permeability to sucrose associated with an induced increased expression of tight junctions (Romero *et al.,* 2003). In addition, horseradish peroxidase, a marker of BBB integrity, is stopped at the level of the tight junction (Sedlakova *et al.,* 1999).

Tight junctions consist of:

1. Junctional adhesion molecules: thought to mediate adhesion at cell apices and contribute to paracellular permeability

2. Occludins: which form the structural basis of tight junctions and which interact with the cytoskeleton via membrane associated guanylate kinase proteins

3. Claudins: which form strong homologous dimers with claudins on adjacent endothelial cells.

In addition to the junctional complexes, gap junctions exist between endothelial cells, which facilitate cell-cell communications (Bazzoni and Dejana, 2004)

3.1.3.2 Pericytes

Pericytes are located on the abluminal surface of the endothelium, and together with the endothelial layer are ensheathed by the basement membrane. They are thought to facilitate endothelial-astrocyte interaction (Ramsauer *et al.,* 2002). *In vitro* studies (Hori *et al.,* 2004) also indicate that pericytes stimulate the manufacture of occludin, a constituent protein in tight junctions. Finally, evidence of the contractile protein α actin in pericytes *in vitro* (Bandopadhyay *et al.,* 2001) also suggests an additional role for pericytes which is not dissimilar to that of smooth muscle in larger blood vessels.

3.1.3.3 Basal Lamina

The basal lamina is the extracellular matrix on the abluminal surface of the endothelium. It is trilaminar in structure, with an endothelial layer (lamina rara interna), an astrocytic layer (lamina rara externa) and an intermediate layer consisting mainly of the structural constituent, collagen type IV. It provides physical support to microvessels, and provides the anchor for endothelial cells via the interaction of proteins intrinsic to the basal lamina such as laminin and integrin receptors on endothelial cells (Hawkins BT *et al.,* 2005). Proteins found in basal lamina also modulate the expression of occludin in endothelial cells (Savettieri *et al.,* 2000) and can stimulate high electrical resistance in endothelial cells *in vitro* (Tilling *et al.,* 1998). The basal lamina also filters macromolecules and therefore affords a degree of protection to the brain against extravasated proteins.

3.1.3.4 Astrocytes and Neurons

Astrocytes belong to a subgroup of glial cells, which have a star-shaped morphology. They are characterized by long processes which form close apposition with synapses and blood vessels. The proximity of astrocytic foot processes with brain microvasculature is thought to induce BBB characteristics in the endothelium (Stewart and Wiley, 1981; Tao-Cheng *et al.,* 1987, *Neuhaus et al.,* 1991*).* In addition, their continued association with endothelial cells is necessary for the maintenance of the BBB phenotype, with the injection of gliotoxic substances causing a consequent BBB breakdown (Bondan *et al.,* 2002). Astrocytes are thought to induce changes in endothelium through secreted factors (Maxwell *et al.,* 1987), possibly through substances such as nitric oxide, endothelin and TNF α (Abbott *et al.,* 2006).

Although the interaction between neurons and the microvasculature is less well understood than that of astrocytes, there is evidence of direct innervation of the neurovasculature (Cohen *et* al., 1997; Tong and Hamel, 2000; Vaucher *et al.,* 1997). However, the significance of the role of neurons in inducing or maintaining the integrity of the BBB is unclear.

3.1.4 Transport across the BBB

The controlled transit of substances across the BBB between the brain parenchyma and blood is essential for normal brain function. This is achieved by a variety of mechanisms, depending on the fat- solubility of the substance in question.

Efficient exchange of lipid soluble gases such as O_2 and CO_2 occurs through direct diffusion across the BBB, driven by concentration differences between brain and blood. The permeability coefficient of the BBB for many substances is directly proportional to the lipid solubility of the substance.

For water soluble, or lipophobic molecules, transport across the BBB occurs through specific carrier-mediated transport systems. For instance, glucose is transported primarily through the GLUT1 transport system. Three distinct carrier systems exist for the transport of amino acids. These are the L, A and ASC systems, each system transporting a different set of amino acids depending on the polarity and size of the amino acids concerned. MDR transmembrane proteins, or P-glycoproteins, are thought to be involved in the expulsion of harmful substances, and MDR deletion mice are more sensitive to circulating neurotoxins such as ivermectin (Schinkel *et al.,* 1994). Electrolyte balance and trans-BBB polarity is maintained by specific ion channels and transporters, especially a high concentration of Na/K ATPase exchange transporters on the abluminal surface of the endothlial layer.

3.1.5 Pathological BBB disruption

Besides BBB disruption in MS, BBB disruption also occurs in a wide range of conditions, as listed below.

- Tumours (Davies, 2002)
- Trauma (Povlishock *et al.,* 1978)
- Infection (Clawson *et al.,* 1966)
- Ischaemic Injury (Kuroiwa *et al.,* 1988)
- Alzheimer's Disease (Berzin *et al.,* 2000)
- Epileptic seizures (Cornford and Oldendorf, 1986)
- Diabetes Mellitus (Mooradian, 1997)

Hypoxia induces BBB leakage (Kempski, 2001; Witt *et al.,* 2003), and vasogenic oedema frequently follows ischaemia-reperfusion events. A number of possible mechanisms for BBB disruption in hypoxia have been proposed, including tight junction disruption (Mark and Davis, 2002; Fischer S *et al.,* 2002) and increased transcellular pathways (Cipolla *et al.,* 2004; Plateel *et al.,* 2004). Also thought to be involved in the process are nitric oxide (Mark *et al.,* 2004) and vascular endothelial growth factor (VEGF) (Fischer S *et al.,* 2002). Co-culture with astrocytes and pericytes has been observed to ameliorate the effects of hypoxia on BBB disruption (Abbruscato and Davis, 1999; Fischer S *et al.,* 2000; Hayashi *et al.,* 2004). In this respect, astrocytes and pericytes may play a protective role against hypoxic insult.

BBB disruption is also well recognised in the two commonest intracranial malignancies: high grade gliomas and metastatic adenocarcinoma. BBB leakage in these circumstances leads to the vasogenic oedema which contributes to the morbidity and mortality associated with these tumours. Microvessels in metastatic adenocarcinomas are phenotypically similar to vessels in the tissue from which the tumours are derived. They therefore do not form as many tight junctions as are observed in cerebral microvessels (Long, 1979).

The mechanism for the breakdown of the BBB in gliomas is less certain. One possibility is that the loss of differentiation in glial cells causes a disruption of the secretion of factors necessary to maintain the BBB. An alternative explanation is that gliomas display accelerated angiogenesis associated with high levels of VEGF (Davies, 2002).

Disruption of the BBB also appears to occur in sepsis, as evidenced by the increased passage of albumin through the BBB in rats treated with endotoxin (Deng *et al.,* 1995). Microscopically, BBB of disruption in sepsis is associated with swelling of astrocytic end feet, neuronal degeneration and microvessel oedema (Papadopoulos *et al.,* 1999).

3.1.5.1 BBB disruption in MS

The existing evidence for BBB disruption in acute and, to a lesser extent, chronic MS lesions has been discussed in chapter 2. Breakdown of the BBB is most dramatic in the early stages of lesion formation, although histological and limited radiological evidence exists for persisting BBB leakage in more long-standing and (on MRI) visibly non-enhancing lesions. The following section will focus on postulated mechanisms governing BBB breakdown in acute and chronic lesions in MS

3.1.5.1.1 BBB breakdown in acute lesions

Histological studies on active MS lesions reveal the presence of local oedema, lymphocytic infiltration and extravascular fibrin deposition (Adams *et al.,* 1985), all indicative of a breakdown of the BBB. Gd-enhanced MRI studies indicate that BBB disruption is a consistent finding in new or actively inflamed lesions. (Bruck *et al.,* 1997; Grossman *et al.,* 1986; Katz *et al.,* 1993; Miller DH *et al.,* 1988; Lai *et al.,* 1996) Disruption of tight junctions in vessels within acute lesions has also been demonstrated in confocal laser microscopic studies (Plumb *et al.,* 2002).

BBB breakdown in acute lesions is thought to result from the migration, proliferation and activation of leucocytes, with consequent cytokine release. (Minagar and Alexander, 2003). Cytokines and oxidants compromise the BBB by the phosphorylation of occludin and associated proteins, causing dissociation from the cytoskeleton and tight junction breakdown. *In vitro* studies indicate that chronic exposure of endothelium to cytokines involved in the T_h1 immune response (central in the acute inflammatory process in MS) is associated with reduced tight junction expression and trans-endothelial resistance (Oshima *et al.,* 2001; Minagar *et al.,* 2003). This process was ameliorated if the endothelium was pre-treated with IFN-β (Minagar *et al.,* 2003).

VEGF may also contribute to BBB breakdown in acute lesions. Elevated levels of VEGF have been found in MS plaques, and the administration of VEGF to myelin basic protein sensitized rats is associated with an increase in EAE plaques (Proescholdt *et al.,* 2002), although a similar reaction is not observed in non-sensitized rats, suggesting that VEGF can amplify the inflammatory process and associated BBB breakdown, but is not on its own sufficient to trigger disease.

3.1.5.1.2 BBB breakdown in non-active and more longstanding MS lesions

Confocal laser microscopy studies provide evidence of abnormal tight junctions in lesions which do not show evidence of active inflammation (Leech *et al.,* 2007). In addition, extravascular fibrin deposits are found in chronic, non-active MS lesions, (Claudio *et al.,* 1995; Adams *et al.,* 1985; Kwon and Prineas, 1994). Taken together, these studies provide histological evidence of BBB disruption in such lesions. Vessels in non-active lesions often exhibit reparative wall thickening in concert with fibrin deposition, (Adams *et al.,* 1985) suggesting that leakage from these lesions might at least in part be due to incomplete BBB repair, with some permanent structural and functional changes following resolution of inflammation. Supporting this hypothesis are findings from morphometric analysis of capillaries in non-active MS lesions, which have demonstrated a reduction in mitochondria and a rise in pinocytic vesicles, in concert with evidence, in terms of extravascular fibrin deposits, of BBB disruption. (Claudio *et al.,* 1995) Such findings imply a shift in the physiology of these vessels to a more energy deficient state, hindering the energy dependent transport mechanisms essential in maintaining the BBB. It is conceivable that such changes could contribute to the low grade BBB leakage detected in chronic MS lesions.

3.2 $\alpha 4\beta 1$ integrin and other molecules involved in the MS inflammatory process

The following sections give a brief description of some of the key molecules contributing to leucocyte adhesion and activation. In particular, very late antigen-4 (VLA-4), or $\alpha 4\beta 1$ integrin, which mediates the adhesion of leucocytes onto the endothelial wall and subsequent trans-BBB migration.

3.2.1 Cell adhesion molecules

Cell adhesion molecules are a diverse group of cell-surface and extracellular glycoproteins which are involved in cell-cell or cell-matrix interaction, adhesion, and cell recognition. They consist of 4 classes of molecules: selectins, cadherins, integrins and members of the immunoglobulin superfamily, including inter-cellular adhesion molecule 1 (ICAM-1) and vascular cell adhesion molecule 1 (VCAM-1)

Selectins are molecules expressed on leucocytes (L-selectin) and endothelial cells (P-selectin). They have a lectin-like domain, and are involved in the initial contact between leucocyte and endothelium in leucocyte adhesion.

Cadherins are calcium dependent cell adhesion molecules which form homophilic bonds to other cadherins. They form a major constituent of the previously mentioned intercellular adherens junctions.

Integrins are integral membrane proteins involved in cell signalling and interaction between cells or between the cell and the extracellular matrix. Integrins are heterodimers, consisting of an α and a β subunit. Cell signalling following contact with ligand is mediated through protein kinase. Integrins which contain the $\alpha4$ subunit are expressed on most leucocytes, with the exception of neutrophils. $\alpha4$ dimerises with either $\beta1$ or $\beta7$ (Rice *et al.,* 2005). $\alpha4\beta1$ integrin plays an important role in the adhesion and migration of leucocytes across the BBB, whereas $\alpha4\beta7$ facilitates the migration of leucocytes across the intestinal mucosa. $\alpha4$ integrin blockage is the probable mechanism of the therapeutic trial agent reported in this thesis.

$\alpha4\beta1$ integrin interacts principally with the immunoglobulin VCAM-1. VCAM-1 is expressed on activated endothelial cells and in astrocytes in response to cytokines (Rosenman *et al.,* 1995; Lee and Benveniste, 1999). The VCAM-1-$\alpha4\beta1$ interaction is thought to underlie many of the processes in leucocyte adhesion, migration and activation within the context of MS.

Fibronectin and osteopontin also form ligands for interaction with $\alpha4\beta1$.

Fibronectin is abundant in the extracellular matrix (Guan and Hynes, 1990) and plays important roles in cell adhesion, migration, growth and differentiation (Pankov and Yamada, 2002). CD3 mediated proliferation of T-cells is co-stimulated by concurrent interaction between fibronectin and the integrins VLA-4 ($\alpha4\beta1$) and VLA-5 (Shimizu *et al.,* 1990).

Osteopontin is a matrix protein that has both adhesive and Th-1-like cytokine activity. Osteopontin cDNA is found in higher levels in MS plaques and in mice with EAE (Chabas *et al.,* 2001). Mice deficient in osteopontin exhibit a relative resistance to EAE.

3.2.2 Chemokines and matrix metalloproteinases

Chemokines are 8-10kDa proteins secreted by activated macrophages and microglia. They consist of 4 subfamilies: α,β,δ, and γ, and can be divided broadly into inflammatory and homeostatic chemokines. Whereas homeostatic chemokines are constitutively expressed and can play roles in neuronal migration and synaptic modulation, inflammatory chemokines are are secreted in response to cytokines, and modulate the interaction between endothelial cells and leucocytes. Inflammatory chemokines from the α subfamily affect T-cells and those from the β subfamily affect monocytes/macrophages. Both these classes of chemokines have been reported to be raised in MS (Trebst *et al.,* 2003) and are thought to convert the leucocyte- endothelial cell interaction from one of low affinity (selectin mediated) to high affinity (integrin mediated) (Minagar and Alexander, 2003)

Matrix metalloproteinases are Zn dependent peptidases which degrade protein components of extracellular matrix. These molecules, especially MMP9, are implicated in MS. Elevated levels of MMP7 and MMP9 are found in MS lesions (Cossins *et al.,* 1997; Maeda and Sobel, 1996), and lesion formation is frequently preceded by increase in the serum level of MMP9 (Waubant *et al.,* 1999). IFNβ appears to reduce the level of MMP9 (Trojano *et al.,* 1999)

3.2.3 Overview of the role of $\alpha 4\beta 1$ in cell adhesion and BBB breakdown

Inflammation within the acute MS plaque is a process that is thought to be driven primarily by Th1 cytokines such as IL1-b, IL6, IFNγ and TNFα (Dettke *et al.,* 1997; Beck J *et al.,* 1998). It is thought that the presence of such cytokines activates endothelial cells, with increased expression of MHC II molecules (van der Maesen *et al.,* 1999) and cell adhesion molecules such as VCAM-1 and E-selectin (Pober *et al.,* 1986; Dustin *et al.,* 1986; Dore-Duffy *et al.,* 1993).

Activated endothelium also releases cell adhesion molecules such as VCAM-1 and platelet endothelial cell adhesion molecule (PECAM-1) into the circulation in vesicles called endothelial microparticles. Serum levels of cell adhesion molecules have been correlated with markers of disease severity in MS, including the presence of Gd-enhancing lesions (Giovannoni *et al.,* 1997; Hartung *et al.,* 1995) and relapses (Rieckmann *et al.,* 1994). In addition, high levels of ICAM and TNF have been reported in CSF in patients with relapses (Tsukuda *et al.,* 1993)

The expression of adhesion molecules by activated endothelium is reduced in the presence of steroids (Elovaara *et al.,* 1998) and IFNβ (Jimenez *et al.,* 2005)

The interaction between activated endothelium and leucocytes appears to occur in several stages (Butcher, 1991), with the initial contact being mediated principally by selectins and their respective carbohydrate ligands, resulting in the slowing, or tethering of the leucocyte (Engelhardt and Ransohoff, 2005; Carrithers *et al.,* 2000*)*.

Subsequent ‘rolling’ of the leucocyte along the endothelial surface is facilitated by the interaction between α4β1 integrin and VCAM-1, as well as selectins and their ligands. (Piccio *et al.,* 2002; Carvalho-Tavares *et al.,* 2000; Kerfoot and Kubes, 2002). It is thought that rolling brings chemokines on the endothelial surface into proximity with their respective ligands on the leucocyte, and their interaction initiates a G- protein linked signal within the leucocyte (Piccio *et* al., 2002, Vajkoczy *et al.,* 2001). This results in the activation of integrins expressed on the leucocyte, which facilitates much higher affinity binding between α4β1 and its ligand VCAM-1.

The high affinity binding leads to the arrest of the leucocyte and is known as adhesion. Leucocyte adhesion can be inhibited by antibodies directed against VCAM-1 (Bochner *et al.,* 1991) or α4 integrin (Vajkoczy *et al.,* 2001). A similar adhesion to cytokine-activated endothelium was demonstrated in cells transfected with α4β1 cDNA, a process inhibited once more with antibodies directed against α4 (Elices *et al.,* 1990).

The leucocyte then travels across the BBB, a process known as diapedesis. In the inflamed vessel, the leucocyte adopts both transcellular and paracellular routes (Engelhardt and Ransohoff, 2005; Carman and Springer, 2004), and the process involves other adhesion molecules such as ICAM-1, the integrin Lymphocyte Function Associated Antigen 1(LFA-1) (Laschinger *et al.,* 2002), and monocyte chemoattractant protein-1 (MCP-1) (Weiss *et al.,* 1998) which is expressed on activated astrocytes.

The α4β1-VCAM-1 interaction plays a role in the migration of the leucocyte in the extracellular matrix, most probably through the stimulation of production of the matrix metalloproteinase MMP2 (Madri *et al.,* 1996).

The α4β1-VCAM-1 interaction is also implicated in T-cell proliferation (Burkly *et al.,* 1991; Damle and Aruffo, 1991) and activation (Damle and Aruffo, 1991), in concert with stimulation by locally produced chemokines and cytokines.

Human umbilical vein endothelium expresses VCAM-1 when stimulated with TNF-α. The resultant adherence of lymphocytes is inhibited by VCAM-1 blockade (Carlos *et al.,* 1990)

Evidence that α4β1 integrin plays a role in the pathogenesis of EAE comes indirectly from the finding that encephalitogenic clones from a Th1 cell line had a 10-fold greater surface expression of α4β1 integrin than non-encephalitogenic variants. (Baron *et al.,* 1993) It was also observed, by the same group, that α4β1 positive cells readily crossed the BBB to enter the brain parenchyma in EAE mice, whereas no such migration was observed in α4β1 negative cells. Administration of antibodies to VLA-4 and VCAM-1 hampered the transmigration of leucocytes. The finding that antibodies to α4 integrin can induce a protein kinase dependent apoptosis of CD4 and CD8 cells in mice (Tchilian *et al.,* 1997) and subsequently in Lewis rats (Leussink *et al.,* 2002) might point to an additional role for α4 integrin in the prolongation of the lifespan of inflammatory cells and the prolongation of the inflammatory process itself.

Antibodies to α4 integrin inhibit adhesion of leucocytes onto endothelium in EAE mice (Yednock *et al.,* 1992). In addition to this, the administration of anti-α4 prevents the development of EAE in mice following the injection of encephalitogenic T-cells

(Brocke *et al.,* 1999).

There is considerable evidence that antibodies directed against α4 integrin ameliorate the clinical (Yednock *et al.,* 1992; Van der Laan *et al.,* 2002; Soilu- Hanninen *et al.,* 1997), MRI (Kent *et al.,* 1995a) and pathological (Kent *et al.,* 1995b) changes seen in EAE. Conversely, a study on EAE mice appeared to indicate that the effect of anti−α4 was dependent on the timing of its administration; anti-α4 administered after the peak of EAE or in remission appeared to exacerbate disease (Theien *et al.,*2001) . The findings from this study suggest that the role of α4 integrin in EAE might be a complex one. However, the findings have not been replicated in further animal or human studies.

Anti-α4 also exerts its action on pathways mediated by α4β7, an integrin which is involved in the trafficking of leucocytes across the gastrointestinal mucosa. Studies with the cotton top tamarin, a new-world monkey that has spontaneous colitis, show a limited benefit from treatment with anti α4 (Podolsky *et al.,* 1993).

3.3 Natalizumab

Natalizumab is a humanized anti α4 antibody made from by grafting the complementarity determining region of the murine antibody AN100226m onto an inert human IgG_4 frame (Leger *et al.,* 1997). The grafting to the human IgG frame reduces immunogenicity and improves half life *in vivo*. Natalizumab and AN100226m have nearly identical binding affinities to α4 integrin. Natalizumab appears to follow linear kinetics over a wide range of body weight, and is relatively fat insoluble. Natalizumab has a reported pharmacological half life of 11 days in healthy volunteers (Cada *et al.,* 2005), a shorter half life of 4.8 days has been reported on patients with Crohn disease. (Gordon *et al.,* 2001). 80-90% saturation of α4β1 integrin receptors can be achieved with 3 - 6mg/kg monthly injections (Miller DH *et al.,* 2003).

3.3.1 The use of Natalizumab in MS trials

An early phase II trial involving 72 patients in a single centre examined the effect of two doses of 3mg/kg natalizumab given a month apart on MRI markers of MS. (Tubridy *et al.,* 1999). This demonstrated a 50% reduction in Gd enhancing lesions in the first 12 weeks of the trial, which was not sustained in the second 12 weeks of the trial, with no significant difference in the number of relapses for the period of observation (6 months). A raised lymphocyte count was observed in the treatment group in the first 12 weeks of the trial, and 11% of patients in the treatment group developed antibodies to natalizumab. .

The results of the initial trial provided the impetus for the conduct of a proof of concept phase IIb multicentre trial, examining the effect of natalizumab on patients with RRMS or SPMS with superimposed relapses (Miller DH *et al.,* 2003). Two hundred and thirteen patients were involved in the trial, and patients were randomized to receive placebo, natalizumab 3mg/kg and 6mg/kg. They received monthly injections for 6 months and had a follow-up period of a year. Natalizumab was found to markedly reduce the number of new Gd enhancing lesions (9.6 in the placebo group as opposed to 0.7 in the 3mg/kg group and 1.1 in the group receiving 6mg/kg) and the number of persistent Gd enhancing lesions (3.6 in the placebo group vs 0.8 in the 3mg/kg group and 1.3 in the 6mg/kg group), with a reduction in relapse rate of 50%, and no significant treatment difference seen in the 2 dosage groups. Adverse events were similar in all 3 arms. A lymphocytosis in the treatment arms, similar to that seen in the previous trial (Tubridy *et al.,* 1999)

A substudy of the above trial demonstrated that administration of natalizumab also influenced the evolution of Gd enhancing lesions into T_1 hypointense lesions, which are generally associated with greater axonal damage and extracellular matrix disruption. Administration of natalizumab was associated with an odds ratio of conversion to T_1 hypointense lesions of roughly 0.5, (Dalton *et al.,* 2004a). This finding suggests that in addition to suppressing the formation of new lesions, natalizumab ameliorates destructive $\alpha 4\beta 1$ mediated processes once inflammation has started.

Based on the results of the phase IIb proof of concept study, two further placebo-controlled phase III trials were organised.

The first such phase III placebo controlled trial (AFFIRM) compared the use of monthly administration of natalizumab as monotherapy against placebo in 942 patients over two years. Natalizumab was associated with a 68% reduction in relapse rate and a 42% reduction in disability progression when compared against placebo (Polman *et al.,* 2006). The use of natalizumab was also associated with a significant reduction in MRI markers of disease activity and severity (Miller DH *et al.,* 2007). This will be described in more detail in chapter 4 of this thesis.

The second phase III trial (SENTINEL) recruited patients who were already receiving

IFNβ-1a (avonex) but had experienced at least one documented relapse in the previous year. This study compared the use of IFNβ-1a and placebo against the combination of IFNβ-1a and natalizumab in 1171 patients. The use of IFNβ-1a – natalizumab combination resulted in significant reductions in relapse rate and disability progression when compared against the group receiving IFNβ-1a and placebo (Rudick *et al.,* 2006).

Patients from the two aforementioned phase III trials were also tested for visual acuity and the ability to distinguish letters of low contrast. Natalizumab was associated with a reduction in risk of low level visual loss in both these trials (Balcer *et al.,* 2007)

Another randomized multi-centre placebo controlled trial of natalizumab investigated the effect of a single dose given during acute relapse on relapse outcome. (O' Connor *et al.,* 2004). The study was based on the principle that the reduced trafficking of leucocytes across the BBB into the brain parenchyma may shorten the period of lesion inflammation and therefore improve outcomes from relapses. Patients who had developed relapse symptoms in the preceding 24 to 96 hours were recruited into the study, received a single intravenous infusion of agent, and were then followed up for 14 weeks. Although the treatment cohort had an overall smaller volume of Gd enhancing lesions than those receiving placebo after 14 weeks, no significant difference in the change in clinical relapse outcome was detected between the treatment groups.

3.3.2 The use of natalizumab in treatment trials of Crohn's disease

As natalizumab is directed against the α4 component of the integrin subtype α, it was postulated that it would exhibit efficacy in antagonising α4β7, an integrin involved in the migration of leucocytes in Crohn's disease. Animal studies supported this postulate, with anti α4 ameliorating the symptoms of colitis in golden top tamarin monkeys (Podolsky *et al.,* 2003). In controlled clinical trials in Crohn disease, natalizumab has been associated with modest improvements in clnical indices (Sandborn *et al.,* 2005) and in remission and response rates (Ghosh *et al.,* 2003)

3.3.3 Adverse effects of natalizumab

Natalizumab appeared on the whole to be fairly well tolerated, with generally similar rates of adverse events between natalizumab and treatment groups, in the phase II clinical trials (Keeley *et al.,* 2003; Miller DH *et al.,* 2003;). In the phase III treatment trial of natalizumab monotherapy against placebo, fatigue and hypersensitivity were found to be more frequent in the natalizumab treated group (Polman *et al.,* 2006). Postmarketing reports of clinically significant liver injury have recently been made, (Food and Drug Administration, 2008), with a recommendation to discontinue natalizumab in the presence of clinical or laboratory evidence of hepatic derangement.

A number of cases of progressive multifocal leukoencephalopathy (PML) have been reported on patients receiving natalizumab (Kleinschmidt-DeMasters and Tyler, 2005; Langer-Gould *et al.,* 2005; Van Assche *et al.,* 2005; Hartung, 2009). PML is a potentially fatal glial infection by the polyoma JC virus. The emergence of PML, which is usually seen in immunocompromised patients, was an unexpected consequence of the drug. A retrospective study conducted of 3417 patients exposed to the agent to date estimated an annual risk of 1.0 per 1000 patients, with necessarily wide confidence intervals (0.2 to 2.8 per 1000) given the paucity of available data. (Yousry *et al.,* 2006)

It is not known exactly how treatment with natalizumab gives rise to PML. It has been suggested that natalizumab interferes with the normal ingress of lymphocytes into the nervous system and compromises the normal immune surveillance, allowing unchecked replication of JC virus (Berger and Koralnik, 2005). CSF studies on patients receiving natalizumab reveal a marked reduction in leucocyte counts which persists up to 6 months after the discontinuation of the drug (Stuve *et al.,* 2006).

The first reported cases of PML emerged after more than 2 years of otherwise uneventful exposure to natalizumab. This late emergence of a serious adverse event underlines the need for long term careful and sustained follow-up in the monitoring of patients who are receiving new treatments for which previous long term data is lacking.

Thesis outline

This thesis describes the imaging results of the trial of an agent that acts at the level of the BBB by blocking $\alpha 4$ integrin, and in doing so investigates the role of the BBB in the pathogenesis of MRI-measured disease activity in MS.

Chapter four reports the main MRI outcomes in the phase III placebo-controlled trial of natalizumab in relapsing MS (AFFIRM). 942 patients participated in the trial, whose MRI outcomes included the number of new Gd enhancing lesions, new or enlarging T_2 lesions, and new T_1-hypointense lesions. Lesion volumes were also studied. In addition, the ratio of volume between T_1-hypointense lesions and T_2 lesions was studied to ascertain whether natalizumab influenced the formation of T_1 hypointense lesions *per se*.

The subsequent two chapters describe substudies of the AFFIRM trial which employed additional MRI measures to assess the effect of natalizumab therapy on segmental brain atrophy (Chapter five) and on low grade BBB leakage, inferred by measuring T_1 weighted signal change after administration of triple dose Gd (Chapter six).

In chapter five the effect of natalizumab on segmental atrophy in a patient population of fifty-seven patients was investigated. GM and WM segments were obtained from 3D volumetric scans taken at baseline, year 1 and year 2 using an automated segmentation procedure. GMF, WMF and BPF were then calculated as a fraction of total intracranial volume. Correlations between atrophy measures and measures of disability as well as lesion load were sought.

Chapter six describes a further substudy of the AFFIRM trial involving 40 patients, in which low grade BBB leakage from visibly non-enhancing lesions was investigated by studying T_1 weighted signal intensity change following the administration of triple dose Gd. Leakage was compared between patients receiving natalizumab vs placebo, leakage was also compared between T_1 hypointense and T_1 isointense lesions.

Chapter seven describes a pilot study of a non-trial MS cohort (19 patients, 10 RRMS and 9 SPMS) wherein the post-Gd change in the $1/T_1$ (ΔR_1) is used to infer BBB leakage in visibly enhancing and visibly non-enhancing lesions. ΔR_1 represents a more reproducible and potentially more sensitive marker of subtle BBB disruption. Comparisons were made between disease subtypes and lesion types. A number of patients who participated in the study were receiving disease modifying therapy, either IFNβ or glatiramer acetate. This allowed for the investigation of possible effects of these agents on subtle BBB permeability. Correlations were also sought between inferred BBB disruption and disability.

CHAPTER 4

MRI results from a phase III trial of natalizumab vs placebo in subjects with relapsing MS

4.1 Introduction

4.1.1 α4β1 integrin and lesion formation in multiple sclerosis

The role of α4β1 integrin in the formation and continued activity of MS lesions has been described at length in chapter 3. α4β1 integrin, through its interaction with its principal ligand VCAM1, and to a lesser extent with its supplementary ligands osteopontin and fibronectin, plays an integral role in leucocyte adhesion (Yednock *et al.,* 1992; Bochner *et al.,* 1991; Elices *et al.,* 1990; Carlos *et al.,* 1990), intraparenchymal activation (Damle and Aruffo, 1991), migration (Madri *et al.,*1996) and proliferation (Burkly *et* al., 1991). Antibodies directed against α4β1 integrin ameliorate disease progression in animal models of MS (Yednock *et al.,*1992; Kent *et al.,* 1995b)

Limited Phase I and II clinical trials of natalizumab versus placebo have demonstrated the efficacy of the agent in reducing relapse rates and disease progression (Miller DH *et al.,* 2003; Tubridy *et al.,*1999). Over a period of 6 months, the use of natalizumab was associated with a 90% decrease in the number of Gd enhancing lesions (Miller DH *et al.,* 2003). Further analysis of the trial data has demonstrated that the use of natalizumab is associated with a reduced likelihood of new lesions evolving into T_1-hypointense lesions (Dalton *et al.,* 2004a) a subset of lesions associated with a greater degree of axonal loss and demyelination and disability (van Waesberghe *et al.,* 1999; Barkhof *et al.,* 2003; Truyen *et al.,* 1996).

4.1.2 Phase III clinical trials involving natalizumab

The results of the clinical trials described in the previous section provided the impetus for 2 large, randomized multi-centre placebo controlled trials involving either natalizumab as monotherapy (AFFIRM trial) (Polman *et al.,* 2006; Miller DH *et al.,* 2007) or in combination with IFNβ−1a (SENTINEL trial) (Rudick *et al.,* 2006). These trials provided the opportunity to determine if the natalizumab-mediated effects seen in the previous trials were sustained over 2 years.

The primary clinical efficacy end points in the trials were the clinical relapse rate at 1 year, and cumulative probability of sustained disability progression at 2 years, defined as an EDSS progression of 1, or (if baseline EDSS was 0) of 1.5 with no improvement over 12 weeks. The trials demonstrated that natalizumab as monotherapy was associated with a 68% reduction in annualised relapse rate and a 42% reduction in sustained disability progression when compared against placebo (Polman *et al.,* 2006), and natalizumab in combination with IFNβ-1a was associated with a significant reduction in annualised relapse rate (54% in the 1st year and 55% in the 2nd year) and a 24% reduction in disability progression compared with IFNβ −1a alone in subjects who had previously had a limited response to IFNβ-1a. This chapter will describe the methodology and results of the MRI scans that were obtained in the natalizumab monotherapy (AFFIRM) trial.

4.2 Methods

4.2.1 Trial Design

The study was a multi-centre, randomized, double-blind, placebo controlled, parallel group treatment trial. The protocol was developed by the trial sponsors (Biogen Idec and Elan) and a central investigator advisory committee, and was approved by central and local ethics committees.

4.2.2 Recruitment

942 subjects from 99 centres in Europe, North America, Australia and New Zealand were recruited into the study. Informed consent was obtained from each subject participating in the trial. Criteria for trial participation are described in FIG 4.1.

Inclusion Criteria

1. Diagnosis of Relapsing MS, as according to 2001 McDonald Criteria (McDonald *et al.,* 2001)

2. Age between 18 and 50, inclusive

3. EDSS between 0 and 5.0 inclusive

4. One or more documented relapse in the 12 months prior to randomization

5. Cranial MRI demonstrating changes consistent with MS

6. Provision of written informed consent for participation in the study

Exclusion Criteria

1. Primary Progressive, Secondary Progressive or Relapsing Progressive MS (Lublin and Reingold, 1996)

2. Documented MS relapse within 50 days prior to randomization

3. Clinically significant infectious illness within 30 days prior to randomization.

4. Abnormal investigation results suggestive of condition that may preclude administration of agent

5. Abnormal blood tests at the screening visit as defined below:

    a) Alanine transaminase or aspartate transaminase > 3 times upper limit of normal.

    b) Total white blood cell count < 2,300/mm3.

    c) Platelet count < 100,000/mm3.

    d) Creatinine > 2 times upper limit of normal

    e) Prothrombin time > Upper imit of normal

6. History of severe allergic or anaphylactic reactions or known drug hypersensitivity.

7. Unable to perform MSFC

8. Prior treatment with

    a) cladribine

    b) any monoclonal therapeutic antibody

    c) total lymphoid irradiation

    d) T-cell receptor vaccination

FIG 4.1 Inclusion and exclusion criteria for trial entry

4.2.3 Randomization

Subjects were randomized during the baseline visit to receive infusions of either natalizumab 300mg or placebo every 4 weeks up to 116 weeks at a ratio of 2:1 (ie, twice as many subjects receive natalizumab than placebo) Randomization was stratified by centre, using a centralized computer-generated block randomization schedule to balance treatment group assignments within centres. Subjects and study personnel were blinded to treatment assignment.

4.2.4 MRI protocol

Each participating centre designated a specific MRI technician who was responsible for the site-specific implementation of the trial MRI protocol. These scans were undertaken at baseline, year 1 and year 2 of the study as according to a standard acquisition protocol which defined allowable ranges for all scanning parameters. The protocol consisted of (i) PD/T_2-weighted FSE (TR = 2000 to 3200 ms; TE = 20 to 50 ms [short] / TE = 80 to120 ms [long]); (ii) pre- contrast T_1-weighted SE (TR = 500 to 600 ms; TE = 10 to 20 ms); (iii) IV injection of 0.1 mmoL/kg of a Gd-chelated MRI contrast agent; (iv) post- contrast T_1-weighted SE starting 5 minutes after the injection of contrast. The slice thickness was 3 mm and the matrix size was 256 x 256, with contiguous oblique-axial plane slices (parallel to the line joining the anterior and posterior commissures) being obtained through the entire brain. Repositioning of follow-up scans was achieved using a protocol based on the identification of predefined anatomic landmarks (Gallagher *et al.,* 1997).

4.2.5 MRI Analysis

Hard copy films and electronic data from image acquisitions were sent to the central MRI analysis centre at the Institute of Neurology, London, where MRI analysis was performed by investigators blinded to subject designation and treatment code. Newly-arrived scans were checked for compliance with study protocol such as slice thickness, TR and TE, FOV and matrix, slice positioning as well as for lack of artefact. In cases where significant protocol deviation occurred, the relevant centre was notified and scans were repeated and resent within 4 weeks.

4.2.5.1 Identification and marking of lesions

Two clinical fellows (DS and KF) received training and validation in the identification and marking of lesions on hard copy films by an expert neuroradiologist (TY) using non-trial MRI data. To minimise error caused by inter-observer variation, each clinical fellow analysed scans for the same subjects throughout the study. Lesion identification was supervised by TY throughout the study.

Lesions were identified as follows: T_2-hyperintense lesions (lesions which appeared more intense than surrounding NAWM on T_2 weighted scans) were identified and marked on PD weighted hard copy films after confirmation of their presence on the more heavily T_2 weighted scans.

The identification of T_1-hypointense lesions (lesions which have a lower intensity than surrounding NAWM on pre- contrast T_1 weighted scans) and Gd enhancing lesions

(lesions which have a higher intensity on post-contrast T_1 weighted scans when compared against pre-contrast T_1 weighted scans) also involved confirmation of the presence of a corresponding T_2-hyperintense lesion in an anatomically analogous position.

Analysis of scans from subsequent timepoints (year 1 and year 2) involved comparison with the previous scans to detect new or enlarging T_2-hyperintense lesions and new T_1-hypointense lesions. T_2-hyperintense lesions were identified as enlarging if they either a) appeared larger than previously on 2 contiguous slices, or b) were at least twice the diameter compared with the diameter from the previous image. Lesions less than 5 mm had to satisfy both criteria before being marked as enlarging lesions. (Molyneux *et al.* 1999)

4.2.5.2 Calculation of lesion volume and T_1/ T_2 lesion volume ratio

Total lesion volume was calculated from electronic data following conversion to a standard format (Supervised by trial and electronic data coordinator, GJB). All lesions previously identified on hard copy films were outlined on the electronic images. This was performed by a team of raters using a semi-automated lesion contouring protocol (Plummer, 1992) based on local intensity thresholding, with manual editing when necessary. Volumes of ring enhancing lesions included everything within it if the ring was complete, or if the ring was incomplete, only the area of enhancement itself. All raters underwent a formalised training programme in the contouring of T_2-hyperintense, T_1-hypointense and Gd enhancing lesions using non-trial MRI data. Target intra-rater coefficients of variation for lesion volumes in contour re-contour exercises (on a predetermined set of scans) were as follows: <3% for T_2 lesion volume, <5% for T_1-hypointense lesion volume, <5% for volume of Gd enhancing lesions. Validation of raters was performed before analysis of trial data, and repeated before the reception of data from year 2. All contoured electronic data at each timepoint was checked by clinical fellows (DS and KF) for consistency. Once the volumes for T_1-hypointense and T_2-hyperintense lesions were determined, the ratio of volume of T_1-hypointense lesions over that of T_2-hyperintense lesions (T_1/ T_2 lesion volume ratio (LVR)) was calculated at each timepoint. The purpose of this was to explore whether natalizumab had an additional effect on T_1-hypointense lesions *per se*, over and above a general effect on T_2-hyperintense lesions (of which T_1-hypointense lesions form a subset).

4.2.6 Trial end points

A set of pre-determined clinical and MRI end points were devised prospectively. These were broadly designed to assess for i) ongoing inflammatory activity (rate of clinical relapse, number of new or enlarging T_2-hyperintense lesions, number and volume of Gd enhancing lesions); and ii) evidence of more persistent deficit or pathology (sustained EDSS progression, progression on MSFC assessments and total T_2 hyperintense and T_1 hypointense MRI lesion volume measures, although it was recognised that reversibility of a portion of these total lesion volumes may occur).

4.2.6.1 Clinical end points

Clinical end points formed the primary outcome measures of the trial. EDSS and MSFC assessments were performed at each site by specified assessing physicians blinded to treatment assignment. Subjects underwent these assessments in 12 weekly visits throughout the trial duration. The primary clinical end points for the trial were i) annual rate of documented relapse, defined as the presence of new or recurrent neurological symptoms in the absence of fever or infection, lasting 24 hours or more, and accompanied by the presence of new neurological findings on clinical examination; ii) cumulative probability of disability progression with secondary clinical end points as follows: i) proportion of relapse free subjects; ii) MSFC progression. All end points were calculated at year 1 and year 2 of the trial

4.2.6.2 MRI end points

Pre-specified MRI end points for the trial were i) The number of Gd enhancing lesions at each timepoint; ii) the number of new or enlarging T_2-hyperintense lesions at year 1 and 2; iii) the number of new T_1-hypointense lesions at year 1 and 2; iv) volume of T_2-hyperintense, Gd enhancing lesions and T_1-hypointense lesions at baseline, year 1 and year 2. Additional end points were T_1/ T_2 LVR at year 1 and 2, as well as the absolute and relative changes of T_1/ T_2 LVRs over the trial period.

4.2.7 Statistical analysis

All analysis followed the intention to treat principle, and all reported P values are 2-tailed

4.2.7.1 Power calculations

Sample size estimates were based on data from previous trial of natalizumab (Miller DH et al., 2003) and IFNb-1a (Jacobs et al., 1996). To determine sample size required for 90 percent power with a 2:1 ratio of natalizumab to placebo, likelihood-ratio tests were employed based on predicted relapse rates of 0.6 with natalizumab and 0.9 with placebo. For an annualized relapse rate, a likelihood-ratio test was used to determine the sample size required for 90% power (n = 765), with a 2:1 ratio of natalizumab to placebo. With an assumed drop-out rate of 15% and rounding, the number of patients needed was estimated to be 900.

In order to power the study for the two-year end point of disability progression, progression rates at the end of two years were assumed to be 34.9% for the placebo group and 22.7 percent for the natalizumab group. Simulations of log rank test for survival were run with a 60 percent accrual in the first 24 weeks and the remainder in the next 24 weeks, assuming a 20 percent dropout rate over the 2 year study. The sample size of 900 provided 90 percent power with the use of a Bonferroni adjustment for multiple end points, maintaining the type 1 error rate of 0.05.

4.2.7.2 Statistical analysis of clinical outcome measures

Annual documented relapse rate was calculated using Poisson regression, while cumulative probability of sustained disability progression was assessed by an analysis of the time until the onset of the disability progression with the use of the Cox proportional-hazards model. Additional baseline factors were tested for inclusion in each of the models. This included the EDSS score, presence or absence of Gd enhancing lesions, the number of T_2-hyperintense lesions (<9 or >9) and age (Beck RW *et al.,* 2002; Weinshenker *et* al., 1989). Only statistically significant covariates were included in the models.

Differences between treatment groups with regard to adverse events were analyzed by the chi-square test, and serious adverse events were analyzed by Fisher's exact test. Poisson regression was used to calculate the difference between the rates of infection in each treatment group.

4.2.7.3 Statistical Analysis of MRI data

Ordinal logistic regression was used to analyse MRI lesion numbers. For the analysis of Gd enhancing lesions and new/enlarging T_2-hyperintense lesions, terms were included for treatment group and respective baseline measures, i.e. number of Gd enhancing lesions at baseline and number of T_2 hyperintense lesions (less than 9 vs 9 or more) as covariates. The number of new T_1-hypointense lesions was analyzed using ordinal logistic regression that included only a term for treatment group. This was because the number of T_1-hypointense lesions at baseline was not found to be a statistically significant covariate.

Absolute and percentage change in volumes of Gd-enhancing, T_2-hyperintense, T_1-hypointense lesions, as well as T_1/ T_2 LVR were analyzed using Friedman's analysis of covariance (ANCOVA), and included a term for treatment group and baseline values.

Sensitivity analysis was conducted for each MRI endpoint. This consisted of 1) analysis that included only available MRI data (not imputed) and 2) analysis which imputed missing values at any timepoint. In the latter case, missing values at baseline and 1 year were imputed using the mean volume in the study population. Missing values at 2 years were imputed using last observation carried forward (LOCF), or if there was no value to carry forward, the mean of the observed population at 2 years was used. All analyses followed the intention-to-treat principle. All reported *p*-values are two-tailed with $p \leq 0.05$ as statistical significance.

Additional pre-specified subgroup analyses were performed on lesion measures using logistic regression that included a term for treatment group and its respective baseline measure as a covariate. The subgroups analysed were as described below:

(i) baseline age (<40 or ≥40 years);

(ii) baseline EDSS score (≤ 3.5 or > 3.5);

(iii) presence or absence of baseline Gd-enhancing lesions;

(iv) number of baseline T_2-hyperintense lesions (< 9 or ≥ 9);

(v) gender

(vi) number of relapses in the year prior to study entry (1, 2, or ≥ 3).

4.3 Results

4.3.1 Study Population

Among the 942 subjects, 627 were assigned to receive natalizumab and 315 to receive placebo. There were no significant differences in baseline characteristics between the treatment groups (Table 4.1)

Depending on the MRI measure, analyzable scans were not available for 4-5% patients at year 1 and 8-9% patients at year 2. (Tables 4.2-4.8) The main reason for missing data (>80%) was the scan not being performed because patient withdrew from study; in the remainder (<20%), although the patient was still in the study, the scan was either not performed, or had not been received at the Central MRI Analysis Center, or had been received but was of inadequate quality for analysis.

Table 4.1 Baseline demographic and clinical characteristics of subjects. IR = interquartile range.

Characteristic	Natalizumab (n = 627)	Placebo (n = 315)
Age, yr		
Mean ± SD	35.6 ± 8.5	36.7 ± 7.8
Range	18- 50	19- 50
Gender, no (%)		
Female	449 (72)	211 (67)
Male	178 (28)	104 (33)
Disease duration, yr		
Median (range)	5 (0- 34)	6 (0- 33)
EDSS score		
Mean ± SD	2.3 ± 1.2	2.3 ± 1.2
Range	0- 6	0- 6
Gd-enhancing lesions, no (%)		
Mean ± SD	2.2 ± 4.7	2.0 ± 4.8
Median	1	0
Range	0- 36	0- 39
Gd-enhancing lesion volume, mm^3		
Mean ± SD	363.5 ± 797.5	332.7 ± 866.0
Median	31.0	0
IR	0- 353	0- 297
T_2-hyperintense lesions, no (%)		
<9	29 (5)	15 (5)
≥9	597 (95)	299 (95)
Missing	1 (< 1)	1 (< 1)
T_2 lesion volume, mm^3		
Mean ± SD	15627.4 ± 17142.4	14962.3 ± 15792.5
Median	9772	9315
IR	3830- 21839	3790- 21022
T_1-hypointense lesion volume, mm^3		
Mean ± SD	5752.4 ± 8182.5	5692.9 ± 7633.0
Median	2743	2681
IR	870- 7132	878- 7467
T_1/ T_2 LVR		
Mean ± SD	0.328 ± 0.19	0.343 ± 0.19
Median	0.319	0.349
IR	0.18- 0.46	0.19- 0.46

4.3.2 Treatment arm comparisons in clinical endpoints

While it is not within the scope of this chapter to describe the clinical findings of the study in detail, a brief summary of the clinical findings is nonetheless relevant in the reporting of the MRI end points. Natalizumab reduced the risk of sustained progression of disability by 42 % over 2 years (Relative risk 0.58, 95% CI 0.43 to 0.77, P<0.001).

The cumulative probability of progression (based on Kaplan Meier analysis) was 17% in the natalizumab group vs 29% in the placebo group. Natalizumab treated subjects had a 68% reduction in relapse rate compared with placebo subjects (0.26 relapses per year compared with 0.81 in placebo subjects P<0.001), an effect which was maintained over 2 years (P<0.001) (Polman *et al.,* 2006).

4.3.3 Treatment arm comparisons in MRI end points

4.3.3.1 Number of Gd Enhancing lesions (Table 4.2)

There were 92% less Gd-enhancing lesions in the group receiving natalizumab compared with placebo at both year 1 (0.1 vs 1.3; $p < 0.001$), year 2 (0.1 vs 1.2; $p < 0.001$) and at both timepoints combined (0.2 vs 2.5; $p<0.001$). 97% of subjects receiving natalizumab had no Gd-enhancing lesions on the year 2 MRI scan compared with 72% of subjects receiving placebo.

Table 4.2 Number of Gd enhancing lesions detected in the trial (Intention-to-treat population, N=942) P<0.001 in comparisons at all timepoints (including year 1 and year 2 combined)

Number of Gd enhancing lesions	Year 1		Year 2		Year 1 & 2	
	Natalizumab	Placebo	Natalizumab	Placebo	Natalizumab	Placebo
N (observed n)	627 (606)	315 (296)	627 (580)	315 (282)	627 (579)	315 (281)
Mean ± SD	0.1 ± 1.3	1.3 ± 3.2	0.1 ± 1.4	1.2 ± 3.9	0.2 ± 2.7	2.5 ± 6.7
Median	0	0	0	0	0	0
Min., max.	0, 32	0, 33	0, 32	0, 48	0, 64	0, 57

4.3.3.2 Number of new or enlarging T_2 lesions (Table 4.3)

Compared with placebo, the natalizumab treated group had 83% fewer new or enlarging

T_2-hyperintense lesions (11.0 vs 1.9; $p < 0.001$) over 2 years. This effect was seen both in new (82% less than that observed in placebo treated arm) and enlarging (88% less when compared with placebo) lesions. However, there was more than 10 times the number of new lesions as compared with enlarging lesions in each study arm. 57% of subjects in the natalizumab group developed no new or enlarging T_2-hyperintense lesions over the 2-year treatment period compared with 15% of placebo subjects.

Table 4.3 Number of new or enlarging T_2-hyperintense lesions detected in the trial. P<0.001 for treatment arm comparisons at all timepoints in new, enlarging and combined lesion measures.

	Year 1		Year 2		Year 1 & 2	
	Natalizumab	Placebo	Natalizumab	Placebo	Natalizumab	Placebo
New lesions						
N (observed n) Mean ± SD Median Min., max.	627 (606) 1.1 ± 4.5 0 0, 96	315 (297) 5.8 ± 8.3 3.0 0, 69	627 (581) 0.7 ± 4.7 0 0, 96	315 (283) 4.4 ± 7.8 2.0 0, 65	627 (580) 1.8 ± 9.0 0 0, 192	315 (282) 10.2 ± 14.4 5 0, 87
Enlarging lesions						
N (observed n) Mean ± SD Median Min., max.	627 (606) 0.1 ± 0.3 0 0, 3	315 (297) 0.4 ± 1.1 0 0, 8	627 (581) 0.0 ± 0.3 0 0, 4	315 (283) 0.4 ± 1.4 0 0, 11	627 (580) 0.1 ± 0.5 0 0, 5	315 (282) 0.8 ± 2.2 0 0, 18
New/ Enlarging Lesions (combined)						
N (observed n) Mean ± SD Median Min., max.	627 (606) 1.2 ± 4.7 0 0, 98	315 (297) 6.1 ± 9.0 3.0 0, 77	627 (581) 0.7 ± 4.8 0 0, 98	315 (283) 4.9 ± 8.5 2.0 0, 66	627 (580) 1.9 ± 9.2 0 0, 196	315 (282) 11.0 ±15.7 5.0 0, 91

4.3.3.3 Number of new T_1-hypointense lesions (Table 4.4)

The mean number of new T_1-hypointense lesions detected over 2 years was 1.1 in the natalizumab treated group, vs 4.6 in the placebo treated group. The natalizumab treated group therefore had 76% fewer new T_1-hypointense lesions compared with the placebo group (p<0.001). This difference was observed over the two years of the trial (74% and 83% fewer new T_1-hypointense lesions in the natalizumab treated group at year 1 and year 2 respectively; $p < 0.001$). In line with the findings in other lesion types, a higher percentage of natalizumab-treated subjects (63%) had no new T_1-hypointense lesions compared with placebo-treated subjects (27%), and substantially fewer natalizumab-treated subjects (11%) had three or more new T_1-hypointense lesions compared with placebo-treated subjects (44%). Analysis of post-Gd scans showed that the mean number of non-enhancing new T_1-hypointense lesions on Gd-enhanced scans over 2 years was 1.0 in the natalizumab group and 3.8 in the placebo group. This represented a 74% reduction in new non-enhancing T_1-hypointense lesions with natalizumab ($p<0.001$) and was very similar to the results from the analysis performed on precontrast scans (76%, $p<0.001$).

Table 4.4 Number of new T_1-hypointense lesions detected in the trial. All treatment arm comparisions revealed significant differences between arms ($p<0.001$)

New T_1-hypointense lesions	Year 1		Year 2		Year 1 & 2	
	Natalizumab	Placebo	Natalizumab	Placebo	Natalizumab	Placebo
N (observed n)	627 (606)	315 (297)	627 (581)	315 (283)	627 (580)	315 (282)
Mean ± SD	0.6 ± 1.9	2.3 ± 4.0	0.4 ± 1.8	2.3 ± 4.5	1.1 ± 3.3	4.6 ± 7.3
Median	0	1.0	0	1.0	0	2.0
Min., max.	0, 27	0, 27	0, 27	0, 53	0, 54	0, 60

Sensitivity analyses of data on the number of lesions showed results that were consistent with the primary analyses (data not shown).

4.3.3.4 Gd enhancing lesion volumes (Table 4.5)

Volume of Gd-enhancing lesions was significantly lower in subjects treated with natalizumab compared with those on placebo at both year 1 (mean 21 vs 207 mm^3; $p < 0.001$) and year 2 (mean 32 vs 192 mm^3; $p < 0.001$); representing 90% and 83% reductions in volume at the year 1 and year 2 time points, respectively. In both treatment arms, Gd enhancing lesion volumes were lower during the trial than baseline values. The reduction in volume was greater in the natalizumab treated groups in both year 1 (-343 mm^3 vs -126 mm^3; $p < 0.001$) and year 2 (-332 mm^3 vs -141 mm^3; $p < 0.001$).

Table 4.5 Gd enhancing lesion volumes (mm3). IR= Interquartile Range

	Baseline		Year 1		Year 2	
	Natalizumab	Placebo	Natalizumab	Placebo	Natalizumab	Placebo
Gd-enhancing lesions						
N (observed N) Mean ± SD Median IR	627 (626) 363.5 ± 797.5 31.0 0- 353	315 (313) 332.7 ±866.0 0 0- 297	627 (605) 20.7 ± 279.2 0 0- 0 *p* < 0.001	315 (295) 206.9 ± 671.8 0 0- 88	627 (580) 31.8 ± 330.3 0 0- 0 *p* < 0.001	315 (282) 191.5 ± 706.4 0 0- 72
Change from baseline						
N (observed N) Mean ± SD Median IR			627 (604) -342.8 ± 810.8 -11.0 -343 to 0 *p* < 0.001	315 (294) -125.8 ± 840.1 0 -168 to 0	627 (579) -331.6 ± 821.5 0 -334 to 0 *p* < 0.001	315 (281) -141.2 ± 922.0 0 -194 to 0
% Change from baseline*						
N (observed N) Mean ± SD Median IR			320 (313) -93.3 ± 51.7 -100.0 -100.0 to -100.0 *p* < 0.001	145 (133) -33.4 ± 448.7 -88.3 -100.0 to -18.1	320 (302) -90.7 ± 61.9 -100.0 -100.0 to -100.0 *p* < 0.001	145 (126) -25.2 ± 188.9 -100.0 -100.0 to -43.1

*calculated for subjects with baseline values >0

4.3.3.5 T_2-hyperintense lesion volumes (FIG 4.2, table 4.6)

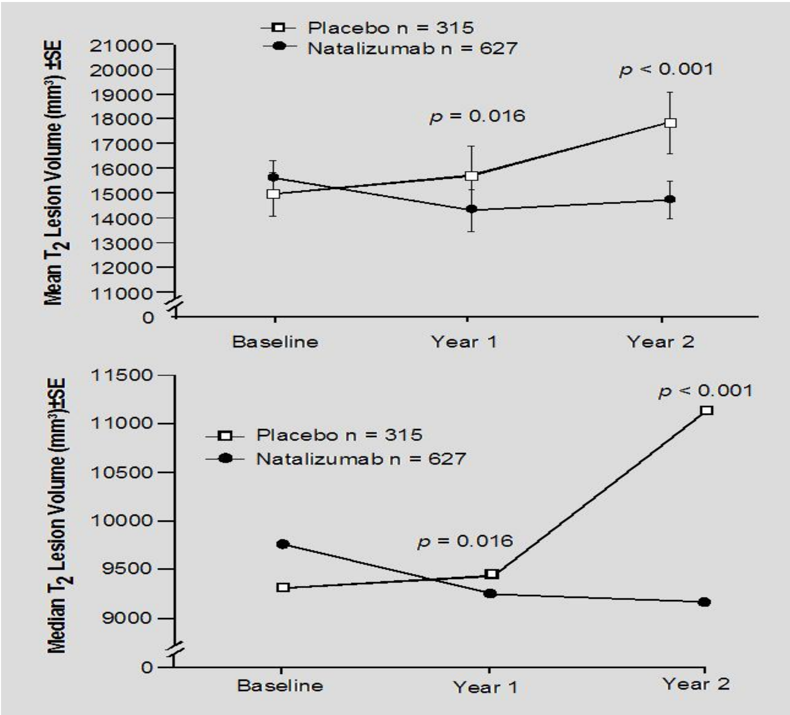

FIG 4.2 Mean (top) and median (bottom) volumes (mm^3) of T_2-hyperintense lesions for natalizumab and placebo treated arms

T_2-hyperintense lesion volumes are shown in FIG 4.2. Over the first year of treatment, T_2-hyperintense lesion volumes decreased in the natalizumab group and increased in the placebo group; the difference in volume between the treatment groups was statistically significant ($p = 0.016$). During the second year of treatment, T_2-hyperintense lesion volume continued to increase in the placebo group and remained stable in the natalizumab group ($p < 0.001$). Overall, mean T_2 lesion volume was significantly lower in natalizumab-treated subjects (14,722 [95% CI: 13,238 to 16,206]) compared with placebo-treated subjects (17,853 [95% CI: 15,414 to 20,292]) ($p < 0.001$) after 2 years. The mean change and median % change in T_2-hyperintense lesion volume over 2 years was also significantly different between the two treatment arms (mean volume change of -905 mm^3 for natalizumab vs 2,891 mm^3 for placebo; Median percentage change of -9.4% for natalizumab vs 8.8% for placebo; $p < 0.001$ for inter-treatment arm comparisons of both these measures). Although mean percentage change measures also reflect a marked difference between treatment arms, the apparent discrepancy in magnitude of percentage change between median and mean is explained by a skewing effect from very large percentage increases in a small number of individual subjects, especially among those who started with small lesion volumes.

Table 4.6 T_2-hyperintense lesion volumes (mm3). IR= interquartile range

	Baseline		Year 1		Year 2	
	Natalizumab	Placebo	Natalizumab	Placebo	Natalizumab	Placebo
T_2 -hyperintense lesions						
N (observed N) Mean ± SD Median IR	627 (626) 15627 ± 17142 9772 3830-21839	315 (313) 14962 ± 15792 9315 3790-21022	627 (605) 14303 ± 20982 9260 3665-17670 *p* = 0.016	315 (296) 15703 ± 21055 9447 3647-20157	627 (577) 14722 ± 18918 9175 3611-18699 *p* < 0.001	315 (280) 17853 ± 21997 11137 4112-23811
Change from baseline						
N (observed N) Mean ± SD Median IR			627 (604) -1324 ± 16861 -819 -2975 to 202 *p* < 0.001	315 (295) 741 ± 13278 -115 -1481 to 1098	627 (576) -905 ± 12781 -548 -2852 to 405 *p* < 0.001	315 (279) 2891 ± 15068 583 -549 to 3218
% Change from baseline*						
N (observed N) Mean ± SD Median IR			626 (603) - 8.1 ± 160.2 -12.1 -26.2 to 4.4 *p* < 0.001	315 (295) 43.5 ± 365.0 -2.3 -19.2 to 14.8	626 (575) -10.1 ± 153.8 -9.4 -22.4 to 6.8 *p* < 0.001	315 (279) 67.2 ± 412.7 8.8 -9.7 to 35.9

*calculated for subjects with baseline values >0

4.3.3.6 T_1-hypointense lesion volumes (FIG 4.3, Table 4.7)

Median and mean T_1-hypointense lesion volumes are shown in FIG 4.3. T_1-hypointense lesion volumes decreased over the first year in both treatment groups; however, the reduction in lesion volume was significantly greater in the natalizumab group compared with the placebo group ($p = 0.004$). T_1- hypointense lesion volume was significantly increased in the placebo group over the second year, while remaining the same in the natalizumab group ($p < 0.001$). Mirroring the changes observed in T_2 lesion volumes, the natalizumab arm experienced a greater mean reduction in T_1-hypointense lesion volume compared against placebo (-1508mm^3 vs 548 mm^3; $p < 0.001$) and, accordingly, a greater median percentage change (-24% vs -2%; $p<0.001$) over the 2 years of the trial.

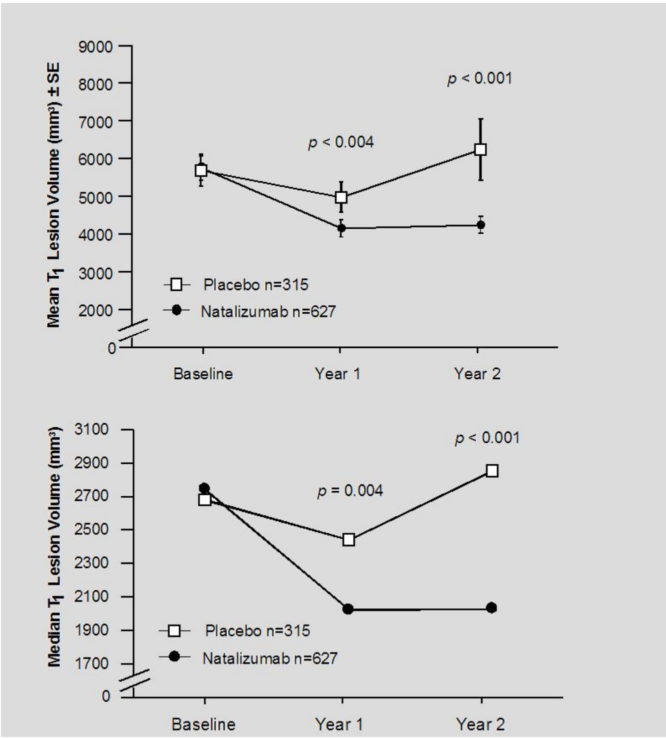

FIG 4.3 Mean (top) and median (bottom) T_1-hypointense lesion volumes for natalizumab and placebo treated arms

As with T_2 volume measures, the mean percentage change, while showing clear differences between treatment arms, is much larger than the median percentage change, due to the presence of a small number of subjects with small baseline lesion volumes and consequently large percentage change in lesion volume over the 2 years.

Table 4.7 T_1-hypointense lesion volumes. IR= interquartile range

	Baseline		Year 1		Year 2	
	Natalizumab	Placebo	Natalizumab	Placebo	Natalizumab	Placebo
T_1- hypointense lesions						
N (observed N) Mean ± SD Median IR	627 (626) 5752 ± 8183 2743 870-7132	315 (313) 5693 ± 7633 2681 878-7467	627 (606) 4149 ± 5591 2025 598-5030 *p* = 0.004	315 (297) 4979 ± 7303 2444 846-6137	627 (582) 4244 ± 5652 2031 672-5169 *p* < 0.001	315 (283) 6241 ± 14394 2855 1026-6801
Change from baseline						
N (observed N) Mean ± SD Median IR			627 (605) -1604 ± 4677 -556 -1753 to -55 *p* < 0.001	315 (296) 714 ± 5086 -254 -1274 to 106	627 (581) -1508 ± 4759 -449 -1786 to -3 *p* < 0.001	315 (282) 548 ± 12314 -6.0 -881 to 475
% Change from baseline*						
N (observed N) Mean ± SD Median IR			610 (588) 14 ± 291 -24 -46 to -7 *p* < 0.001	308 (290) 75 ± 1073 -13 -37 to 7	610 (565) 20 ± 322 -22 -43 to -4 *p* < 0.001	308 (278) 109 ± 1362 -2 -28 to 25

*calculated for subjects with baseline values >0

4.3.3.7 T_1/ T_2 Lesion Volume Ratio (Table 4.8)

Table 4.8 T_1/ T_2 LVR at each trial timepoint. IR = interquartile range

T_1/ T_2 LVR	Baseline		Year 1		Year 2	
	Natalizumab	Placebo	Natalizumab	Placebo	Natalizumab	Placebo
Mean ± SD Median IR	0.328 ± 0.19 0.319 0.18-0.46	0.343 ± 0.19 0.349 0.19-0.46	0.275 ± 0.18 0.261 0.15- 0.38 *p*=0.012	0.298 ± 0.16 0.300 0.18- 0.39	0.270 ± 0.17 0.256 0.15- 0.37 *p*=0.002	0.311 ± 0.24 0.295 0.18- 0.40
Change from baseline						
Mean ± SD Median IR			-0.053 ± 0.13 -0.044 -0.12 to 0.00 *p*=0.043	-0.045 ± 0.11 -0.037 -0.09 to 0.01	-0.058 ± 0.13 -0.048 -0.12 to 0.01 *p*=0.002	-0.032 ± 0.21 -0.032 -0.11 to 0.03
% Change from baseline						
Mean ± SD Median IR			-9.6 ± 64.1 -17.0 -37.3 to 1.1 *p*=0.024	-0.9 ± 102.2 -12.8 -30.8 to 3.5	-10.0 ± 64.6 -17.4 -36.6 to 2.1 *p*=0.003	7.7 ± 126.2 -12.9 -31.2 to 8.0

Although the T_1/ T_2 LVR was not significantly different between treatment arms at baseline, mean T_1/ T_2 LVR was lower in the natalizumab treated group versus the placebo treated group at year 1 (0.275 vs 0.298, p= 0.012) and year 2 (0.270 vs 0.311 p=0.002) (Table 4.8). In addition, the absolute and percentage reduction in T_1/ T_2 LVR was greater in the natalizumab treated group throughout the trial (table 4.8).

Sensitivity analyses of lesion volume data showed results that were consistent with the primary analyses (data not shown).

4.3.4 Subgroup analysis

Subgroup analysis was performed on pre-specified baseline characteristics as described in the methods section (4.2.7.3) in order to determine whether certain baseline characteristics influenced disease activity and progression, and whether natalizumab exerted a differential effect on any particular subgroup. The results of the analysis will be described in the following sections.

4.3.4.1 Gd enhancing lesions (Table 4.9)

Table 4.9 Number of Gd-enhancing lesions over the trial period: prespecified subgroup analysis. Figures are in mean ± standard deviation. All natalizumab vs placebo comparisons are significantly different to p<0.01 except for subjects with less than 9 T_2 lesions at baseline: in which neither arm exhibited activity within the trial

Subgroups	Natalizumab	Placebo
Age, yr		
<40 (n = 399, 188)	0.1 ± 0.6	1.1 ± 3.0
≥40 (n = 228, 127)	0.2 ± 2.2	1.3 ± 4.9
Gender		
Female (n = 449, 211)	0.1 ± 1.6	1.3 ± 4.4
Male (n = 178, 104)	0.1 ± 0.6	0.9 ± 2.6
EDSS		
≤3.5 (n = 548, 278)	0.1 ± 0.5	1.2 ± 4.1
>3.5 (n = 79, 37)	0.5 ± 3.6	0.8 ± 1.8
No. of relapses in year prior to study		
1 (n = 368, 180)	0.0 ± 0.1	0.8 ± 2.4
2 (n = 197, 102)	0.2 ± 0.9	1.3 ± 3.1
≥3 (n = 56, 27)	0.6 ± 4.3	3.4 ± 10.0
No. of Gd-enhancing lesions		
0 (n = 308, 172)	0.0 ± 0.1	0.4 ± 1.1
≥1 (n = 319, 143)	0.2 ± 1.9	2.1 ± 5.5
No. of T_2 lesions		
<9 (n = 29, 15)	0.1 ± 0.2	0.0 ±0.1
≥9 (n = 598, 300)	0.1 ± 1.4	1.3 ± 3.9

Greater pre-study or baseline disease activity, as measured by number of relapses in the preceding year, and the presence of Gd enhancing lesions, were associated with a greater number of Gd enhancing lesions during the trial study period. Higher number of Gd enhancing lesions during the study period were also found in women, subjects at or over the age of 40, subjects with >9 T_2 -hyperintense lesions at baseline, and paradoxically, subjects with a baseline EDSS score <3.5. Treatment with natalizumab was associated with a significantly lower number of Gd enhancing lesions compared with placebo, regardless of pre-study or baseline characteristics, with the exception of the small group of subjects who had <9 T_2-hyperintense lesions, in which neither treatment arm had demonstrable Gd-enhancing lesion activity.

4.3.4.2 T_2-hyperintense lesions (Table 4.10)

Table 4.10 Number of new or enlargingT_2-hyperintense lesions over 2 years: prespecified subgroup analysis. Figures are in mean ± standard deviation. All natalizumab vs placebo comparisons are significantly different to p<0.001

Subgroups	Natalizumab	Placebo
Age, yr		
<40 (n = 399, 188)	1.7 ± 4.6	12.2 ± 17.2
≥40 (n = 228, 127)	2.2 ± 14.1	9.2 ± 13.2
Gender		
Female (n = 449, 211)	2.0 ± 10.7	11.4 ± 16.5
Male (n = 178, 104)	1.6 ± 3.4	10.1 ± 14.2
EDSS		
≤3.5 (n = 548, 278)	1.8 ± 9.2	11.4 ± 16.1
>3.5 (n = 79, 37)	2.5 ± 9.3	7.9 ± 12.1
No. of relapses in year prior to study		
1 (n = 368, 180)	1.3 ± 3.8	10.0 ± 13.0
2 (n = 197, 102)	2.1 ± 4.6	12.1 ± 16.6
≥3 (n = 56, 27)	5.6 ± 27.9	14.6 ± 26.6
No. of Gd-enhancing lesions		
0 (n = 308, 172)	0.9 ± 2.0	5.8 ± 8.3
≥1 (n = 319, 143)	2.8 ± 12.7	17.3 ± 19.8
No. of T_2 lesions		
<9 (n = 29, 15)	0.2 ± 0.9	2.6 ± 2.8
≥9 (n = 598, 300)	2.0 ± 9.4	11.4 ± 16.0

Disease activity in the year prior to the study and at baseline was associated with a greater number of new or enlarging T_2- hyperintense lesions during the study. These results echoed the findings of the subgroup analysis for the number of Gd-enhancing lesions. In addition, women and subjects with baseline EDSS scores ≤ 3.5 or ≥9 T_2-hyperintense lesions also had higher numbers of new/enlarging T_2-hyperintense lesions on study. There was no effect of age on the number of new/enlarging T_2-hyperintense lesions. Natalizumab treatment was associated with lower numbers of new/enlarging T_2-hyperintense lesions compared with placebo, regardless of prestudy/baseline characteristics.

4.3.4.3 T_1-hypointense lesions

Table 4.11 Number of new T_1-hypointense lesions over 2 years: prespecified subgroup analysis. Figures are in mean ± standard deviation. All natalizumab vs placebo comparisons are significantly different to p<0.001

Subgroups	Natalizumab	Placebo
Age, yr		
<40 (n = 399, 188)	1.1 ± 2.5	4.9 ± 7.6
≥40 (n = 228, 127)	1.0 ± 4.2	4.2 ± 6.7
Gender		
Female (n = 449, 211)	1.1 ± 3.7	4.6 ± 7.6
Male (n = 178, 104)	0.9 ± 1.8	4.6 ± 6.6
EDSS		
≤3.5 (n = 548, 278)	1.0 ± 3.1	4.9 ± 7.6
>3.5 (n = 79, 37)	1.5 ± 3.9	2.6 ± 3.3
No. of relapses in year prior to study		
1 (n = 368, 180)	0.7 ± 1.5	4.7 ± 7.5
2 (n = 197, 102)	1.4 ± 3.3	4.3 ± 6.1
≥3 (n = 56, 27)	2.1 ± 8.1	5.5 ± 10.3
No. of Gd-enhancing lesions		
0 (n = 308, 172)	0.6 ± 1.2	2.4 ± 3.4
≥1 (n = 319, 143)	1.5 ± 4.3	7.3 ± 9.5
No. of T_2 lesions		
<9 (n = 29, 15)	0.3 ± 0.5	1.5 ± 2.0
≥9 (n = 598, 300)	1.1 ± 3.3	4.8 ± 7.4

Subjects with Gd-enhancing lesions at baseline had more on-study new T_1-hypointense lesions. The relationship between number of relapses prior to study and number of new T_1-hypointense lesions is less clear cut, although in general, it appears to show a trend toward a positive relation between number of pre-study relapses and number of new T_1-hypointense lesions. In addition, subjects with baseline EDSS scores ≤ 3.5 or ≥9 T_2-hyperintense lesions also had higher numbers of new T_1-hypointense lesions on study. There was no clear effect of age or gender on the number of new T_1-hypointense lesions. In line with the other subgroup analyses, treatment with natalizumab was associated with significantly fewer T_1-hypointense lesions compared with placebo in all prespecified subgroups.

4.4 Discussion

Treatment of subjects with natalizumab was associated with marked improvements in MRI indices (number of Gd enhancing lesions, new/enlarging T_2-hyperintense, new T_1-hypointense lesions) of MS when compared against placebo. These effects were sustained over the 2 year period of the study, and were consistent with the clinical findings of the study. In addition, they confirmed and extended the findings of the previous 6 month proof-of-concept trial (Miller DH *et al.,* 2003).

4.4.1 Effect of natalizumab on Gd- enhancement

Treatment with natalizumab was associated with a 92% reduction in the number of Gd-enhancing lesions over 2 years. The changes in lesion volume mirrored the number of lesions, and an equally clear cut-difference was observed between treatment groups. Gd enhancing lesions represent areas of overt BBB breakdown. As such, these findings emphasize the efficacy of natalizumab in the suppression of lesions associated with overt BBB leakage, and are consistent with its mechanism as an $\alpha 4\beta 1$ antagonist.

4.4.2 Effect of natalizumab on new lesion formation and lesion volume

Natalizumab was associated with a significant and sustained reduction in the accumulation of new lesions, seen either as areas of T_2 hyperintensity (83% reduction) or T_1 hypointensity (74% reduction), the latter representing about one-third of the former. While a clear difference in T_2-hyperintense and T_1-hypointense lesion volume evolution was also seen in favour of the natalizumab-treated group, the longitudinal pattern of change was nonlinear in both groups and warrants more detailed consideration.

4.4.2.1 Changes in the volume of T_2-hyperintense lesions

Changes in total lesion volume are a result of the net effect from volume expansion through new and enlarging lesions against volume reduction through the resolution of pre-existing lesions. Within the placebo group, the relatively stable lesion volume over the 1st year was followed by a clear increase in volume in the 2nd year. Seen in the terms above, the results indicate that accumulation of new or enlarging lesions matched the resolution of pre-existing lesions during the 1st year, with a much greater accumulation of new or enlarging lesions in the second year than lesion resolution. Because the number of new T_2-hyperintense lesions in the placebo arm was similar in both years, the relative stability of lesion volume in the 1st year compared with the 2nd year is likely to be due to a greater proportion of potentially reversible subacute inflammatory lesions at study entry than was the case later on in the study. This idea of greater inflammatory activity at baseline is supported by the observation that the total volume of Gd enhancing lesions in the placebo group was roughly 50% higher at baseline than at latter timepoints, and by the observation that the relapse rate during the year prior to study entry was 1.3 compared with 0.7 in the 1st year of study.

It may also be possible that enlargement of pre-existing lesions occurred which escaped visual detection, which was employed according to conservative criteria (Molyneux *et al.,* 1999). Such enlargement may have contributed to the greater observed increase in total volume of T_2-hyperintense lesions in the 2^{nd} year of the study, in the face of little apparent increase in the number of new or enlarging lesions.

In the natalizumab-treated arm, there was a clear reduction in T_2-hyperintense lesion volume in the 1^{st} year of study, with little change in the 2^{nd} year. These findings indicate that resolution of pre-existing lesions outweighed the development of new lesions (which were very few for subjects on treatment) in the 1^{st} year, while in the 2^{nd} year, when there were few lesions either resolving or appearing, total volumes were predictably stable.

The relative stability of T_2-hyperintense lesion volume in placebo-treated subjects in the first year of the study emphasizes the crucial importance of having a parallel control group to distinguish the effects of spontaneous regression in disease activity from genuine treatment effects.

4.4.2.2 T_1-hypointense lesion volume changes in the placebo treated arm

The changes seen in T_1-hypointense lesion volume changes were similar to those seen for lesion volume of T_2-hyperintense lesions. Hence, the placebo treated arm experienced a relatively minor drop in T_1-hypointense lesion volume over the 1^{st} year of the trial, followed by a clear increase in volume during the 2^{nd} year of the trial. The mechanisms underlying this evolution are likely to be similar to that seen for T_2-

hyperintense lesion volumes, but the sharper initial drop in T_1-hypointense lesion volume may reflect a relatively high proportion of subacute lesions at study entry that had resolution of edema and/or remyelination, both of which will favor evolution from T_1 hypointensity to T_1 isointensity.(Barkhof *et al.,* 2003)

The large drop in T_1-hypointense volume in the natalizumab-treated group during the 1st year is consistent with partial resolution of preexisting lesions, in addition to there being very few new lesions. As expected, with few new lesions in the second year and a stable pre-existing lesion load at year 1, the T_1-hypointense lesion volumes were relatively stable during year 2.

4.4.3 Changes in T_1/ T_2 LVR

As T_1-hypointense lesions form a subset of T_2-hyperintense lesions associated with more profound damage, the observation that natalizumab treatment was associated with a reduced T_1/ T_2 LVR is an important one. It indicates that the effect of natalizumab on T_1-hypointense lesion volume cannot merely be attributable to a 'blanket effect' on T_2-hyperintense lesions as a whole, but an additional effect on the volume of T_1 hypointense lesions *per se*, most likely by reducing the likelihood of new T_2-hyperintense lesions evolving into regions of T_1-hypointensity, and therefore reducing the accumulation of the total T_1 hypointense lesion load. Evidence that natalizumab treatment is associated with a reduced likelihood of evolution into T_1-hypointense lesions stems from a study of data from the previous trial (Dalton *et al.,* 2004a) and is consistent with postulated downstream effects of the agent on lymphocyte activation and inflammatory processes, once leucocyte adhesion and migration have occurred. The effect of natalizumab on lesion formation and evolution are therefore potentially twofold. Firstly, to avert new lesion formation. Secondly, once lesion formation has occurred, to suppress ongoing inflammation and therefore reduce the likelihood of axonal loss and damage.

4.4.4 Subgroup analysis

The effect of natalizumab treatment on MRI lesion number was evident in all subgroups studied. Although there was little treatment arm difference in Gd enhancing lesions in subjects with <9 T_2 lesions, the group was small, and very little clinical or MRI evidence of disease activity was present during the study. This finding suggests that subjects with relapsing MS who have few MRI lesions are likely to experience a more quiescent disease course during clinical trials. There may therefore be a case for requiring a minimum number of lesions as a criterion for entry to future studies of relapsing MS.

Higher levels of MRI activity during the trial were associated with higher levels of disease activity at baseline, most notably a higher relapse rate during the year prior to study entry and the presence of Gd-enhancing lesions at baseline. Similar observations were made in subgroups of the previous smaller Phase II study. (O'Connor *et al.,* 2005). This observation suggests that subgroups selected for having more frequent recent relapses or Gd-enhancing lesions will be more sensitive when evaluating MRI lesion activity measures in treatment trials since they are likely to have more on-study activity. In a similar vein, an analysis of placebo data from multiple trials showed that prior relapse rate is correlated with the likelihood of Gd-enhancement at a single time point.(Barkhof *et al.,* 2005)

4.4.5 The use of the number of new T_2-hyperintense lesions as an outcome measure

It was observed during the trial that the number of new T_2-hyperintense lesions considerably exceeds (by 10 times) the number of Gd-enhancing lesions. As such, in trials where annual scans are performed, new T_2-hyperintense lesions may be a more sensitive outcome measure than the number of Gd-enhancing lesions. This is because the T_2 measure visualizes new T_2-hyperintense lesions that may have appeared at any time during the year, since the majority of such lesions become persistent areas of T_2 hyperintensity. In contrast, Gd-enhancement is a transient feature of new lesions that typically lasts for only a few weeks, and therefore depicts only active lesions at the time of MRI.

It was also observed that new T_2-hyperintense lesions are much more common (>10 times) than enlarging lesions. Although this partly reflects the use of conservative criteria for enlargement that had been previously developed by an expert group (Molyneux *et al.,* 1999), the approach was considered necessary since it is difficult to be certain of enlargement during analysis of scans, as the appearance of lesions is susceptible to change with minor differences in repositioning. For future studies, it may be considered more efficient to report new T_2 lesions only and not expend extra effort in detecting (with less certainty) a few enlarging lesions unless there is a hypothesis that therapy will have a discordant effect on new vs enlarging T_2-hyperintense lesions. In addition, genuine biological enlargement of lesions, even if not appreciated visually, should also be reflected in the measure of total lesion volume.

4.4.6 The use of new T_1-hypointense lesions as an outcome measure

The total count of new T_1- hypointense lesions on the precontrast scans included Gd enhancing lesions which may have been acute and reversible. Therefore, to determine the contribution of such lesions to the outcome measure, an additional analysis was performed on the post-contrast scans. This revealed that the majority of new T_1-hypointense lesions were non-enhancing, and therefore more likely to reflect areas of persistent hypointensity associated with a greater degree of tissue matrix damage, including axonal loss when compared with isointense lesions (Barkhof *et al.,* 2003; van Waesberghe *et al.,* 1999). The number of new T_1-hypointense lesions is a potentially useful outcome measure as it is more likely to reflect just such a subset of lesions, which are associated with more axonal loss and tissue damage, and provides more specific information than T_2 lesion load. The reduction of such a measure and its related measure of T_1/ T_2 LVR in natalizumab treated subjects indicates the potential of natalizumab to reduce the accumulation of axonal loss arising from new inflammatory lesions in RRMS.

4.4.7 Conclusion

In conclusion, treatment with natalizumab is associated with a marked and sustained reduction in brain MRI lesions in subjects with relapsing MS. These changes mirror the improvements in clinical indices of the disease (Polman *et al.,* 2006), and are consistent among subgroups of subjects with more or less active inflammatory disease. Taken together these results suggest that natalizumab is a promising new therapy for the treatment of relapsing MS, although account will also need to be taken of the potential for adverse effects, in particular the risk for PML (Kleinschmidt-Demasters and Tyler., 2005; Langer-Gould *et al.,* 2005; van Assche *et al.,* 2005), which has been estimated to be about 1 in 1000 over the first 18 months of treatment (Yousry *et al.,* 2006*).* Continued longer term follow-up with conventional MRI will be useful to explore the persistence of therapeutic effect on the lesion activity and volume measures reported herein.

CHAPTER 5

A study of grey and white matter atrophy in a placebo-controlled trial of natalizumab in relapsing remitting multiple sclerosis.

5.1 Introduction

Histological and MRI studies support a growing body of evidence for axonal loss within MS lesions and, to a lesser extent, in NAWM. Serial volumetric MRI scans, through the observation of changes in brain volume, provide a reproducible method for following brain volume change (atrophy) and inferring neuroaxonal loss over time (Anderson *et al.,* 2006). This substudy of the natalizumab trial in RRMS (AFFIRM) utilised MRI to examine segmental (GM, WM and BP) atrophy in study subjects treated with natalizumab or placebo. The data was also analysed for relationships between atrophy, disability and MRI lesion load.

5.1.1 Evidence for axonal loss or degeneration in MS

The MR spectroscopy metabolite NAA is contained almost exclusively in neurones and axons in the human adult CNS. Reduced NAA, indicating neuroaxonal damage or loss, is observed in MS lesions (Fu *et al.,* 1996), NAWM (Siger-Zajdel and Selmaj, 2005; Chard *et al.,* 2002c), GM (Chard *et al.,* 2002c; Van Au Duong *et al.,* 2007) and in whole brain measures (Filippi *et al.,* 2003) even in the earliest clinical stage of disease. Such reductions correlate with axonal loss and disability in early disease (De Stefano *et al.,* 2001; Fu *et* al., 1998). The findings echo those of histological studies which demonstrate a reduction in axonal density within MS lesions (van Waesberghe *et al.,* 1999) and evidence of axonal transection and axonal damage in MS lesions and surrounding NAWM (Trapp *et al.,* 1998; Kuhlmann *et al.,* 2002). In addition, axonal damage originating within the lesion can have more widespread anatomical effects, through antegrade or retrograde degeneration and neuronal cell body apoptosis. This is supported by the finding of reduced axonal density in the corpus callosum (a structure with widespread cortical and subcortical connections) in a manner which correlates with white matter lesion load (Evangelou *et al.,* 2000)

5.1.2 Sequential volumetric MRI as a marker of brain atrophy

Sequential volumetric MRI measures of the whole brain provide a reproducible and often sensitive marker of brain tissue loss (atrophy), and have been used in the study of neurodegenerative diseases such as Alzheimer disease (Fox and Freeborough, 1997). In MS, this approach has allowed the study of brain atrophy in vivo (Anderson *et al.,* 2006). In CIS, conversion to MS is associated with ventricular enlargement (Dalton *et al.,* 2002b) and GM atrophy (Dalton *et al.,* 2004b). In early disease (within two and a half years of onset of first symptoms), average brain volumes – and the volumes of grey and white matter - of MS sufferers are lower than healthy counterparts (Chard *et al.,*2002a), with increasing atrophy over time again being predominantly seen in the GM (Tiberio *et al.,* 2005).

The relationship between atrophy and MS lesion load is a complex one, with conflicting findings emerging from different studies (Tiberio *et al.,* 2005; Filippi *et al.,* 2004; Molyneux *et al.,* 2000; Gasperini *et al.,* 2002, Rudick *et al.,* 2000). Atrophy appears to be temporally linked to MS lesion formation, with rates of atrophy being related to preceding MS lesion load, sometimes many years before. (Gasperini *et al.,* 2002, Rudick *et al.,* 2000, Chard *et al.,* 2003). A correlation with disability has also been demonstrated in some, but not all studies (Rudick *et al*, 2000; Losseff *et al.,* 1996; Gasperini *et al.,* 2002).

5.1.3 Natalizumab, new lesion formation and secondary neuronal damage

The effect of natalizumab on MRI-visible MS lesions in the AFFIRM monotherapy trial was described in detail in the preceding chapter. Natalizumab, a humanized monoclonal antibody directed against the $\alpha4$ subunit of the leucocyte cell adhesion molecule $\alpha4\beta1$ integrin, was associated with a 68% reduction in annualized relapse rate and a 42% reduction in risk of sustained disability progression compared with placebo (Polman *et al.,* 2006). Its effects on MRI-visible lesions is similarly dramatic (92% reduction in Gd enhancing lesions, 83% reduction in new or enlarging T_2- hyperintense lesions and 76% reduction in new T_1- hypointense lesions), and sustained over 2 years(Miller DH *et al.,* 2007). In patients who were still experiencing relapses on IFN$\beta-$1a, the addition of natalizumab to the existing therapy (SENTINEL Trial, Biogen Idec) was associated with a 54% reduction in annualized relapse rate and a 24 % reduction in risk of disability progression compared with IFN$\beta-$1a and placebo. (Rudick *et al.,* 2006).

Treatment with natalizumab was also associated with a reduced likelihood of new Gd enhancing lesions evolving into persistent T_1- hypointense lesions (Dalton *et al.,* 2004a), a subset of lesions associated with greater incidence of disruption to the extracellular matrix, axonal loss and persistent demyelination (van Waesberghe *et al.,* 1999; van Walderveen *et al.,* 1998; Barkhof *et al.,* 2003).

Such studies are compatible with an action of natalizumab that, while primarily disrupting overt BBB breakdown and associated new lesion formation, may also limit axonal damage and degeneration by the disruption of downstream processes such as leucocyte activation and proliferation once the BBB has been breached (Dalton *et al.,* 2004a, Damle *et al.,* 1991, Burkly *et al.,* 1991)

A subsidiary endpoint of the AFFIRM monotherapy study was atrophy as measured by changes in BPF as defined by Rudick and colleagues as the ratio of brain parenchymal volume over the total volume within the surface contour of the brain (Rudick *et al.,* 1999). Over the 2 years of the trial, there was no significant difference between the treatment arms in the total change in BPF. However, BPF reduction in the group receiving natalizumab was significantly higher than placebo between baseline and year 1, and lower than placebo between year 1 and year 2. (Miller DH *et al.,* 2007) The difference in the BPF trajectory may be attributable to the initial resolution of inflammation-associated oedema in the treated cohort in the first year and to reduced neuroaxonal loss secondary to the suppression of new inflammatory lesions in the second year.

The present study aimed to look at segmental atrophy by applying an automated brain segmentation programme (SPM99, Wellcome Institute of Cognitive neuroscience)(Ashburner and Friston, 1997; 2000) to examine changes in normalised volumetric measures of GM and WM and whole brain parenchyma (BP=GM+WM) in a subpopulation of patients participating in the AFFIRM trial. Treatment effect on rates of

GM, WM and BP atrophy was looked for, as were correlations between rates of atrophy, disability and lesion load.

5.2 Methods

5.2.1 Recruitment

Recruitment was from 3 centres (National Hospital for Neurology and Neurosurgery, London UK, VU Medical Centre, Amsterdam Netherlands and St Michael's Hospital, Toronto Canada) participating in the AFFIRM trial, the details of which have already been reported in the Chapter 4. The institutional review board and ethics committee for each centre approved the substudy protocol for each site, and written, informed consent separate from the main trial was obtained from each patient participating in the substudy.

5.2.2 MRI Protocol

Patients were scanned in 1.5T MRI scanners in their respective centres at baseline, year 1 and year 2 of the treatment trial. At each scan session, in addition to the sequences obtained as part of the main trial protocol (PD/ T_2 weighted fast spin echo sequence; pre and post-contrast T_1 weighted spin echo sequence (4.3.4)), an additional 3D Inversion Prepared FSPGR Echo sequence was performed at the beginning of each session. (TI=450ms; TR=13.5-15ms; TE=4.2-7ms; 1 excitation; 256X256 matrix; 250X180mm

FoV; 124-128 contiguous axial oblique slices with a z interval and slice thickness of 1.5mm). These produced T_1 weighted sequences of high volumetric precision and good WM/GM contrast.

5.2.3 Image processing and analysis

Electronic data for the scans were forwarded to the central MRI analysis centre (NMR Research Unit, Department of Neuroinflammation, Institute of Neurology, London). SPM99 was then used to perform automated segmentation of the images into GM, WM and CSF fractions (Ashburner and Friston, 1997; 2000), through the calculation of the probability (based on location and signal intensity thresholds) of each voxel being in GM, WM or CSF. Using corresponding T_2 weighted sequences as reference, WM lesions were identified on the 3D FSPGR scans. ROI were then drawn around the lesions and empirically assigned as WM, to avoid the erroneous assignation by SPM99 (based partly on signal intensity) of these lesions as GM or CSF (Chard *et al.,* 2002b). Binary maps of each specific tissue segment within the total intracranial volume ie GM, WM or CSF were then constructed (FIG 5.1), from which the volumes of individual segments (GM, WM or CSF) were measured.

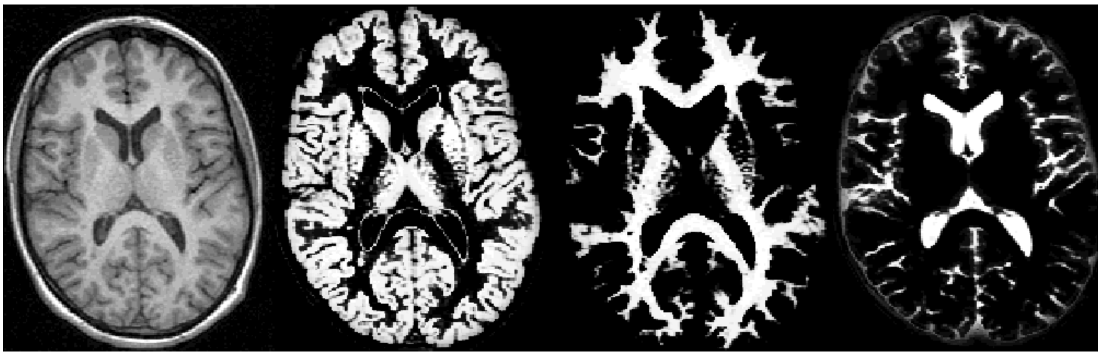

FIG 5.1 (From left to right) Axial brain, binary maps of GM segment, WM segment and CSF segment. The latter 3 obtained through automated segmentation of the 1st using SPM99

Scan rescan studies on healthy controls, employing SPM99 for brain segmentation on 3D FSPGR sequences have produced coefficients of variation of 0.5%, 0.7% and 1.1% for normalised BP, GM and WM volumes respectively (Chard *et al.,* 2002b).

5.2.4 Calculation of GMF, WMF and BPF

The volume of each segment (GM, WM and CSF) was calculated from the binary maps. Volumes of GM, WM and BP were expressed as a fraction of the total intracranial volume (which was calculated as the sum of volumes from GM, WM and CSF) to produce a normalised value of GM fraction (GMF), WM fraction (WMF) and BP fraction (BPF). Normalising to intracranial volume was intended to reduce variations caused by differences in subject head size, FoV and positioning.

5.2.5 Change across scanner upgrade

One of the centres (London) underwent a scanner software upgrade during the second year of the study. Consequently, 13 of the 19 patients in that centre underwent their year 2 scans after the scanner upgrade. 5 Healthy controls were scanned in London before and after the scanner upgrade, and WMF, GMF and BPF were obtained, to help determine if the aforementioned measures were influenced by the upgrade. While measures of WMF were stable across the upgrade, GMF was underestimated in post-upgrade scans, possibly due to subtle changes in the GMF/CSF contrast seen mainly around the gyrus rectus and temporal lobe. The underestimation of GMF in post-upgrade scans proved difficult to characterise. Treatment arm comparisons and linear regression analyses took into account changes that may have been seen as a result of the upgrade.

5.2.6 Statistical Analysis

Mann-Whitney independent sample rank sum tests were employed on baseline parameters (Age, Gender, disease duration, lesion loads, EDSS) to determine any differences between the treatment groups.

The atrophy measures were log-transformed so that any changes and accompanying CI were expressed as percentages. A paired t-test was used to look for significant atrophy between baseline and year 1 with regression of change performed to determine if atrophy differed between centres. Analysis of atrophy at year 2 then used multiple regression, with log(atrophy measure) as response variable and treatment, centre, gender and baseline or year 1 log(atrophy measure) as covariates. An additional site x upgrade interaction term was included to accommodate for the scanner upgrade in London. There was no evidence of non-normality of residuals.

An independent samples t-test, correcting for baseline values, was used to determine if there was an effect of natalizumab on change in the volume of T_1- hypointense, or T_2-hyperintense lesions

Spearman's correlation coefficients were obtained for associations between atrophy and measures of disability and MRI visible lesion load, with regression analysis performed when multiple (confounding) associations were detected to determine the independent association.

5.3 Results

5.3.1 Descriptive Data (Table 5.1)

Table 5.1 Baseline descriptive data of patients volunteering in the study. Values are in median (range) unless otherwise stated.

	Placebo Group (n=18)	Treated Group (n=39)	Entire Substudy group (n=57)
Age	38 (25-50)	38 (19-51)	38 (19-51)
Number of Males (%)	4 (22)	12 (31)	16 (28)
Disease Duration at baseline	6 (1-26)	5 (1-26)	6(1-26)
EDSS at baseline	1.5 (0-4.5)	2 (0-5.5)	2 (0-5.5)
Mean Total T_2 -hyperintense lesion load per patient in mls (SD)	15739 (20440)	17639 (13751)	17039 (15998)
Mean Total T_1-hypointense lesion load per patient in mls (SD)	6570 (10336)	7231 (7963)	7022 (8692)
Mean Total Gadolinium enhancing lesion load in mls (SD)	379 (759)	527 (897)	480 (851)

Fifty-seven patients participated in the study, (twenty-five in Toronto, nineteen in London and thirteen in Amsterdam). Thirty-nine of the patients had been randomized to the treatment cohort and were receiving monthly intravenous infusions of natalizumab 300mg. At baseline, age, disease duration, EDSS and treatment ratio were similar between treatment arms and centres. Males constituted a higher proportion of patients in the natalizumab arm when compared with the placebo arm (30 vs 22 per cent) but this was not statistically significant on the Mann-Whitney test. Nonetheless, differences in gender distribution were taken into account while performing the treatment arm analysis. Of the fifty-seven subjects who were scanned at baseline, fifty-six subjects returned for the scan at year 1 and fifty-three at year 2.

5.3.2 Changes in normalised brain volume (FIG 5.2; Table 5.2)

Given the cross-upgrade discrepancies in brain volume estimation described earlier, mean values of normalised brain volumes at year 2 and estimated volume changes between baseline and year 2 are reported excluding those who underwent their scans after the scanner upgrade (n=40). However, as the upgrade took place after all the year 1 scans were performed, the corresponding values reported at year 1 include data from all who participated in the year 1 scan (n=56). All values are reported with treatment arms combined.

Estimation of percentage change in normalised brain volume employed a regression model which took into account differences in centre, gender and baseline values (Table 5.2). Calculation of normalised brain volumes involved obtaining the mean values and standard deviation for the cohort at each timepoint (FIG 5.2). As such, apparent discrepancies may exist between the figures reported in Table 5.2 and FIG 5.2. However, the figures derived from regression analysis (Table 5.2) provide a more statistically robust reflection of change in normalised brain volume between timepoints.

Table 5.2 Estimated percentage change in normalised brain volume using multiple regression (baseline to year 2) and paired t-test (baseline to year 1). Negative values denote a reduction in normalised volume. Values are reported for both treatment arms combined. Numbers in parenthesis are 95% CIs.

	Baseline to year 1 (n=56)	Baseline to year 2 (n=40)
BPF	-0.81% (-0.49%, -1.13%) P<0.001	-1.12% (-0.67%, -1.56%) P<0.001
GMF	-1.01% (-0.58%, -1.43%) P<0.001	-1.36% (-0.81%, -1.9%) P<0.001
WMF	-0.50% (-1.00%, 0.002%) P=0.051	-0.73% (-1.38%, -0.08%) P=0.030

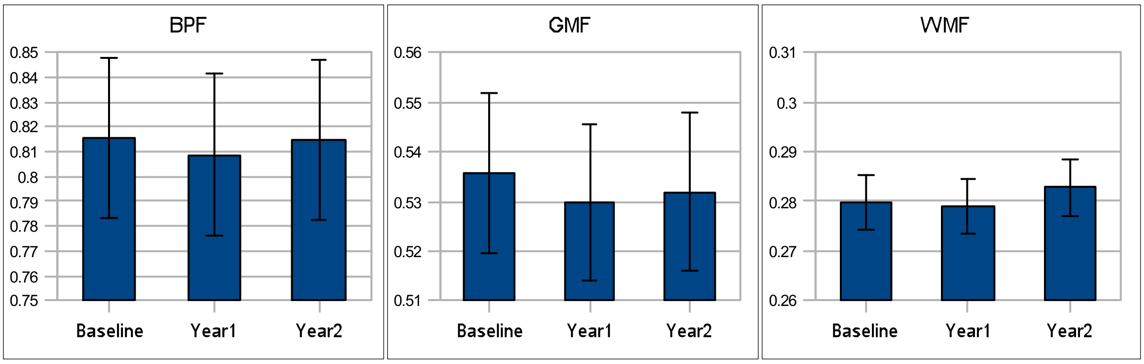

A B C

FIG 5.2 Mean values (+/- standard deviation) of BPF, GMF and WMF at baseline(n=57), year 1(n=56) and year 2(n=40).

5.3.2.1 BPF: mean values and estimated changes (Table 5.2; FIG 5.2A)

The mean BPF at each timepoint (0.816, 0.809, 0.815 at baseline, year 1 and year 2 respectively with standard deviation of 0.03) is shown in FIG 5.2A.

There was a statistically significant estimated 0.81% fall (95% CI: 0.49% lower, 1.13% lower; P<0.001) in BPF from baseline to year 1 and a 1.12% fall (95% CI: 0.67% lower, 1.56% lower; P<0.001) between baseline and year 2 (Table 5.2). There was no evidence that the fall in BPF varied between centres (P=0.14).

5.3.2.2 GMF: Mean values and estimated changes (Table 5.2;FIG5.2B)

Mean GMF was 0.536, 0.53 and 0.532 at baseline, year 1 and year 2 respectively with a standard deviation of 0.02. (FIG 5.2B)

There was an estimated 1.01% reduction in GMF (95% CI 0.58% lower, 1.43% lower, P<0.001) from baseline to year 1 and a 1.36% fall (95% CI: 0.81% lower, 1.9% lower, P<0.001) from baseline to year 2. (Table 5.2) There was no evidence that these changes varied by centre (P=0.84)

5.3.2.3 WMF: Mean values and estimated changes (Table 5.2; FIG 5.2C)

Mean WMF was 0.280, 0.279 and 0.283 in baseline, year 1 and year 2 respectively. Standard deviation at each timepoint was 0.04. (FIG 5.2C)

Statistical analysis revealed that changes in WMF were less clear cut across the 2 years, with a borderline significant 0.50% fall (95% CI 1.00% lower, 0.002% higher; P=0.05) from baseline to year 1 and a significant 0.73% fall (95% CI: 1.38% lower, 0.08% lower; P=0.030) in WMF between baseline and year 2 (Table 5.2). Once more, there was no evidence that changes in WMF varied between centres (P=0.84)

5.3.3 Treatment arm analysis

Treatment arm analysis was performed taking all data (pre and post upgrade) into account, with a correction factor for post-upgrade data.

5.3.3.1 Treatment arm comparison of changes in MRI visible lesion load (FIG 5.3)

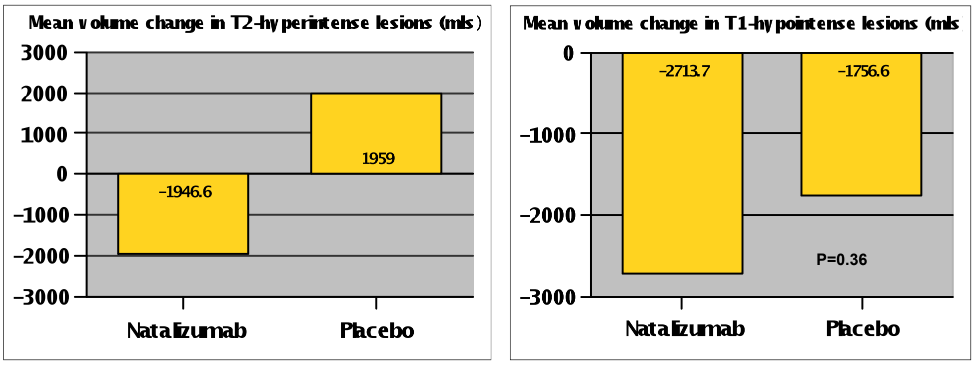

A **B**

FIG 5.3 Mean volume change from baseline to year 2 in T_2-hyperintense lesions (A) and T_1-hypointense lesions (B)

Natalizumab was associated with a greater reduction in the volume of T_2 hyperintense lesions compared to placebo (Baseline-adjusted mean treatment arm difference -3741mls 95% CI -6689, -793 mls, P=0.01). However, no significant treatment effect was demonstrated on the volume of T_1- hypointense lesions (Baseline-adjusted mean treatment arm difference -709mls 95% CI -2257, 837, P=0.36).

5.3.3.2 Treatment arm atrophy comparison (Table 5.3; Fig 5.4)

Table 5.3 Active vs Placebo differences in BPF, GMF, WMF, adjusting for baseline values. Figures represent differences as a percentage of placebo (95% CIs). Negative values denote greater atrophy in the active arm. All differences are non-significant to p=0.05

	Year 1	Year 2
BPF	0.29% (-0.42%, 1.0%) P=0.41	-0.16% (-1.05%, 0.74%) P=0.73
GMF	0.70% (-0.21%, 1.6%) P=0.49	-0.23% (-0.87%, 1.33%) P=0.68
WMF	-0.40% (-1.5%, 0.75%) P=0.13	-0.81% (-2.1%, 0.47%) P=0.21

Multiple regression analysis of normalised brain volume adjusted for baseline values, centre and gender differences. It demonstrated no significant difference in atrophy between treatment arms at year 1 or year 2 (Table 5.3)

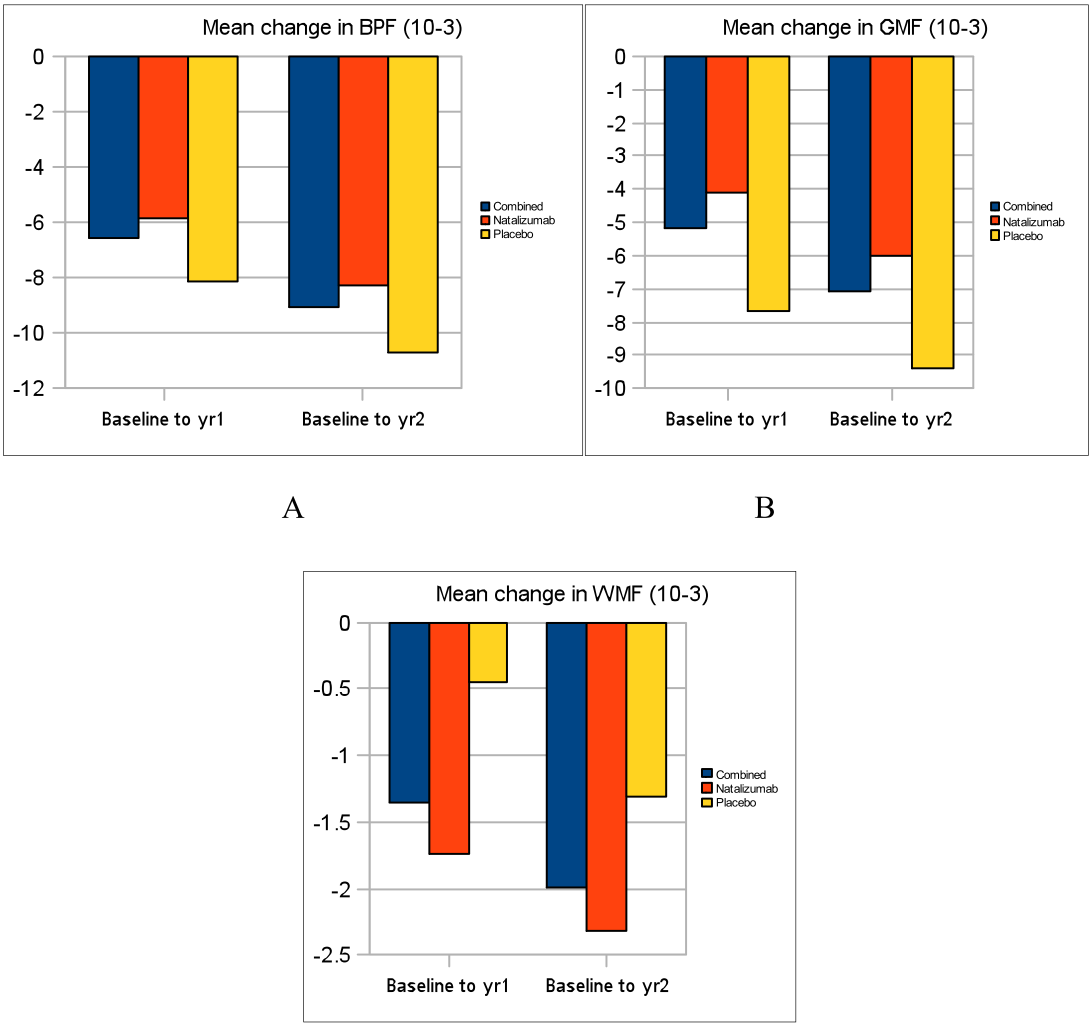

A

B

C

FIG 5.4 Mean change in BPF (A), GMF (B) and WMF (C) over the course of the trial. Units expressed in 10^{-3}. As calculated by multiple regression (Table 5.3), changes seen in natalizumab, placebo and combined arms were not significantly different.

FIG 5.4 displays the mean changes in normalised brain volume over the course of the trial, as calculated by subtracting the baseline value from values at latter timepoints.

Although multiple regression detected no statistically significant differences between the treatment arms, the charts in FIG 5.4 appear to reflect a trend toward a lower rate of GM atrophy in the natalizumab treated arm when compared against the placebo at both timepoints (GMF reduction of $-4.1*10^{-3}$ vs $-7.7*10^{-3}$ for natalizumab and placebo respectively at year 1 and $-6.0*10^{-3}$ vs $-9.4*10^{-3}$ for natalizumab and placebo respectively at year 2), and similarly a trend toward a greater rate of WM atrophy in natalizumab treated patients compared with placebo at both timepoints.

5.3.4 Relationship between atrophy and other measures of disease

5.3.4.1 Relationship between EDSS and normalised brain volumes (Table 5.4).

Table 5.4 Spearman's rank correlation coefficient between normalised brain volume (BPF, WMF, GMF) and disability as measured by EDSS at baseline and Year 2. Significant relationships in bold

Associations between EDSS and normalised brain volume		BPF	WMF	GMF
Baseline (n=57)	Spearman's rank correlation coefficient (ρ)	**-0.45**	-0.0115	**-0.48**
	Significance (P)	**0.0005**	0.93	**0.0002**
Year 2 (n=56)	Spearman's rank correlation coefficient (ρ)	**-0.41**	-0.13	**-0.43**
	Significance (P)	**0.0024**	0.42	**0.001**

There was a negative association between GMF and EDSS at baseline ($\rho=-0.48$, $p=0.0002$) and year 2 ($\rho=-0.43$ $P=0.001$). No such relationship existed between WMF and EDSS at baseline or year 2 ($P=0.9$ and 0.4 respectively). The negative association observed between BPF and EDSS at baseline and year 2 therefore most probably results from the association with GMF. Bootstrap analysis revealed no difference in the relationship between EDSS and brain volume in the 2 treatment groups.

5.3.4.2 Relationship between atrophy MRI lesion load measures (Table 5.5, Table 5.6)

Table 5.5 Multiple bivariate spearman correlation coefficients (ρ) between GMF/WMF atrophy from baseline to year 2 and various MRI visible lesion measures. Significant bivariate correlations are in bold

Baseline Lesion Volumes		GMF Change	WMF Change
T_2- hyperintense lesions	Spearman Correlation Coefficient (ρ)	-0.212	**-0.414**
	P value (2-tailed)	0.128	**0.002**
T_1- hypointense lesions	Spearman Correlation Coefficient (ρ)	-0.096	**-0.347**
	P value (2-tailed)	0.494	**0.011**
Gd enhancing lesions	Spearman Correlation Coefficient (ρ)	-0.175	**-0.443**
	P value (2-tailed)	0.209	**0.001**
Lesion volume change over 2 years		GMF Change	WMF Change
T_2- hyperintense lesions	Spearman Correlation Coefficient (ρ)	0.168	0.144
	P value (2-tailed)	0.228	0.304
T_1- hypointense lesions	Spearman Correlation Coefficient (ρ)	-0.004	0.212
	P value (2-tailed)	0.979	0.127
Gd enhancing lesions	Spearman Correlation Coefficient (ρ)	0.234	**0.392**
	P value (2-tailed)	0.095	**0.004**

Multiple bivariate correlation analysis revealed no significant association between GMF change and any of the lesion volume measures (table 5.5).

Although a number of significant bivariate correlations existed between WMF change and lesion volumes at baseline (T_2- hyperintense lesions, T_1- hypointense lesions and Gd enhancing lesions), a multiple regression analysis revealed that only the relationship with Gd enhancing lesions was independently significant (r=-0.349, P=0.014)(Table 5.6)

Table 5.6 Multiple regression analysis of change in WMF over 2 years and baseline lesion load measures. Significant multivariate correlations in bold.

Baseline lesion volumes	Standardized Coefficients (r)	Sig. (P)
T_2- hyperintense lesions	-0.463	0.173
T_1- hypointense lesions	0.386	0.255
Gd Enhancing lesions	**-0.349**	**0.014**

Apart from a positive association with the change in volume of Gd enhancing lesions (ρ=0.392, P=0.004), change in WMF was not associated with the change in volume of MRI visible lesions (Table 5.5).

Change in WMF was therefore negatively associated with baseline volume of Gd enhancing lesions (r=-0.349, P=0.014) and positively associated with the change in volume of Gd enhancing lesions (ρ=0.392, P=0.004). The high correlation between these 2 measures of Gd enhancing lesions (ρ=0.983, P<0.001) precluded any multiple regression analysis to discern if either influence was independent of the other.

5.4 Discussion

This substudy of the AFFIRM trial utilised SPM99 to analyse segmental atrophy in patients with RRMS. Although atrophy occurred in both GM and WM, GM atrophy appeared to predominate over the 2 years.

GM atrophy was not related with MRI-visible MS lesion load. The positive association of WMF change with change in Gd enhancing lesion volume suggests that such variations in WMF are driven by changes inflammation-associated oedema.

In keeping with the AFFIRM study, treatment with natalizumab reduced the expansion of T_2- hyperintense lesions. The lack of observed effect on T_1- hypointense lesions is most probably a result of the small cohort (N=56), as a significant effect was observed in the main study (N=942)(Chapter 4).

No significant difference in atrophy rate was demonstrated between the treatment arms receiving natalizumab and placebo at any timepoint within the study using multiple regression. However, trends toward a treatment effect may exist. These are discussed in more detail in section 5.4.4.

5.4.1 Rates of Atrophy

The rates of atrophy observed in the substudy (1.12%, 1.36% and 0.73% in BPF, GMF and WMF respectively over 2 years) are in keeping with those reported from other studies (Rudick *et al.,* 2000; Kalkers *et al.,* 2002; Tiberio *et al.,* 2005), and further endorse the use of serial 3D volumetric MRI to measure atrophy in RRMS. Both GM and WM atrophy was observed, with GM atrophy occurring at a greater rate than WM atrophy over the 2 years (1.36% vs 0.73%), a finding consistent with observations from other studies which detected predominantly GM atrophy in early disease (Dalton *et al.,* 2004b; Tiberio *et al.,* 2005).

5.4.2 Relationship between atrophy and EDSS

BPF and GMF at baseline and year 2 correlated with EDSS at these timepoints. This finding is largely consistent with findings from other studies to date investigating the relationship between disability and brain atrophy, using a variety of brain atrophy measurement approaches (Rudick *et al.,* 2000; Bermel *et al.,* 2003; Rovaris *et al.,* 2001; Paolillo *et al.,* 2002; Fisher *et al.,* 2008; Fisniku *et al.,* 2008b). Being less subject to inflammation-associated oedema (Pirko *et al.,* 2007), GMF, rather than WMF is potentially a more accurate reflection of underlying neuronal loss and related disability.

5.4.3 Relationship between atrophy and MRI visible lesion load

WMF change was significantly and positively associated with the change in the volume of Gd enhancing lesions, a subpopulation of lesions associated with active inflammation and oedema (Grossman *et al.,* 1986; Katz *et al.,* 1993; Miller DH *et al.,* 1988). Such a relationship points to oedema playing a significant role in influencing WMF fluctuation in this study.

No relationship was detected between GM atrophy and lesion load. Other studies have failed to demonstrate a clear relationship between atrophy and lesion load (Gasperini *et al.,* 2002; Molyneux *et al.,* 2000). Using a methodology very similar to that adopted in the current study, Tiberio and colleagues demonstrated atrophy in early RRMS confined mainly to the GM, which was unrelated to the underlying lesion load(Tiberio *et al.,* 2005).

The reasons for the apparent dissociation between GM atrophy and MRI visible lesion load are not altogether clear. A possible explanation may be that GM atrophy is influenced by demyelinating lesions within the GM itself. Such lesions form a significant portion of the total lesion load in MS (Pirko *et al.,* 2007), and the existence of such lesions do not correlate well with white matter lesion load (Kutzelnigg *et al.,* 2005). The majority of these lesions are invisible on standard MRI sequences(Geurts *et al.,* 2005, Kidd *et al.,* 1999), including the ones used in this study. They are associated with activation of cortical microglia (Bo *et al.,* 2003, Peterson *et al.,* 2001) and increased expression of inducible nitric oxide synthase, factors contributory to axonal loss (Smith KJ *et al.,* 2001). It is conceivable that a population of MRI-invisible GM lesions, which are not necessarily associated with WM lesions, may be the principle stimulus for GM atrophy and explain the apparent dissociation between GM atrophy rate and WM lesion load.

An alternative explanation may lie in the temporal relationship between focal inflammation and atrophy. In a long-term follow-up study, whole brain measures of volume were examined in MS patients 14 years after their first clinical event. Inferred atrophy was significantly related with change in T_2- hyperintense lesion load between baseline and 5 years later (Chard *et al.,* 2003), indicating that the effect of focal inflammation on atrophy in MS may be temporally remote from the inflammatory event itself, through relatively slow processes such as antegrade or retrograde degeneration originating from the site of inflammation or nitric oxide- induced damage to more vulnerable demyelinated axons (Smith KJ *et al.,* 2001). Such processes may result in axonal loss and consequent atrophy in the GM once a significant length of time has passed, beyond the duration of the current study.

5.4.4 Effect of natalizumab on lesion measures and atrophy

Natalizumab reduced the proliferation of T_2- hyperintense lesions, a finding in keeping with those from existing trials (Miller DH *et al.,* 2007; Rudick *et al.,* 2006). The apparently discrepant lack of a significant effect on T_1- hypointense lesions is most probably attributable to differences in the sample population.

In spite of a clear effect on MRI visible lesions, multiple regression failed to demonstrate any significant effect of natalizumab on segmental atrophy (GMF, WMF, BPF) at any timepoint (year 1 or year 2) in the study. Non-significant trends appeared to suggest a greater rate of WM atrophy and lower rate of GM atrophy in the natalizumab treated group in the duration of the trial. The trend toward a greater rate of WM atrophy in natalizumab treated patients may reflect a natalizumab-mediated suppression of inflammation associated oedema within the WM. Similarly, the lower rate of atrophy in GM, which is unrelated to WM lesion load, may be an effect of natalizumab on GM atrophy itself. However, it must be stressed that none of these trends approach significance, and therefore, such findings should be taken with caution.

The absence of a statistically significant treatment effect of natalizumab on atrophy is a finding which only partly agrees with those of the whole AFFIRM cohort. This found a significantly greater rate of reduction in BPF in the natalizumab-treated arm in the 1st year (thought to be due to an initial reduction in inflammation-related oedema) and a lower rate of atrophy in the treatment arm between year 1 and year 2, resulting in no overall difference in BPF between treatment arms in the 2nd year (Miller DH *et al.,* 2007). The discrepancy in the findings of the 2 studies may be explained by the different methods adopted at measuring atrophy in the 2 studies (SPM assisted brain segmentation vs BPF), or by the differences in the size of the study populations, as already alluded to above.

A recent study calculated population sample sizes required to demonstrate a change in rate of atrophy using a selection of atrophy measures (Structural image evaluation using normalization of atrophy; segmented brain volume difference; brain boundary shift interval). The study findings indicated that in order to demonstrate a 30% reduction in atrophy rate over 2 years, drug trials required the recruitment of at least 123 subjects (Anderson *et al.,* 2007). The ability to detect differences in atrophy was influenced by the number of study participants (the larger the study, the more sensitive), the duration of the study (longer studies were able to detect smaller differences in atrophy rates) and the method of atrophy measures. Although measurement of SPM99-segmented brain volumes was not amongst the approaches examined in this study, it is possible that with 57 patients, this substudy was of insufficient power to demonstrate a treatment effect of natalizumab on atrophy.

However, if the findings of this study (that is, the absence of a natalizumab-mediated effect on atrophy) are taken to be true, they would echo the findings of other trials of disease modifying agents which have not shown any significant effect on brain atrophy (Molyneux *et al.,* 2000, Rovaris *et al,.* 2001) despite a clear effect on MRI-visible lesions. Together, such evidence would appear to suggest that atrophy is driven by processes not immediately or entirely related to focal white matter inflammation.

The possibility remains that the temporal relationship between focal inflammation and axonal loss and atrophy may be a protracted one, with atrophy resulting from lesions occuring years before (Chard *et al.,* 2003). This may provide an explanation for the apparent lack of effect of natalizumab on atrophy, despite a clear effect on WM lesion formation. Follow-up studies would be required to verify if this is the case.

It is also possible that Natalizumab may exert a more modest effect on GM lesions. Such lesions are associated with less BBB breakdown and leucocyte infiltration (Peterson *et al.,* 2001), processes mediated by the interaction of VLA-4 and its associated ligands. If such lesions influence and drive atrophy within the GM, the lack of effect of natalizumab on GM atrophy may be a reflection of its effect on such GM lesions. However, it is not possible to verify this hypothesis given the MRI sequences undertaken in the current study, which do not detect the majority of GM lesions.

5.4.5 Summary

The study has demonstrated measurable brain atrophy over 2 years, predominantly in the GM, driven by processes independent from concurrent WM lesions. Normalised GM volume is inversely related to disability as measured by EDSS. The positive association between WMF change and the change in volume of Gd enhancing lesions points to fluctuations in the WM being largely secondary to inflammation associated oedema. Natalizumab, having influenced the formation of WM lesions, did not appear to have an effect on atrophy. This could be due to a lack of power (Anderson *et al.,* 2007). However, if the findings of the study do actually reflect a lack of treatment effect of natalizumab on atrophy, it would indicate that atrophy does not immediately arise from VLA-4 mediated processes or inflammation. Further studies are required to determine if the influence of natalizumab on WM lesions results in a moderation of atrophy in the long term.

CHAPTER 6

Subtle blood brain barrier disruption in a placebo-controlled trial of natalizumab

6.1 Introduction

Overt BBB disruption, as detected by visible Gd enhancement on MRI, is a consistent finding in new MS lesions in patients with relapsing MS. (Kermode *et al.,* 1990). Histological studies of active MS lesions demonstrate the extravascular deposition of fibrinous exudates, indicative of BBB disruption, in conjunction with perivenular inflammation, lymphocyte infiltration and oedema (Adams *et al*., 1985). Additional evidence of BBB disruption in chronic, non-active lesions has come from histological studies, including the demonstration through confocal microscopy of disruption of the intercellular network of tight junctions which form the physical BBB (Kirk *et al.,* 2003), and the widespread histological finding of extravascular deposition of fibrin in non-active MS lesions (Kwon and Prineas, 1994; Claudio *et al.,* 1995 ; Adams *et al.,* 1985). The former, when chronic and persistent, are associated with a greater degree of axonal loss, extracellular matrix destruction (van Walderveen *et al.,* 1998) and disability (Truyen *et al.,* 1996; van Walderveen *et al.,* 2001).

Natalizumab has been shown to suppress overt BBB disruption (Miller *et al.,* 2003;2007; Tubridy *et al.,* 1999). Its effect on low grade BBB leakage was examined in this study by comparing the leakage from visibly non-enhancing lesions in the placebo group, vs the natalizumab treated group.

6.2 Methods

6.2.1 Recruitment

The subjects involved in the study were recruited from 3 centres (National Hospital for Neurology and Neurosurgery, London UK, VU Medical Centre, Amsterdam Netherlands and St Michael's Hospital, Toronto Canada) participating in the AFFIRM trial, the details of which have already been described in chapter 4. Subjects and study personnel were unaware of the treatment assignments. Subjects from the 3 aforementioned centres were given the option of participating in this additional substudy of the main trial. The institutional review board and ethics committee for each centre approved the substudy protocol for each site, and written, informed consent was obtained from each subject participating in the substudy.

6.2.2 MRI protocol (FIG 6.1)

Subjects were scanned in their respective centres 24 weeks after the start of the treatment trial. All scans were performed on 1.5T scanners. Sequences were prescribed as 46 contiguous axial oblique 3mm slices with a 256 x 256 matrix and a 250mm x 188mm FOV. Before scanning, a cannula attached to a long line was inserted into the antecubital vein of each subject, to allow for the administration of Gd-DTPA while keeping the subject's position constant within the scanner. A pre-contrast FSE sequence (TR= 3000 to 3300 ms; TE= 15 to 24 ms and 90 to 98 ms; 1 excitation; acquisition time approximately 5 min) was taken initially. This produced a T_2 weighted and a PD weighted image, both of which were used for lesion identification. T_1 weighted SE sequences (TR= 500 to 650 ms; TE= 15 to 20 ms; 1 excitation; acquisition time approximately 6 min) were then obtained prior to, and starting 2, 9, 20 and 40 minutes following a bolus intravenous injection of Gd-DTPA (0.3mmol/kg London, Amsterdam, 0.15mmol/kg Toronto). The timings at which SI was read at each scan were taken to be at the completion of each scan, i.e. at 8, 15, 26 and 46 minutes following contrast administration respectively. To ensure comparable intensity in T_1 weighted images before and after contrast administration, the initial radiofrequency amplifier gains for T_1 weighted sequences in each subject were kept constant throughout.

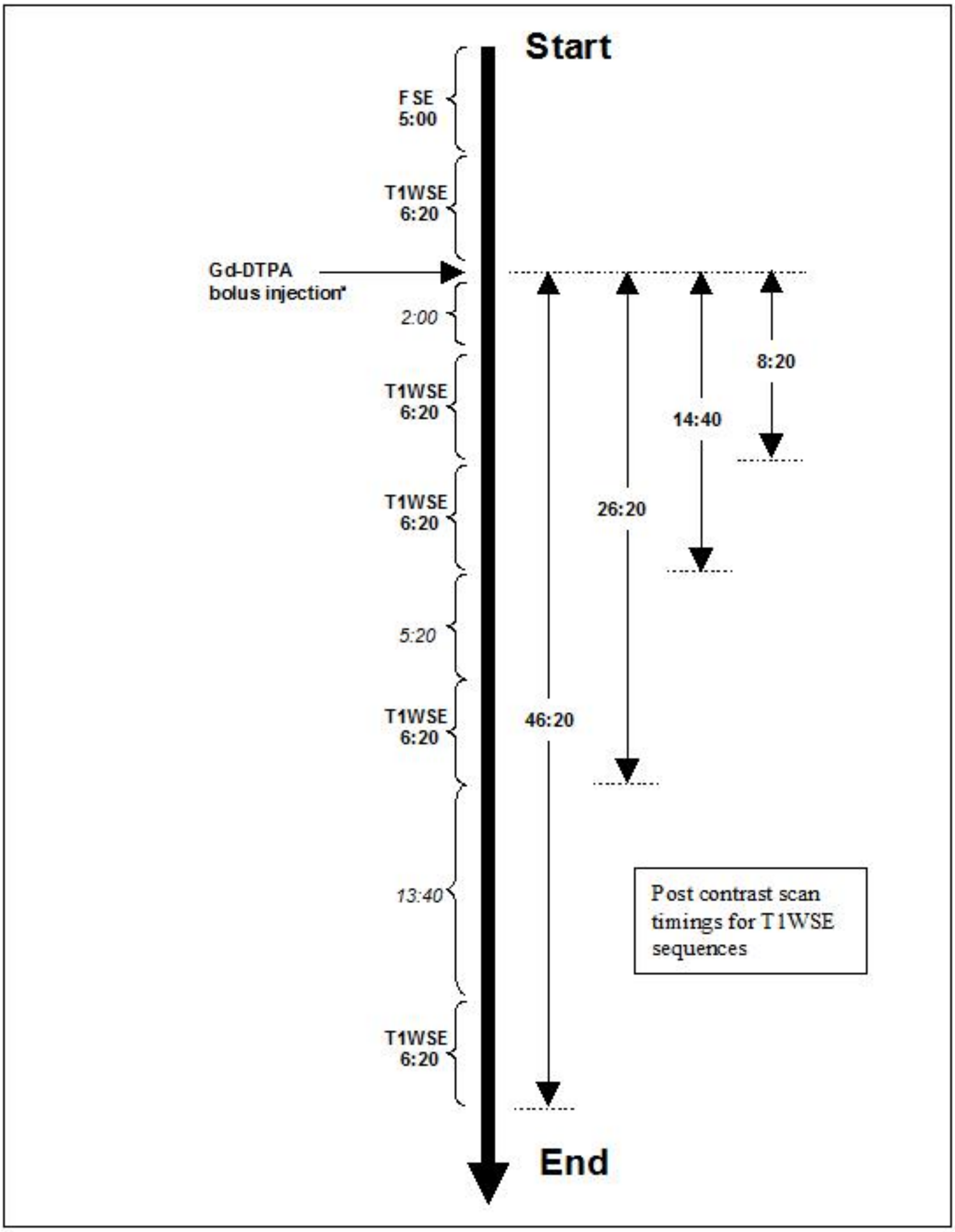

FIG 6.1 Scan protocol timeline for each subject. Unless otherwise specified, figures are in minutes and seconds. Figures to the left of the central vertical arrow represent the time elapsed for subsequent MR sequences and related actions. Figures in italics represent the time intervals between subsequent sequences. Double-headed arrows represent the post-contrast timing of the serial T_1 weighted scans. Gd-DTPA was administered as a bolus injection over 2 minutes, with scanning resuming 2 minutes after its completion. Abbreviations: FSE-Fast Spin Echo, T1WSE-T_1 weighted spin echo

[a]0.3mmol/kg for 18 subjects, 0.15mmol/kg for 22 subjects

6.2.3 Image Registration

For each subject, the PD weighted component of the FSE sequence was registered to the pre-contrast T_1 weighted sequence using a mutual information registration programme (Studholme *et al.,* 1999). Subsequent, post-contrast T_1 weighted sequences were then registered to the pre-contrast T_1 weighted sequence using an adapted co-registration protocol (Woods *et al.,* 1992). Co-registration spatially aligned the images within a series, allowing the accurate evaluation of T_1-weighted SI change resulting from Gd administration.

6.2.4 Image Analysis:

Images were analysed by a single observer (DS), unaware of the subjects' history and treatment, using a Sun workstation (Sun Microsystems, Mountain View, CA, USA) and dispimage display software (Plummer, 1992). Visibly non-enhancing lesions were defined as being hyperintense on pre-contrast T_2 and PD weighted sequences, but which did not enhance to the eye on post-contrast T_1 weighted scans. These were identified on the co-registered PD weighted sequence, where ROIs were described around them. Lesions which showed visible enhancement on post-contrast T_1 weighted scans were excluded from the analysis. For each ROI describing a lesion (ROI_{lesion}), a matched ROI was placed in the contralateral NAWM (ROI_{NAWM}) (FIG 6.2). Where it was not possible to do this, the lesion was excluded from the analysis. ROI_{NAWM} provided a basis of comparison from which the SI change of the ROI_{lesion} could be measured in the primary analysis. Each visibly non-enhancing lesion described on the PD weighted image was also designated as T_1- hypointense or isointense. A lesion is designated as

T_1- hypointense if it has a lower SI to the eye than the surrounding NAWM in the pre-Gd T_1 weighted sequence. SI change in response to Gd was quantified, and was used to infer BBB leakage.

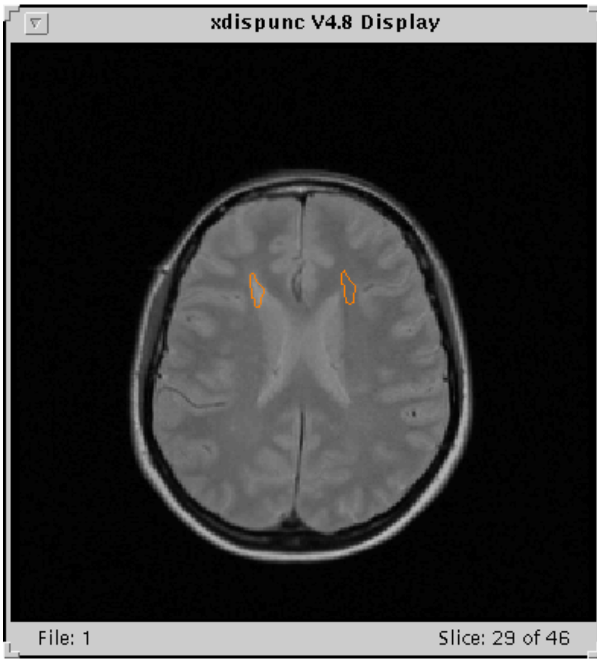

FIG 6.2 ROI_{lesion} were described on a PD weighted image which was registered to the pre-contrast T_1 weighted sequence. For each ROI_{lesion}, a paired ROI_{NAWM} was described in the contralateral NAWM

6.2.5 Outcome measures and statistical analysis

As log transformation of the SI improved the normality of the data and stabilised variance, the analysis was performed with log (SI).

The primary aim of the study was to investigate for low grade BBB leakage from visibly non-enhancing lesions in a multi-centre setting using contrast-enhanced MRI, and to explore whether there might be a modifying influence of natalizumab treatment on such leakage from visibly non-enhancing lesions, using NAWM as a covariate.

Secondary outcome measures assessed for a modifying influence of natalizumab treatment in:

1.SI change in ROI_{lesion} alone, (without SI in paired ROI_{NAWM} as a covariate)
2. SI change in ROI_{NAWM}

SI change in T_1- hypointense and T_1- isointense lesions were also compared, and the influence of natalizumab on SI change was compared in either lesion subtype.

Primary analysis was performed using a multilevel, multivariate model (Goldstein, 1995), allowing for possible dependencies within lesions belonging to the same subject, with a separate response variable for each of the post-contrast time points. Other covariates taken into account by the model were centre/Gd dosage differences, pre-contrast SI in $ROI_{lesion,}$ and paired ROI_{NAWM} SI. The model allowed for testing for differences between treatment arms at individual time points, as well as a joint (global) test which assessed the null hypothesis of no differences between treatment arms at any of the last three time points. The pre-specified selection of the last three time points in the joint test was because of the potentially larger contribution of intravascular Gd to the initial rise in SI on the first post-contrast scan. Secondary analyses were implemented within this model framework by altering the covariate terms. Statistical significance was taken to be at $p<0.05$. Analysis was implemented using MLwiN2.0

6.3 Results

6.3.1 Descriptive data (Table 6.1)

Table 6.1 Descriptive data of subjects volunteering in the study. Values are in median(range) unless otherwise stated. Total T_2 lesion load per subject is from data taken from the AFFIRM study for the relevant subjects at week 0. Age, gender distribution, EDSS and distribution of treatment arms were similar across the 3 centres

	Placebo Group (n=13)	Treated Group (n=27)	Entire study (n=40)
Age	33 (25-48)	38(19-50)	38 (19-50)
Male (%)	4 (30%)	10 (37%)	14 (35%)
Disease Duration	5.5 (1.5-21.5)	6.5 (1.5-23.5)	6.0 (1.5-23.5)
EDSS	1.5 (0-5.5)	3.0 (0-4.5)	2.25 (0-5.5)
Total T_2 lesion load per subject in mls	8.6 (1.0- 83.3)	12.9 (0.9-44.0)	10.4 (0.9- 83.3)

40 subjects were scanned (22 in Toronto, 7 in London and 11 in Amsterdam). 27 of the subjects had been randomized to the treatment cohort and were receiving monthly infusions of natalizumab 300mg. Age, gender distribution, disease duration and EDSS were similar between treatment arms and centres. 8 out of 13 subjects (62%) in the placebo cohort and 1 out of 27 subjects (4%) in the treatment cohort showed visible enhancement with Gd. This difference in the number of subjects showing Gd enhancement between the treatment and placebo cohort at 24 weeks is in keeping with findings in the main AFFIRM trial after 52 and 104 weeks of treatment(Miller *et al.,* 2007, Polman *et al.,* 2006).

In total, 1812 ROI pairs were studied, of which 1159 ROI's were of T_1- hypointense lesions. Between 4 and 111 ROI pairs were studied per subject, the median number studied per subject being 40.5 (Table 6.2). The number of ROI pairs studied per subject did not differ significantly between centres.

Table 6.2 Median number of Paired ROIs studied per subject, categorised by centre. Unless otherwise specified, numbers in brackets are the range of values. The numbers of ROIs studied per subject did not differ significantly between the centres.

	London (n=7)	Toronto (n=22)	Amsterdam (n=11)	**Total study (n=40)**
T_1- hypointense lesions	22 (7-44)	22.5 (2-87)	31 (4-79)	**25 (2-87)**
T_2 hyperintense lesions	56 (18-73)	36.5 (4-97)	39 (7-111)	**40.5 (4-111)**

6.3.2 Low grade BBB leakage in visibly non-enhancing lesions (Table 6.3)

Table 6.3 Mean percentage change from pre-contrast SI in ROI_{lesion} and ROI_{NAWM} . All paired differences between changes in ROI_{lesion} and ROI_{NAWM} are significant to $p<0.01$

Centre	**1st timepoint**		**2nd timepoint**		**3rd timepoint**		**4th timepoint**	
	Lesion	**NAWM**	**Lesion**	**NAWM**	**Lesion**	**NAWM**	**Lesion**	**NAWM**
Toronto	**2.5**	**1.2**	**1.7**	**0.4**	**1**	**-0.3**	**0.7**	**-0.9**
Amsterdam	**3.3**	**2.5**	**3.3**	**2.3**	**3**	**2**	**2**	**1.1**
London	**4.1**	**2.5**	**3.5**	**2**	**2.8**	**1.4**	**1.9**	**0.7**
Entire Study	**3.1**	**1.9**	**2.6**	**1.2**	**1.9**	**0.7**	**1.3**	**0**

SI change in visibly non-enhancing lesions was consistently greater than in paired NAWM at all post-contrast time points in all centres ($P<0.01$), indicating subtle, but consistent and detectable leakage in visibly non-enhancing lesions.

6.3.3 Treatment arm analysis (Table 6.4)

Table 6.4 Mean percentage change in ROI[a] SI at each post-contrast timepoint, divided into treatment arm. Numbers in parentheses are standard deviations. Analysis adjusting for centre and baseline values found no significant difference between treatment arms in any of the ROI types below.

	T_2 lesions		NAWM		T_1- hypointense lesions		T_1- isointense lesions	
Timepoint	natalizumab	placebo	natalizumab	placebo	natalizumab	placebo	natalizumab	placebo
1	3.2 (3.1)	3.0 (2.5)	1.8 (2.6)	2.1 (2.5)	3.5 (3.2)	2.9 (2.6)	2.6 (3.0)	3.1 (2.3)
2	2.1 (2.5)	2.7 (2.8)	1.0 (2.6)	1.6 (2.6)	2.8 (3.3)	2.6 (3.0)	2.1 (3.0	2.8 (2.5)
3	2.0 (3.4)	1.7 (3.0)	0.7 (3.2)	0.6 (2.7)	2.4 (3.6)	1.6 (3.1)	1.3 (2.9)	1.9 (2.7)
4	1.3 (3.1)	1.4 (2.8)	0.0 (2.7)	0.0 (2.5)	1.6 (3.2)	1.5 (3.1)	0.8 (2.9)	1.2 (2.3)

[a]crude means, not adjusted for centre and baseline values, and will thus not correspond closely to the model-based estimated treatment effects given in the text.

Analysis of the influence of natalizumab on BBB leakage revealed no evidence of a treatment x centre/Gd dosage interaction (P=0.90 for the global test), indicating that there was no evidence of a different natalizumab effect in different centres/Gd dosages.

6.3.3.1 Treatment arm analysis of SI change in ROI_{lesion}

A joint test involving the last 3 timepoints revealed no evidence of difference in SI change in ROI_{lesion} between treatment and placebo groups (chi-square 4.2 (df=3),P=0.24), adjusting for pre-contrast lesion SI, paired contralateral NAWM SI and centre/dosage. Analysis of individual timepoints revealed that treatment with natalizumab was associated with non-significant, small % reductions in SI change in ROI_{lesion} when compared against the placebo group at each post-Gd timepoint. (Mean natalizumab-associated change in SI at 1st timepoint: -0.37%; 95%CI -1.1%, 0.3%, P=0.30; 2nd timepoint: -0.65%; 95%CI -1.4%, 0.1%, P=0.08; 3rd timepoint: -0.30%; 95%CI -1.2%, 0.6%, P=0.5; and 4th timepoint: -0.52%; 95%CI -1.3, 0.2, P=0.16).

Removing SI in paired ROI_{NAWM} as a covariate did not substantially change the findings of the influence of natalizumab on SI change in ROI_{lesion}. (Joint test chi-square 3.7 (df=3), P=0.29, with no substantial alteration of the p values in individual timepoints).

6.3.3.2 Treatment arm analysis of SI change in ROI_{NAWM}

No difference was observed between treatment arms in the SI change of NAWM (n=1812, joint test chi-square 3.1 (df=3), P=0.37, P values for respective timepoints 0.30, 0.19, 0.84, 0.55).

6.3.4 Leakage from T_1- hypointense vs T_1- isointense lesions

A variation existed between different centres in the proportion of ROI_{lesion} that were classified as T_1- hypointense lesions (Table 6.2). This could have arisen from a number of contributing factors, including differences in scanners and sequences, as well as differences in the sampling of lesions. Alternatively, such an observed difference could reflect real differences in the composition of visibly non-enhancing lesions in the subjects participating in the study. However, by adjusting for centre (as well as pre-contrast lesion SI and contralateral NAWM SI and treatment group), the analysis by lesion subtype allowed for centre differences in the proportion of T_1- hypointense lesions.

When comparing the post-contrast SI change between T_1- hypointense and T_1- isointense ROI_{lesion}, a borderline difference was detected in the 2nd post-contrast timepoint (mean SI change of hypointense ROI_{lesion} was 0.28% less than isointense ROI_{lesion}; 95%CI 0.56%, 0.002%; P=0.049). No difference was detected in any of the other timepoints (P= 0.43, 0.80, 0.21 for the 1st, 3rd and 4th timepoints respectively) or when the last 3 timepoints were tested jointly (P=0.12). When comparing the influence of natalizumab on lesion subtypes, ie hypointense vs isointense, no evidence was found of an interaction between lesion subtype and treatment over the last three time points (chi-square 2.074, df=3, P=0.557).

6.4 Discussion

6.4.1 Possible contribution of intravascular Gd to observed changes

A possible confounding factor in the usage of T_1 weighted SI change in the inference of BBB leakage would be the contribution of intravascular Gd to SI change. Following a bolus injection, intravascular Gd concentration reaches a peak rapidly, before following a biexponential curve with a mean distribution half life of the order of 10 minutes,(Tofts and Berkowitz, 1994) diffusing into the extracellular spaces of the body, and being excreted principally through the kidneys. In this study, the contribution of intravascular Gd would have been greatest at the initial post-contrast timepoint, receding steadily with each successive timepoint. The selection of the latter 3 timepoints in the joint statistical tests was designed to take into account the lower contribution of intravascular Gd in these timepoints.

6.4.2 Low grade BBB leakage in visibly non-enhancing lesions

A consistent finding in this study was the low grade, detectable leakage in visibly non-enhancing lesions, compared with contralateral NAWM which was present up to 45 minutes following the administration of contrast. This was apparent in all centres, and in both T_1- hypointense as well as T_1- isointense lesions. That such differences were sustained over all timepoints up to 45 minutes strongly indicates BBB leakage, rather than a larger blood volume, or higher perfusion, in visibly non-enhancing lesions. This is in agreement with findings from the previous, single centre contrast-enhanced study in multiple sclerosis (Silver *et al.,* 2001b), and supports the approach of quantitative contrast-enhanced imaging as a way of detecting low grade BBB leakage in visibly non-enhancing lesions in a multi-centre study. These findings are also in line with histological evidence, in terms of tight junction disruption (Kirk *et al.,* 2003) and fibrin deposition (Claudio *et al.,* 1995 ,Kwon and Prineas, 1994), of widespread BBB leakage from non-active lesions.

6.4.3 Treatment arm analysis of BBB leakage in visibly non-enhancing lesions

The ability of natalizumab to suppress new lesion formation and acute, overt BBB disruption has been demonstrated in a series of animal (Yednock *et al,.* 1992) and human (Tubridy *et al.,* 1999; Miller *et al.,* 2003; 2007) studies. It is thought that natalizumab, in blocking α4 integrin, interferes not only with the initial event of lymphocyte adhesion and trafficking, but also with the subsequent events of activation (Damle and Arrufo, 1991), proliferation (Burkly *et al.,* 1991) and cytokine release-events critical in the formation of lesions and in the initial, overt BBB breakdown (Minagar and Alexander, 2003). The lack of a significant difference in post-contrast signal changes in non-enhancing lesions between treatment arms suggests that the more subtle leakage from such lesions is due to processes that are largely or entirely independent of $\alpha 4$ integrin. Histologically, vessels in non-active MS lesions often exhibit reparative wall thickening in concert with fibrin deposition, (Adams *et al.,* 1985) suggesting that leakage from such lesions might at least in part be due to incomplete BBB repair, with some permanent structural and functional changes following resolution of inflammation. Supporting this hypothesis are findings from morphometric analysis of capillaries in non- active MS lesions, which have demonstrated a reduction in mitochondria and a rise in pinocytic vesicles, in concert with evidence, in terms of extravascular fibrin deposits, of BBB disruption. (Claudio *et al.,* 1995) Such findings imply a profound shift in the physiology of these vessels to a more energy deficient state, hindering the energy dependent transport mechanisms essential in maintaining the BBB. It is conceivable that such changes could contribute to the low grade BBB leakage detected in the MS lesions in this study.

6.4.4 Leakage from T_1- hypointense vs T_1- isointense lesions

The finding of a slightly higher (0.28%) SI change in T_1- isointense than in hypointense lesions in the 2^{nd} post-contrast timepoint (15 minutes post-contrast) is an isolated finding. No similar difference is seen in the other timepoints, most notably in the 1^{st} post-contrast timepoint, indicating that the difference in the 2^{nd} timepoint is not due to differences in intravascular Gd. Moreover, a joint test involving the last 3 timepoints, including the 2^{nd} post-contrast timepoint, revealed no difference in SI change between hypointense and isointense lesions. The overall picture in this study is therefore of very little difference in BBB leakage between T_1- hypointense and T_1- isointense lesions. Such a finding suggests that low grade leakage in both types of lesions may occur through common or similar mechanisms, involving more permanent changes to the BBB. The absence of a differential effect of natalizumab on leakage in the 2 lesion subtypes suggests that such mechanisms in both subtypes are largely independent of $\alpha 4 \beta 1$ integrin.

6.4.5 SI change in NAWM

This study found no evidence of any difference in the SI change in NAWM between natalizumab and placebo treated groups. However, as there were no healthy controls for comparison, it is uncertain if the post-Gd SI changes seen in NAWM reflect abnormal BBB leakage *per se*.

6.4.6 Limitations imposed by the use of contralateral NAWM as a covariate

In order to incorporate contralateral NAWM as a covariate, a number of visibly non-enhancing lesions were excluded as it was not possible to find a contralateral area of NAWM in which to place a matching ROI_{NAWM}. This was more likely in subjects with lesions covering large areas on both sides of the brain. There is therefore a possibility that lesions in subjects with larger T_2 lesion loads are under represented. Total T_2 lesion volume per subject however, did not differ significantly between the natalizumab and the placebo group. It is unlikely therefore that the main analyses by treatment arm would be affected by this methodological limitation. It was found in this study that analysis without including contralateral NAWM as a covariate did not change the study findings, and there was no significant change in the related P values. This suggests that it is feasible to modify the design of future contrast enhanced BBB studies to include all visibly non-enhancing lesions, with a related, smaller analysis employing the SI change in contralateral NAWM as a covariate, where possible. Such a modification in design would incorporate a greater proportion or visibly non-enhancing lesions, and has been undertaken in the study described in the next chapter.

6.4.7 Gd Dosage differences between centres

Subjects from a single centre inadvertently received 0.15mmol/kg of Gd-DTPA instead of a triple dose (0.3mmol/kg). These constituted 22 out of the 40 subjects studied. The different dose of Gd-DTPA resulted in post-contrast SI curves of different magnitude. Moreover, a proportion of lesions which would have visibly enhanced following triple dose Gd-DTPA could have lost their visible enhancement and been re-classified as visibly non-enhancing, with a lower Gd dose. (Silver *et al.,* 1997; Filippi *et al.,* 1996). Nonetheless, the balance between treated and placebo subjects is similar in the 3 centres, and statistical analysis, which took into account centre and Gd dosage differences, revealed an absence of centre/Gd dosage x treatment interaction. Therefore, for the purpose of investigating for differences in post-contrast SI change between treatment and placebo arms, the differences in Gd dosage do not appear to compromise the main findings of the study.

6.5 Summary and conclusion

This substudy of the AFFIRM trial of natalizumab monotherapy versus placebo has demonstrated that quantitative contrast-enhanced imaging is a viable approach in detecting low grade BBB leakage from visibly non-enhancing lesions in a multi-centre trial setting, and that such leakage is a consistent feature in both T_1- hypointense and T_1- isointense lesions in MS. The finding that the detectable BBB leakage is not significantly lower in natalizumab-treated subjects suggests that it occurs predominantly or entirely through mechanisms other than those mediated by $\alpha4\beta1$ integrin. Such leakage may occur through more permanent changes in the vascular wall, with a chronic, incomplete BBB repair, as suggested by findings from histological studies of vessels in non-active lesions, and will be studied in detail in the next chapter using an alternative MRI marker to T_1 weighted SI change.

CHAPTER 7

Quantification of subtle blood brain barrier disruption in non- enhancing lesions in multiple sclerosis: A study of disease and lesion subtypes

7.1 Introduction

The use of Gd chelated contrast agents such as Gd-DTPA has been central to the investigation of BBB disruption using MRI. Gd does not traverse the intact BBB, and local Gd enhancement has been correlated with histological markers of BBB breakdown in EAE - a widely recognized animal model of MS (Hawkins *et al.,* 1990). Gd enhanced MRI studies have been useful in detecting focal BBB disruption in association with new or actively inflamed lesions in MS (Bruck *et al.,* 2007; Grossman *et al.,* 1986; Katz *et al.,* 1993; Miller *et al.,* 1988; Lai *et al.,* 1996).

Most Gd enhanced MRI studies in MS have been qualitative investigations, relying on visible post-Gd enhancement of lesions on T_1 weighted images to identify overt BBB disruption and leakage. Quantitative investigations, where the Gd mediated change is measured, could facilitate the detection of more subtle and low grade BBB leakage. Such studies have been performed in the ischaemic rat brain (Harris *et al.,* 2002) and intracranial tumours (Zhu *et al.,* 2000). Using the proportional change of T_1 weighted signal intensity as a marker for BBB leakage, subtle leakage from visibly non-enhancing lesions up to 40 minutes following triple dose Gd-DTPA has been demonstrated (Silver *et al.,* 2001).

Conventional MRI markers of MS, such as Gd enhancement and T_2 weighted lesion load, correlate only modestly with clinical disability and relapse rate (Kappos *et al.,* 1999; IFNB MS Study Group and University of British Columbia MS/MRI analysis Group, 1995). A potential factor that could lead to such a dissociation is subtle but widespread BBB disruption occurring in the large majority of MS lesions that are non-enhancing, in post-contrast scans, to the eye. Such disruption could, if prolonged and ubiquitous, contribute to ongoing tissue damage (demyelination and axonal loss) and hence disability through the continuous low grade leakage of inflammatory cells and soluble mediators of inflammation into surrounding central nervous system parenchyma. Therefore, the use of MRI to detect such low grade leakage, and to determine if such leakage relates to disease course and disability, is of relevance.

This present study used $\Delta R_1/\Delta t$ as a measure of BBB leakage. $\Delta R_1/\Delta t$ is derived from Gd-induced changes in measured T_1 and represents a more fundamental, more sensitive and potentially more reproducible MR measure than T_1 weighted SI change. Visibly non-enhancing lesions were investigated for subtle BBB disruption. BBB leakage was also compared between non-enhancing lesions which were hypointense on pre-contrast T_1 weighted scans (T_1- hypointense lesions) and those which were isointense (T_1-isointense lesions); the former - when chronic and persistent - are associated with greater axonal loss and extracellular matrix destruction, as well as disability.(van Walderveen *et al.,* 1998, Barkhof *et al.*, 2003). Lesions from RRMS and SPMS patients were studied for possible differences of leakage across the 2 clinical subtypes. As eight of the nineteen patients were on disease modifying treatment, potential interactions with treatment status were also investigated. The relationship of the BBB leakage measure with EDSS, age and gender was also studied.

7.2 Methods

7.2.1 Patients

Nineteen patients with clinically definite MS (Poser *et al.,* 1983) were recruited from the outpatient department at the National Hospital for Neurology and Neurosurgery. All patients had a neurological history taken and a physical examination performed by a single observer (DS). Exclusion criteria included pregnant or breast feeding women, previous allergy to Gd-DTPA and corticosteroid use within the previous 2 months. Each patient gave full, written, informed consent to participate in the study, which was approved by the joint research ethics committee of the National Hospital for Neurology and Neurosurgery and the Institute of Neurology

7.2.2 MRI acquisition protocol

All imaging was performed using a 1.5 T Signa, superconducting system with a standard quadrature headcoil. (GE Medical Systems, Milwaukee, Wisconsin, USA). Sequences were prescribed as 28 contiguous axial oblique 5mm slices with a 256 x 256 matrix and a 240mm x 180 mm Field of View. Before starting to scan, a cannula was inserted into the antecubital vein of the patient. This was connected to a long line which was flushed with normal saline. The use of the long line enabled the patient to be maintained in the same position throughout the whole MR acquisition during and after the administration of Gd-DTPA, which was normally performed over 2 minutes.

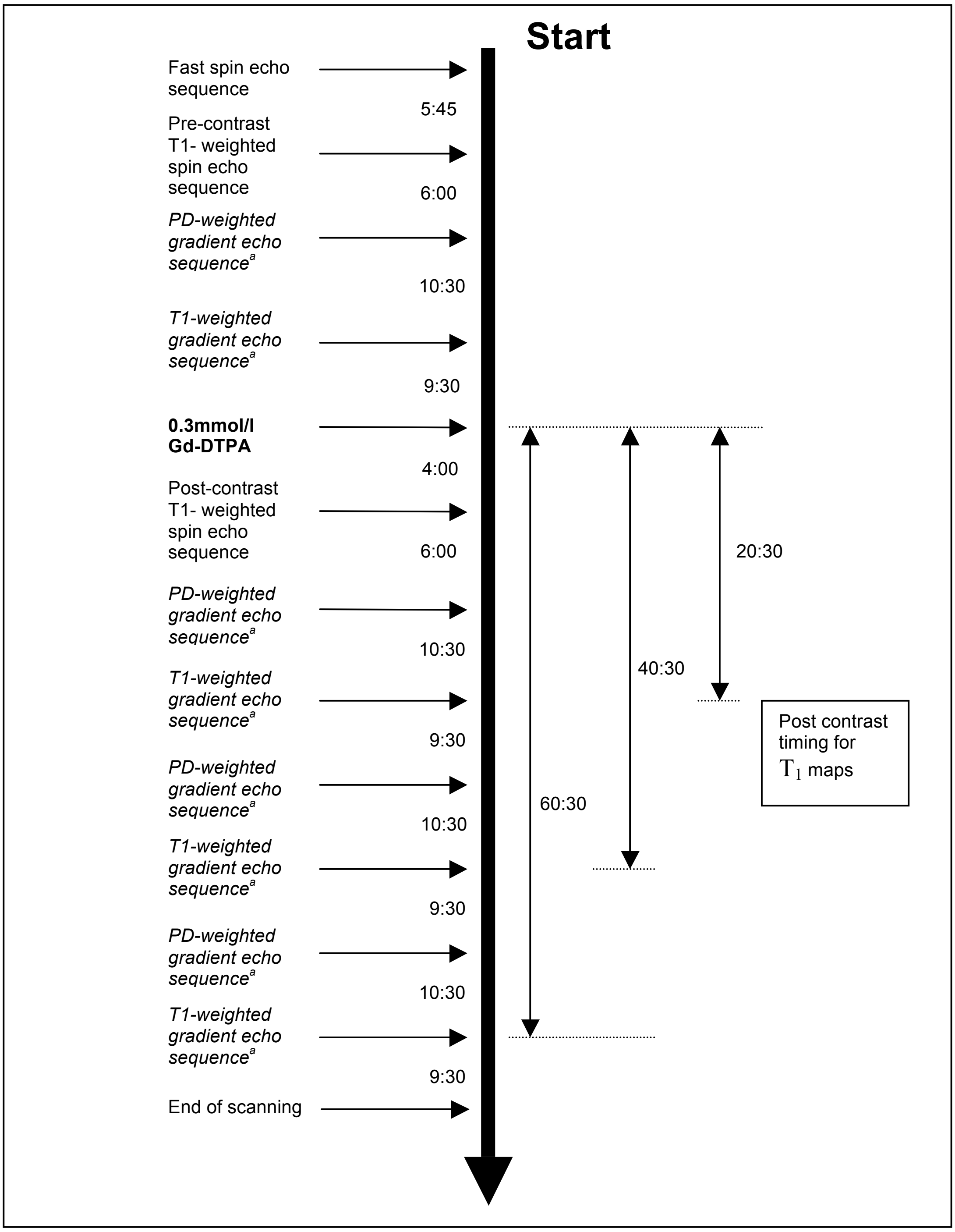

FIG 7.1:Scan protocol timeline for each patient. Unless otherwise specified, figures are in minutes and seconds. Figures to the left of the central vertical arrow represent the time elapsed between subsequent MR sequences and related actions. Figures adjacent to the double-headed arrows represent the post contrast timing of the serial T_1 maps. Gd-DTPA is administered over 2 minutes, with scanning resuming 2 minutes after its completion.

[a]sequences used to make up T_1maps

FIG 7.1 illustrates the order and timing of sequences obtained for each patient. Radiofrequency amplifier gains in each patient were kept constant throughout the scan.

This ensured that images obtained before and after the Gd administration were of comparable intensity, and facilitated the identification and description of lesions (visibly enhancing vs non-enhancing, T_1- hypointense vs T_1- isointense) to be carried out in a standardized manner.

7.2.2.1 Sequences for lesion identification

A pre-Gd FSE sequence (TR= 2000ms; TE= 19ms and 95 ms; ETL=8; acquisition time 5min 45s) was acquired, producing PD and T_2-weighted images on which lesions were identified. A T_1 weighted SE sequence (TR= 540ms; TE= 20ms; NEX=1; Acquisition time= 6min.) was performed before and from 2 minutes after the completion of Gd-DTPA administration (FIG 7.1), to enable the identification of: (i) T_1- hypointense lesions pre-contrast and (ii) visibly Gd enhancing lesions post contrast.

7.2.2.2 T_1 map construction

PD weighted (TR= 1500ms, TE= 11ms, flip angle= 45 degrees, NEX= 1.5, Acquisition time= 10min 30s) and T_1 weighted (TR=50ms, TE =11ms, flip angle= 45 degrees, NEX= 3, Acquisition time= 9min 30s) GE sequences were performed prior to, and in series after the completion of the postcontrast T_1 weighted SE sequence (FIG 7.1). Alignment of the initial PD and T_1 weighted images was achieved using a mutual information registration technique (Studholme *et al.,* 1999). Subsequent T_1 weighted and PD weighted GE sequences were then registered to the initial, co-registered scans using an adapted co-registration protocol (Woods *et al.,* 1992). A T_1 map at each timepoint was then calculated from the registered PD and T_1 weighted images (Parker *et al.,* 2001 *).* This relates the ratio of the PD and T_1 weighted signal intensities to a look-up table, accounting for slice profile and B_1 non-uniformity. The timing of each post-Gd T_1 map was taken as the start of its T_1 weighted GE component, which was roughly 20, 40 and 60 minutes after the start of Gd-DTPA administration. (FIG 7.1)

7.2.3 Image Analysis

All image analysis was performed using a Sun Workstation (Sun Microsystems, Mountain View, CA, USA) and Dispimage display software (Plummer, 1992). All analysis was performed blinded to patient demographic and clinical data.

Visibly non-enhancing lesions were identified on the co- registered PD weighted component of the FSE sequence and checked against the post-Gd T_1 weighted SE sequence to exclude those with visible enhancement. A lesion is defined as showing visible enhancement if on the post-Gd T_1 weighted scan, it appears brighter to the eye than its NAWM and to its corresponding image on the pre-Gd T_1 weighted sequence. The lesions were then outlined on the co-registered PD weighted image using a semiautomated lesion contouring technique (Plummer, 1992). Wherever possible, for each ROI describing a lesion, a matching ROI was placed in the contralateral normal appearing brain tissue (NABT) (FIG 7.2). These paired ROI's formed a subset of data from which leakage from visibly non-enhancing lesions could be compared against that of matched NABT.

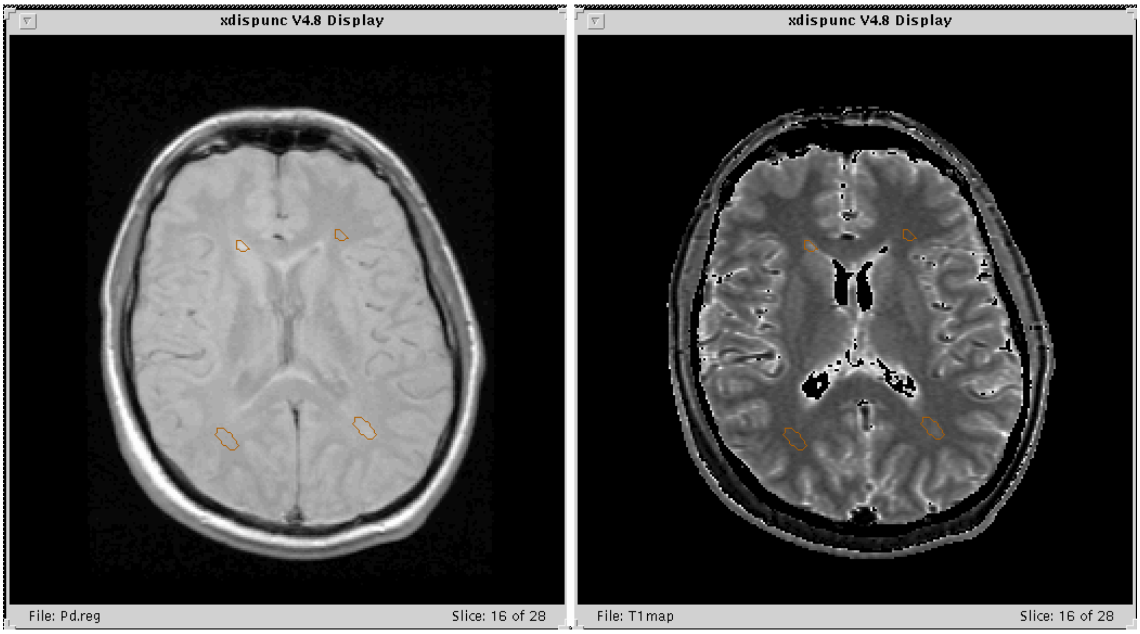

a b

FIG 7.2 Coregistered PD weighted image (a) on which focal non-enhancing lesions are identified. ROIs are placed on the lesions, with matched ROIs in the contralateral NABT. The resultant ROIs are then placed on T_1 maps (b) from which T_1 for the ROI is measured and the R_1 is calculated.

Additionally, each visibly non-enhancing lesion was visually designated as hypointense or isointense relative to the surrounding NAWM in the pre-Gd T_1 weighted SE sequence. The lesion cross sectional area (CSA) was also recorded for each lesion. This was defined as the area of the ROI describing the lesion on the T_2 weighted image, and in the case where a lesion traverses multiple slices, the area of the largest ROI describing the lesion.

ROIs were also described around visibly enhancing lesions identified on the post contrast T_1 weighted image.

All ROIs were superimposed onto the serial T_1 maps (FIG 7.2). The mean T_1 value within each ROI at each timepoint on the T_1 map was then recorded.

7.2.4 Detection of subtle BBB leakage

Longitudinal relaxation rate (R_1), is defined as the inverse of T_1. ΔR_1 is the change in R_1 following Gd administration. This is described in the following equation:

$$\Delta R_1 = \frac{1}{T_1} - \frac{1}{T_{1(0)}} = r_1 C_t(t)$$

$C_t(t)$ = local concentration of Gd at time t following its administration
T_1= value of T_1 at the time t
T_{10}= value of T_1 before Gd administration
r_1= relaxivity of Gd, a constant[1]

From the above equation, the gradient of ΔR_1 over time elapsed ($\Delta R_1/\Delta t$) is proportional to the change in local Gd concentration over time ($C_t(t)$). $\Delta R_1/\Delta t$ was therefore used to infer BBB disruption in this study.

7.2.5 Statistical analysis

For the lesion level analysis, the slice with the largest CSA was chosen to obtain the largest representative sample. Analyses of response variables ($\Delta R_1/\Delta t$) at separate timepoints used hierarchical linear regression (Baltagi, 1995) on two levels, patient and lesion, with random patient intercepts and fixed effects for the covariates of interest. The analysis of paired lesions vs contralateral NABT was similar, but using the

[1] 4.5 s-1mM-1 from in-vitro studies (Tofts and Berkowitz, 1994; Tofts *et al.,* 1999).

difference ($\Delta R_1/\Delta t_{lesion}$ minus $\Delta R_1/\Delta t_{NABT}$) as response variable.

In the case of visibly non-enhancing lesions, the covariate terms included in the regression models were at lesion level: log lesion CSA (log transformation greatly improved normality without affecting the interpretability or validity of the analysis), and whether a lesion was T_1- hypointense. Covariate terms at patient level included age, total lesion volume (continuous variables) and gender, disease subtype, treatment with disease modifying agents such as IFNβ or glatiramer acetate, EDSS > 3 (indicators).

Where Normality of regression residuals could not confidently be assumed, non-parametric bias-corrected bootstrap (Carpenter and Bithell, 2000) estimates (1000 replicates with patient clustered resampling) are reported.

Results of the analyses of post-Gd leakage have been expressed as paired differences in $\Delta R_1/\Delta t$ (as in the analysis of lesions vs contralateral NABT), or, in circumstances where analysis is between non-paired covariates (such as RRMS vs SPMS lesions), in mean differences in $\Delta R_1/\Delta t$. Results were expressed in this manner to convey the magnitude of difference in inferred leakage between the covariates studied. Analyses were implemented in Stata 8.2 (Stata Corporation, College Station, Texas, USA).

7.3 Results

Table 7.1 Demographic data of patients recruited into the study. All values are median (range) unless otherwise stated.

	RRMS (n=10)	**SPMS (n=9)**
Number of male patients (%)	4 (40%)	4 (44%)
Number of patients with visible enhancement (%)	4 (40%)	3 (33%)
Number of patients on disease modifying treatment (%)	4 (40%)	4 (44%)
Age, years	36 (27-53)	46 (26-64)
Disease duration, years	4.5 (1-18)	19 (4-28)
EDSS	2 (1.5-3.5)	6 (3-7.5)
total lesion volume, mls	4.7 (0.2-12.9)	8.4 (3.2- 29.6)

7.3.1 Patient Data

The demographic data of the patients are shown in table 7.1. Nineteen patients (nine with SPMS and ten with RRMS) participated in the study. Due to the extended duration of the scan series, (over 90 minutes for the entire series), five patients (four with SPMS and one with RRMS) were only able to tolerate the acquisition of 2 instead of 3 sets of post-Gd T_1 maps. In addition, a single RRMS patient reported dizziness during Gd-DTPA administration. The administration was discontinued and the patient consequently received 0.1mmol/kg instead of 0.3mmol/kg of Gd-DTPA. There were no adverse events following the procedure.

7.3.2 Lesion Data

A total of 581 visibly non-enhancing lesions were identified in all nineteen patients, 238 lesions in RRMS patients and 343 in SPMS patients. Of these, 156 out of the 343 (45%) of the SPMS lesions were T_1- hypointense, as opposed to 80 out of the 238 (34%) RRMS lesions (odds ratio 0.57, p=0.057). In 449 of the 581 lesions, it was possible to describe matching ROI's in the contralateral NABT. Leakage from this subset of lesions was therefore analysed against anatomically analogous contralateral NABT. Three RRMS and three SPMS patients were identified as having visibly enhancing lesions. Between them, 76 enhancing lesions were identified.

7.3.3 Associations between covariates

T_1- hypointense lesions had larger CSAs than isointense lesions by an estimated factor of 2.0, (P<0.001; 95% CI 1.8, 2.3). RRMS patients tended to have smaller lesion CSAs than SPMS, by a factor of 21.4% (P=0.037; 95% CI 1.5%, 37.3%); however, after adjusting for hypointensity, significance is lost (P=0.156), suggesting the difference in CSA between disease types may be at least partly explained by a borderline significant lower proportion of hypointense lesions in RRMS patients (odds ratio 0.57, p=0.057). No association was detected between lesion CSA and EDSS, disease duration, age or gender but, not surprisingly, patients with larger total lesion volume tended to have larger lesion CSA (P=0.002). There was evidence that patients with an EDSS greater than 3 had a higher proportion of hypointense lesions (odds ratio 2.09, 95% CI 1.22, 3.56; P=0.007), but there were no significant associations between T_1- hypointensity and age, disease duration, gender or total lesion volume once EDSS was taken into account. There was no association between being on disease modifying treatment and the other covariates of T_1- hypointense lesion load, age, disease duration, gender, or total lesion volume, or EDSS.

7.3.4 Post Gd changes

7.3.4.1 Visibly enhancing vs visibly non-enhancing lesions

The mean $\Delta R_1/\Delta t$ in visibly enhancing lesions was significantly greater than that in visibly non-enhancing lesions at all timepoints ($p<0.001$ for each timepoint) with no overlap of 95% CIs or of 95% reference ranges (table 7.2).

Table 7.2 Mean Δ $R_1/\Delta t$ in visibly enhancing vs visibly non-enhancing lesions. Values in curved parenthesis are 95% CIs; values in square parenthesis 95% reference ranges. Units in $10^{-3}s^{-1}min^{-1}$

	1st timepoint	2nd timepoint	3rd timepoint
Enhancing Lesions	**41.1(32.6, 49.6) [25.8, 56.4]**	**20.2 (17.3,23.1) [12.7, 27.7]**	**11.1(8.6,13.6) [8.2, 14.1])**
Non-Enhancing Lesions	**4.2 (3.1, 5.2) [-11.0, 19.3]**	**2.1(1.7, 2.6) [-5.3, 9.5]**	**1.7(1.4, 1.9) [-1.1, 4.5]**
Difference in Mean Δ $R_1/\Delta t$ (Enhancing – Non-Enhancing Lesions)	**36.9 (28.9 , 44.9) P< 0.001**	**18.1 (15.3, 20.8) P< 0.001**	**9.4 (6.8, 12.0) P< 0.001**

7.3.4.2 Visibly non-enhancing lesions vs contralateral NABT

The mean paired difference ($\Delta R_1/\Delta t_{lesion}$ minus $\Delta R_1/\Delta t_{NABT}$) between visibly non-enhancing lesions and contralateral NABT was significant at all 3 post Gd-DTPA timepoints ($p \leq 0.001$ for all lesions overall) (table 7.3).

Overall, the paired difference appears to reduce with time. The difference in ($\Delta R_1/\Delta t_{lesion}$ minus $\Delta R_1/\Delta t_{NABT}$) remained significant at all timepoints for both T_1- hypointense and isointense subgroups and for both RR and SPMS subgroups, with the exception of SPMS subgroup lesions at the 3rd timepoint (table 7.3). The paired differences in the lesion and clinical subgroups were not significantly different from one another at any timepoint(table 7.4).

Table 7.3 Mean paired difference in $\Delta R_1/\Delta t$ between lesions and contralateral NABT. Values in parenthesis are 95% CIs. Units in $10^{-3}s^{-1}min^{-1}$

Mean paired difference in $\Delta R_1/\Delta t$ [($\Delta R_1/\Delta t_{lesion}$ - $\Delta R_1/\Delta t_{NABT}$] [a]			
	1st timepoint 449 lesions	**2nd timepoint 449 lesions**	**3rd timepoint 277 lesions**
All lesions	**1.80 (1.16,2.51);P<0.001 [b]**	**1.02 (0.64,1.40);P<0.001**	**0.61 (0.24,0.97);P=0.001**
Isointense	**1.55 (0.60, 2.49);P=0.001**	**0.86 (0.44,1.28);P<0.001**	**0.45 (0.07,0.84);P=0.02 [b]**
Hypointense	**2.17 (1.14, 3.21);P<0.001**	**1.26 (0.79,1.72);P<0.001**	**0.82 (0.24,1.23);P<0.005 [b]**
SPMS	**1.89 (0.65, 3.13);P=0.003**	**1.01 (0.47,1.56);P<0.001**	**0.48 (0.03,1.02);P=0.08 [b]**
RRMS	**1.72 (0.50, 2.94);P=0.006**	**1.03 (0.49,1.57);P<0.001**	**0.68 (0.24,1.14);P<0.005 [b]**

[a]This is not exactly the difference in raw means due to differential weighting in hierarchical model for patients contributing different numbers of lesions.

[b]Bootstrap derived CI and P-value.

Table 7.4 Differences in mean paired difference ($\Delta R_1/\Delta t_{lesions}$ - $\Delta R_1/\Delta t_{NABT}$) in lesion and disease subtypes. Values in parenthesis are 95% CIs. Units in $10^{-3}s^{-1}min^{-1}$

Difference in ($\Delta R_1/\Delta t_{lesions}$ - $\Delta R_1/\Delta t_{NABT}$) between lesion and disease subtypes			
	1st timepoint 449 lesions	**2nd timepoint 449 lesions**	**3rd timepoint 277 lesions**
Hypointense-Isointense	**0.63 (-0.37, 1.62) P=0.2**	**0.40 (-0.08, 0.87) P=0.1**	**0.37 (-0.23,0.88) P=0.29 [a]**
RRMS- SPMS	**-0.17 (-1.91, 1.57) P=0.8**	**0.02 (-0.74,0.78). P=1.0**	**0.20 (-0.51, 0.80)P=0.8 [a]**

[a] Bootstrap derived CI and P-value.

7.3.4.3 Relationship of $\Delta R_1/\Delta t$ with lesion CSA

There was a significant negative association between $\Delta R_1/\Delta t$ and lesion CSA at all timepoints (table 7.5).

Table 7.5 Association between $\Delta R_1/\Delta t$ and lesion CSA. Coefficient is the change in $\Delta R_1/\Delta t$ per doubling of area ($10^{-3}s^{-1}min^{-1}mm^{-2}$)

	Coefficient	95% CI	P-value
1st timepoint 581 lesions	-0.55	-0.80 to -0.30	P<0.001
2nd timepoint 581 lesions	-0.26	-0.37 to -0.14	P<0.001
3rd timepoint 322 lesions	-0.21	-0.33 to -0.09	P=0.001

7.3.4.4 T_1- hypointense vs Isointense lesions

Although there was no univariate (unadjusted) association between $\Delta R_1/\Delta t$ and T_1 hypointensity, the relationship between the two is complicated by the fact that both had a significant association with lesion CSA; after adjusting for lesion CSA, there was a significantly greater $\Delta R_1/\Delta t$ in T_1- hypointense than in isointense lesions at the 1st and 2nd timepoints post Gd-DTPA. The difference reduced with time and was non-significant at the 3rd timepoint. (Table 7.6).

Table 7.6 Mean difference in $\Delta R_1/\Delta t$ between T_1- Hypointense and Isointense lesions (units in $10^{-3}s^{-1}min^{-1}$)

	Difference[a] in $\Delta R_1/\Delta t$: hypointense – isointense	95% CI	P-value
1st timepoint 581 lesions	1.13	0.44 to 1.82	0.001
2nd timepoint 581 lesions	0.41	0.09 to 0.73	0.013
3rd timepoint 322 lesions	0.15	-0.17 to 0.48	0.353

[a]Difference is adjusted for (log) lesion CSA.

7.3.4.5 Comparison of relapsing remitting & secondary progressive MS

Disease subtype was associated with lesion CSA, so again there is the possibility of area confounding the $\Delta R_1/\Delta t$ differences between subtype. Table 7.7 therefore reports area-adjusted results. There was a greater $\Delta R_1/\Delta t$ amongst lesions in RRMS patients at the 1st (also significant before area adjustment) but not the 2nd or 3rd timepoint (also non-significant before adjustment).

Table 7.7 Mean difference in $\Delta R_1/\Delta t$ between lesions in RRMS and SPMS patients (units in $10^{-3}s^{-1}min^{-1}$)

	Difference[a] in $\Delta R_1/\Delta t$: RRMS – SPMS	95% CI	P-value
1st timepoint 581 lesions	1.22	0.12 to 2.42	P=0.04[b]
2nd timepoint 581 lesions	0.07	-0.61 to 0.74	P=0.848
3rd timepoint 322 lesions	-0.03	-0.49 to 0.43	P=0.895

[a]Difference is adjusted for (log) lesion CSA

[b]Bootstrap derived CI and P-value.

7.3.5 Disease Modifying Treatment and other covariates

At the time of scanning, 8 out of the 19 patients were receiving disease modifying treatment. 7 were receiving IFNβ (3 with RRMS, 4 with SPMS with relapses) and 1 patient with RRMS was receiving glatiramer acetate. $\Delta R_1/\Delta t$ was not associated with disease modifying treatment status at any timepoint, neither was there any association between $\Delta R_1/\Delta t$ and age, gender, disease duration, or EDSS.

7.4 Discussion:

7.4.1 Consistent BBB leakage from visibly non-enhancing lesions

The principal study finding was that visibly non-enhancing MS lesions (identified by careful visual inspection and comparison of the pre- and post-contrast T_1-weighted images) had a $\Delta R_1/\Delta t$ that was significantly higher than contralateral NABT and significantly lower than visibly enhancing lesions at all timepoints up to 60 minutes after the injection of 0.3mmol/kg DTPA. These observations are compatible with a low grade BBB leakage in visibly non-enhancing lesions that is distinct from the more overt BBB leakage seen in enhancing lesions. The distinction between the leakage in visibly enhancing and visibly non-enhancing lesions is unambiguous, with non-overlapping 95% reference ranges and differences in magnitude by a factor of 10. Similar differences in magnitude of post-contrast enhancement between visibly enhancing and non-enhancing lesions were found in a previous study utilising Gd-DTPA (Silver *et al.,* 2002b). Together with the histological studies previously discussed (Adams *et al.,* 1985; Gay and Esiri, 1991; Claudio *et al.,* 1995*;* Kwon and Prineas, 1994), our MR-based findings consolidate the evidence for existence of low grade BBB disruption in visibly non-enhancing lesions, many of which will be longstanding. This discernible BBB leakage in non-enhancing lesions was a consistent feature in all the disease subtypes studied, and was present in both T_1- hypointense and isointense lesions, indicating that low grade BBB leakage is a common and relatively non specific feature of visibly non-enhancing MS lesions.

It is important to stress that although low grade BBB leakage appears to be a consistent feature in visibly non-enhancing lesions, such leakage is different in degree and nature from that seen in visibly enhancing lesions. This is mirrored in the differences in the histological appearances of the two populations of lesions. Lymphocytic infiltration and acute inflammation are features of visibly enhancing lesions. In contrast, acute inflammation is rarely observed in visibly non-enhancing lesions. (Adams *et al.,* 1985; Gay and Esiri 1991; Claudio *et al.,* 1995; Kwon and Prineas, 1994). Such differences point toward distinct underlying mechanisms of BBB breakdown in visibly enhancing and non-enhancing lesions, with inflammation underpinning the more florid breakdown in the former and incomplete BBB repair at least partly responsible for the latter.

7.4.2 Potential contribution of intravascular Gd-DTPA to observed changes

A possible confounder of Gd-DTPA enhanced MRI studies on BBB disruption would be the contribution of intravascular Gd to measured $\Delta R_1/\Delta t$. Intravascular Gd concentration reaches a peak shortly after bolus administration, before declining steadily following a biexponential function with a mean distribution half life of approximately 10 minutes, diffusing into the extracellular spaces within the body and being excreted principally through the kidneys (Tofts and Berkowitz, 1994). Intravascular Gd would therefore exert its greatest influence on local ΔR_1 in the earliest timepoint, with a relatively rapid reduction in contribution as time passes. The observed differences in $\Delta R_1/\Delta t$ between lesions and NABT were sustained over the 3 timepoints up to an hour post-Gd. Such a sustained effect points toward changes secondary to BBB leakage, as opposed to intravascular Gd-DTPA.

7.4.3 T_1- hypointense vs T_1- isointense lesions

Because lesions were described on the PD weighted images, the resultant ROI's around T_1- hypointense lesions were often larger than the areas of actual T_1 hypointensity, encompassing within it additional areas of isointensity (FIG 7.3). This has to be borne in mind when interpreting the results of the lesion subtype comparison.

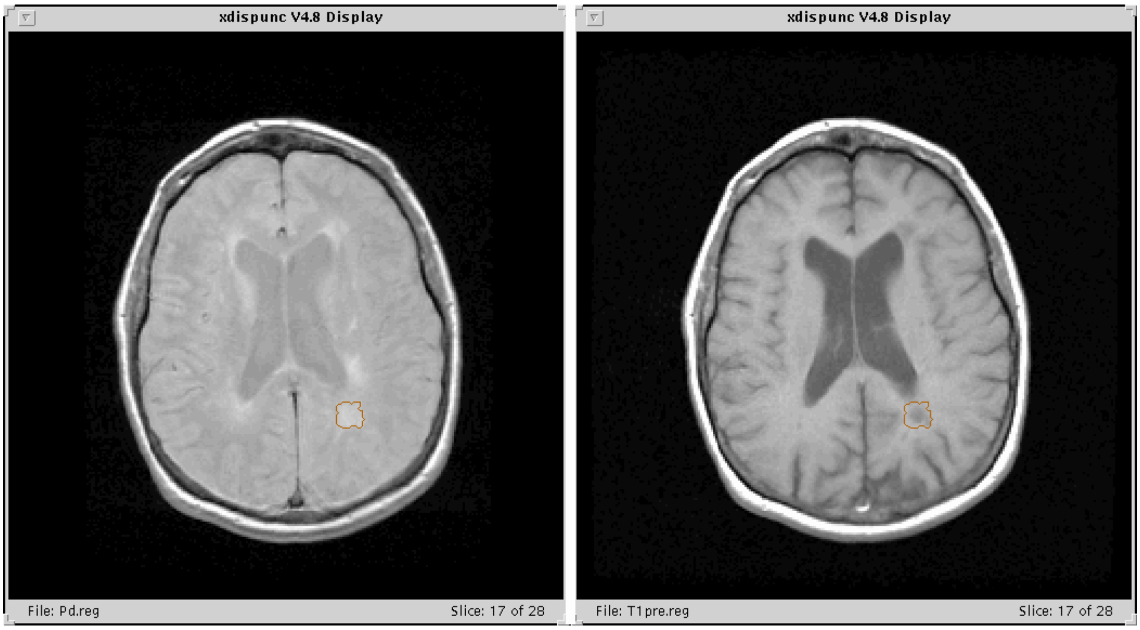

a **b**

FIG 7.3 Non-visibly enhancing lesion described on the PD weighted image (a), with its anatomical and spatial correlate on the T_1-weighted SE image (b). The ROI, described on the PD weighted image, and encompasses an area greater than the area of T_1 weighted hypointensity.

Nonetheless, a clear finding was that after allowing for the negatively confounding effects of lesion CSA, T_1- hypointense lesions had a greater $\Delta R_1/\Delta t$ than isointense lesions at the 1st and 2nd timepoints, with a loss of significance at the 3rd timepoint (table 7.6). In the light of dynamic susceptibility contrast studies on T_1- hypointense lesions, which have revealed both a reduction in cerebral blood volume (Haselhorst *et al.,* 2000, Wuerfel *et al.,* 2004) and cerebral blood flow (Wuerfel *et al.,* 2004), it would seem improbable that the greater post contrast $\Delta R_1/\Delta t$ seen in hypointense lesions could be from greater perfusion in these lesions. Rather it seems more likely that this reflects a greater degree of BBB disruption, and therefore higher permeability in T_1- hypointense lesions. Fewer patients (14 as opposed to 19 patients, with 322 instead of 581 lesions) contributed to the 3rd timepoint analysis, due to the prolonged, and relatively demanding scanning protocol. The resultant smaller sample size might be a possible explanation for the loss of significance at this latter timepoint. An alternative explanation to the loss of a significant difference in $\Delta R_1/\Delta t$ between the lesion subtypes at 60 minutes could be that Gd leakage follows different time courses in T_1- hypointense and isointense lesions, achieving equilibrium with similar local Gd concentration in both lesion subtypes by 60 minutes. This would be compatible with the decreasing difference in $\Delta R_1/\Delta t$ between the 2 lesion subtypes over time (Table 7.6).

There was an association between lesion CSA and T_1 hypointensity- lesions with a larger CSA tending to coincide with an area of hypointensity on the pre-contrast T_1-weighted SE sequence. This could be seen as being compatible with the idea of larger lesions being associated with a greater degree of tissue and axonal damage, the pathological hallmark of T_1- hypointense lesions (Hiehle *et al.,* 1995; Van Walderveen *et al.,* 1998).

In the study, a positive association was noted at patient level between the percentage of lesions which were T_1- hypointense and advanced disability as measured by EDSS. In addition patients with SPMS were noted to have a higher proportion of T_1- hypointense lesions (p=0.057). These findings are in line with those of previous studies, where T_1-

hypointense lesion load was found to correlate with disability as measured by EDSS, and with a SP disease subtype (van Walderveen *et al.,* 2001).

7.4.4 RRMS lesions vs SPMS lesions

RRMS lesions were observed to have a greater $\Delta R_1/\Delta t$ only at the 1st post contrast timepoint when compared with lesions in SPMS patients. Given the borderline significance ($p=0.04$), and the absence of a sustained difference over 40 or 60 minutes, further studies would be required to confirm this finding. Assuming however that this is a real observation, it could be accounted for by differences in lesion composition in the 2 clinical subtypes. As Gd leakage and therefore $\Delta R_1/\Delta t$ is proportional to transfer coefficient across the BBB (K^{trans}) and lesion leakage space (v_e)(Tofts and Kermode, 1991; Tofts *et al.,* 1999), it is possible that the difference in initial $\Delta R_1/\Delta t$ is due to a relatively high permeability (K^{trans}) and low leakage space (v_e) in RRMS lesions.

An alternative explanation for the difference seen in the post contrast $\Delta R_1/\Delta t$ between RRMS and SPMS patients could be increased perfusion in lesions in RRMS, which would be consistent with ongoing active inflammation in a population consisting of newer, more active lesions. Continuous arterial spin labelling studies on perfusion across different MS subtypes (Rashid *et al.,* 2004) have revealed increased perfusion in RRMS compared with SPMS patients. However, this finding was not confined to lesions, but on segmented white matter as a whole. Another study employed dynamic susceptibility contrast enhanced MRI to investigate perfusion in lesions in RRMS patients (Ge *et* al., 2005). This revealed a population of non enhancing lesions which have increased perfusion with vascular changes similar to visibly enhancing lesions consistent with low grade inflammation. However, no SPMS patients were included in this study. Overall, it seems plausible that higher perfusion in the population of lesions seen in RRMS patients could be contributing to clinical subgroup difference seen only at the first post-contrast timepoint.

7.4.5 Associations with lesion CSA

In the present study, a robust negative relationship was found between lesion CSA and $\Delta R_1/\Delta t$. Lesions with a lower CSA had a greater $\Delta R_1/\Delta t$ than larger lesions. The observation is unlikely to be due to partial volume effect, wherein smaller lesions should have a smaller apparent $\Delta R_1/\Delta t$. Neither is it easily explained by errors of alignment or misregistration in the construction of T_1 maps. Although this may conceivably affect smaller lesions more, it is unlikely that such errors would introduce a systemic error resulting in such a robust relationship. In addition, explaining the relationship in terms of differences in perfusion is difficult, as the relationship is significant and present in all timepoints. Perhaps a more likely explanation can be given if one assumes that the chronic BBB leakage occurs from a "central" venule around which the lesion originally developed. Such an origin for MS lesions is well documented in neuropathological studies, where lymphocytic infiltrates and fibrinous exudates follow a perivenular pattern (Adams *et al.,* 1985) Persistent low grade leakage from such a venule is likely to result in a concentration gradient of Gd contrast, with a decrease in concentration further away from the venule. If the permeability of the central venule is the same in small and large lesions, it might be expected that post-Gd $\Delta R_1/\Delta t$ would be greater per unit voxel in smaller lesions. Such an effect could also impede the detection of higher leakage in T_1- hypointense than isointense lesions, because the former are more commonly seen in larger lesions. Further investigation of the relationship between venule location and extent of leakage might be possible by the application of an imaging methodology that enables the detection of venules. (Tan *et al.,* 2000)

7.4.6 Associations with treatment and disability

$\Delta R_1/\Delta t$ was not associated with disease modifying treatment by IFNβ or glatiramer acetate at any timepoint, suggesting that the low grade BBB leakage in visibly non-enhancing lesions reported in this study were not materially influenced by inter-current disease modifying therapy. Persistent low grade BBB leakage is likely due to relatively permanent structural changes that have been reported in pathological studies e.g. reparative thickening in the vessel walls in longstanding MS lesions (Adams *et al.,* 1985). Although no correlation was found between $\Delta R_1/\Delta t$ and concurrent disability as measured by EDSS, long term follow up will be required to determine whether the extent of BBB leakage in visibly non-enhancing lesions is related to future accumulation of disability.

7.4.7 Limitations

The present study had a number of limitations. The long acquisition time for each T_1 map limited the temporal resolution of the study, making accurate modelling and estimation of intravascular Gd concentration difficult. The construction of serial T_1 maps involved multiple steps of registration, which could introduce an element of error in the estimation of T_1. The describing of ROI's over areas of PD weighted abnormality complicated the interpretation of comparisons between T_1- hypointense and isointense lesions. The study design was cross sectional and the exact age of the lesions was not known; nor is there longitudinal data to indicate whether the changes observed alter with time. The absence of healthy controls in the study precluded the investigation of BBB leakage in NAWM, where a number of studies using measures such as spectroscopy, magnetization transfer and diffusion weighted imaging have indicated the presence of abnormality in MS (Fernando *et al.,* 2004; Kidd *et al.,* 1997; Werring *et al.,* 1999).

7.4.8 Summary and Future Work

The study has clearly demonstrated that low grade BBB leakage is a feature of visibly non-enhancing lesions, and is detectable using contrast enhanced MRI, with $\Delta R_1/\Delta t$ as a quantitative measure. The leakage is distinct from that seen in visibly enhancing lesions, is greater in smaller than in larger lesions, and appears to be greater in T_1- hypointense lesions, compared with size-adjusted T_1- isointense lesions. In addition, there is a borderline observed difference between RRMS and SPMS patients in the initial $\Delta R_1/\Delta t$ value. If true, this may reflect differences in perfusion, or in the permeability characteristics of lesions in RRMS and SPMS.

The findings in this preliminary study justify the use of serial T_1 maps and $\Delta R_1/\Delta t$ as a sensitive measure of low grade leakage, and encourage future work in this approach, which could include a sequence for obtaining T_1 maps with a shorter acquisition time, the inclusion of healthy controls, primary progressive patients, and longitudinal observations.

CHAPTER 8

Summary and Conclusions

Natalizumab and the BBB form the 2 major themes of this thesis. The BBB and its breakdown are central to new lesion formation and inflammation within MS (Adams *et al*., 1985; Bruck *et al.,* 2007; Grossman *et al.,* 1986; Katz *et al.,* 1993; Miller *et al.,* 1988; Lai *et al.,* 1996) The postulated mechanism of action of Natalizumab is principally at the level of the BBB, preventing leucocyte adhesion and transmigration through the BBB. (Rice *et al.,* 2005). Its effect on new lesion formation was studied in a phase III monotherapy trial (chapter 4). Further studies in this thesis investigated the effect of natalizumab on segmental atrophy (chapter 5) and inferred subtle BBB breakdown (chapter 6)

Overt BBB breakdown (as detected by Gd enhancement and histological changes) is an established feature of new lesions and ongoing inflammation in MS. Less is known about low grade BBB leakage in old, non-active lesions. Such leakage could potentially contribute to tissue damage through the attendant leakage of inflammatory cells and soluble mediators of inflammation. The final study described in this thesis attempted to investigate BBB leakage both in visibly enhancing as well as in visibly non-enhancing lesions by utilising changes in R_1 to infer BBB leakage (chapter 7).

8.1 Effect of natalizumab on MRI measures in MS

Several studies to date have demonstrated the efficacy of natalizumab in ameliorating the clinical manifestations of MS, as monotherapy (Miller *et al.,* 2003; Polman *et al.,*

2006) or in combination with IFNβ (Rudick *et al.,* 2006).

Much of this thesis investigated the effect of natalizumab on MS through MRI studies, either through conventional MRI measures of disease activity and severity such as Gd enhancing lesions, T_1- hypointense lesion load and number of new and enhancing T_2 hyperintense lesions (Chapter 4), or through volumetric measures of GM and WM (Chapter 5) and inferred BBB leakage through the measurement of change in T_1 weighted signal (Chapter 6).

8.1.1 Effect of natalizumab on MRI visible lesions: The AFFIRM trial results (Chapter 4)

In this 2 year, placebo-controlled, double-blinded trial, treatment with natalizumab was associated with a 92% reduction in number of Gd enhancing lesions, 83% reduction in number of new or enlarging T_2 hyperintense and a 76% reduction in the number of new T_1 hypointense lesions. Similarly, natalizumab significantly reduced the total volumes of all lesion types studied compared to placebo. Such findings are in line with those of other studies investigating the effect of natalizumab on MRI visible MS lesions (Miller DH *et al.,* 2003; Rudick *et al.,* 2006; Goodman *et al.,* 2009) and complement the clinical results from AFFIRM and SENTINEL (Rudick *et al.,* 2006; Polman *et al.,* 2006). Together, they reinforce the evidence that natalizumab exerts a profound anti-inflammatory effect in MS.

In addition, natalizumab reduced T_1/T_2 LVR, indicating an additional effect on the formation of the more severe subset of T_1- hypointense lesions over and above the general effect of natalizumab on all T_2 hyperintense lesions. Consistent with this is the finding that natalizumab reduces the likelihood that Gd enhancing lesions evolve into permanent T_1-hypointense lesions (Dalton *et al.,* 2004b). Together, these studies suggest that in addition to averting leucocyte adhesion and resultant BBB breakdown, natalizumab also ameliorates axonal damage once inflammation has commenced, presumably by further disruption of α4 integrin mediated processes downstream.

8.1.2 Effect of natalizumab on segmental atrophy (Chapter 5)

In this 2 year substudy of the AFFIRM trial, volumetric measures of GM, WM and BP were obtained. Atrophy over the 2 years occurred predominantly in the GM and was independent of WM lesion load, echoing findings from a previous study (Tiberio *et al.,* 2005). GMF (but not WMF) was negatively related to EDSS.

Although trends were detected for greater rates of WM atrophy and lower rates of GM atrophy in natalizumab treated patients, caution must be exercised in interpreting these findings as none of the trends approach significance. The lack of a significant treatment effect could either reflect insufficient statistical power due to the relatively small study population (Anderson *et al.,* 2007), or could represent a real absence of effect of natalizumab on atrophy, indicating that atrophy does not immediately arise from VLA-4 mediated processes or inflammation. Further studies are required to determine if the influence of natalizumab on WM lesions results in a moderation of atrophy in the long term.

8.1.3 Effect of natalizumab on low grade BBB leakage in visibly non-enhancing lesions (Chapter 6)

In this second substudy of the AFFIRM trial, subtle BBB leakage in visibly non-enhancing lesions was inferred by detecting subtle change in SI at set timepoints up to 40 minutes after the administration of Gd-DTPA. The scans were undertaken 6 months after the start of the trial, by which time the study subjects would have received 6 infusions of either 300mg natalizumab or placebo.

The study demonstrated consistent detectable leakage from non-visibly enhancing lesions up to 40 minutes post-contrast. It validated the use of dynamic contrast enhanced imaging to investigate subtle BBB leakage in a multi-centre setting.

The subtle leakage was not influenced by the administration of natalizumab, implying that such leakage occurs through $\alpha 4\beta 1$ independent processes, ostensibly through permanent structural and physiological changes in the vascular wall, with chronic, incomplete BBB repair, as suggested by findings from histological studies in non-active lesions (Adams *et al.,* 1985; Claudio *et al.,* 1995)

8.1.4 Progressive Multifocal Leukoencephalopathy and natalizumab

The development of PML in a handful of patients receiving natalizumab has caused considerable concern amongst patients and clinicians alike. PML has been reported to develop in patients receiving natalizumab monotherapy (Hartung, 2009) as well as in patients who have undergone previous or ongoing immune modulation or suppression (van Assche *et al.,* 2005; Demasters and Tyler, 2005; Langer-Gould *et al.,* 2005). Retrospective studies on patients receiving natalizumab estimate the annual risk of developing PML at 1 per 1000 patients (Yousry *et al.,* 2006)

The reasons behind the development of PML in natalizumab treated patients are unknown. Studies on natalizumab- treated patients show a marked paucity of leucocytes in CSF (Stuve *et al.,* 2006), as well as reductions in the number of dendritic cells and CD4+ T-cells in the cerebral perivascular spaces (del Pilar Martin *et al*., 2008), consistent with a restriction of α4-mediated adhesion and transmigration of leucocytes. It has been suggested that the disruption of leucocyte transmigration across the BBB compromises normal CNS immune surveillance, thereby allowing unchallenged replication of JC virus and the development of PML(Berger and Koralnik, 2005).

An alternative hypothesis (Ransohoff, 2005) points to the potential for B-cell and B-cell precursors to act as reservoirs of JC virus. Such cells are mobilized from the bone marrow in natalizumab treated patients (Krumbholz *et al.,* 2008).

Published guidelines now inform the selection of suitable candidates for natalizumab therapy, and the subsequent monitoring for PML (Gold *et al.,* 2007; Kappos *et al.,* 2007). The guidelines prescribe specific washout periods for previous immune-suppressive treatments prior to the commencement of natalizumab. The suspicion of PML, based on clinical and radiological evidence, is accompanied by a recommendation for discontinuation. The possibility of a re-emergence of disease activity on drug withdrawal was examined in a recent study, which revealed that clinical, radiological and immunological markers of disease activity were stable up to 14 months following discontinuation of the natalizumab (Stuve *et al.,* 2009).

In a study of 12 patients receiving natalizumab, a 3-day course of plasma exchange was associated with a 92% reduction in serum natalizumab concentration within the 1st week, and with an increased transmigratory capacity of peripheral blood mononuclear cells as measured in vitro (Khatri *et al.,* 2009), suggesting plasma exchange may be of benefit in natalizumab related PML by hastening the clearance of natalizumab from the system and restoring the migratory capacity of immune cells and therefore the immune surveillance of the CNS.

8.2 Usage of $\Delta R_1/\Delta t$ to infer subtle BBB leakage in MS (Chapter 7)

The final study described in this thesis utilised the change in R_1 (the inverse of T_1) to measure local Gd concentration and therefore infer BBB leakage after administration of Gd. The measure used ($\Delta R_1/\Delta t$) represents a more reproducible and potentially more sensitive measure than T_1- weighted signal *per se,* which in addition to being inversely related to T_1, is also directly related to PD, and influenced by amplifier gain at each scan.

Persistent low grade BBB leakage was detected up to 60 minutes after administration of Gd seen in visibly non-enhancing lesions. Such low grade BBB leakage was distinct from the leakage seen in visibly enhancing lesions, in which a 10-fold difference in magnitude and non-overlapping 95% reference ranges were noted. Leakage was greater in size-adjusted T_1-hypointense lesions, indicating that such low grade BBB leakage was more severe in lesions in which there was a greater degree of neuronal damage and extracellular matrix disruption. A robust inverse relationship was observed between lesion CSA and BBB leakage, with lower $\Delta R_1/\Delta t$ in larger lesions. This may be explained by a dilutional effect rather than differences in BBB permeability, with a larger leakage space in large lesions leading to lower local concentration of leaked Gd. No convincing evidence for differences in lesional BBB permeability between RRMS and SPMS was found.

8.3 Conclusion

The efficacy of natalizumab in suppressing new lesion formation and ameliorating the clinical manifestations of MS advocates strongly for the targeting of cell adhesion molecules at the level of the BBB as a potential treatment strategy in MS. The development of PML in a small number of patients receiving natalizumab underlines the need for continued, long term monitoring of patients receiving new agents for which long term data is lacking. It is hoped that published recommendations aimed toward the early detection of PML in natalizumab patients will help to reduce the morbidity and mortality associated with this rare but potentially fatal complication.

Although treatment with natalizumab was not shown to influence segmental atrophy over a 2 year period, this may be due to insufficient statistical power. Non-significant trends appeared to suggest that treatment with natalizumab reduced the rate of GM atrophy and accelerated WM atrophy, ostensibly from resolution of inflammation related oedema. Further, follow-up studies are required to ascertain whether treatment with natalizumab influences atrophy in the long term.

Subtle BBB leakage was investigated in the final 2 studies described in the thesis, the latter study utilising the novel measure $\Delta R_1/\Delta t$ as a reproducible and sensitive measure of BBB leakage. Both studies demonstrated consistent, measurable low grade leakage from visibly non-enhancing lesions. This leakage was distinct from the overt BBB breakdown in visibly enhancing lesions, and was not influenced by treatment with natalizumab. Such findings consolidate the evidence from histological studies of low grade BBB leakage from non-active lesions due to changes in vessel wall structure (Adams *et al.,* 1985) and physiology (Claudio et al., 1995).

Although no correlation was found between inferred BBB leakage ($\Delta R_1/\Delta t$) and EDSS, it is hoped that long term follow up studies will determine whether the extent of BBB leakage in visibly non-enhancing lesions is related to future accumulation of disability.

Reference List

Abbott NJ, Ronnback L, Hansson E. Astrocyte-endothelial interactions at the blood-brain barrier. Nat Rev Neurosci 2006; **7**: 41-53.

Abbruscato TJ, Davis TP. Protein expression of brain endothelial cell E-cadherin after hypoxia/aglycemia: influence of astrocyte contact. Brain Res 1999; **842**: 277-86.

Adams CW, Poston RN, Buk SJ, Sidhu YS, Vipond H. Inflammatory vasculitis in multiple sclerosis. J Neurol Sci 1985; **69**:269-283

Allen IV, McQuaid S, Mirakhur M, Nevin G. Pathological abnormalities in the normal-appearing white matter in multiple sclerosis. Neurol Sci 2001; **22**: 141-144

Anderson VM, Fox NC, Miller DH. Magnetic resonance imaging measures of brain atrophy in multiple sclerosis. J Magn Reson Imaging 2006; **23**:605-618

Anderson VM, Bartlett JM, Fox NC, Fisniku L, Miller DH. Detecting effects on brain atrophy in relapsing remitting multiple sclerosis: Sample size estimates. J Neurol 2007; **254**: 1588-1594

Ashburner J, Friston K. Multimodal image coregistration and partitioning- a unified framework. Neuroimage 1997; **6**: 209–217.

Ashburner J, Friston KJ. Voxel-based morphometry--the methods. Neuroimage 2000; **11**: 805-821.

Association of British Neurologists. ABN Guidelines for Treatment of Multiple Sclerosis with ß-interferon and Glatiramer Acetate. London: ABN, Ormond House; 2007

Bagnato F, Jeffries N, Richert ND, Stone RD, Ohayon JM, McFarland HF, Frank JA. Evolution of T1 black holes in patients with multiple sclerosis imaged monthly for 4 years. Brain 2003; **126**:1782-1789.

Bakshi R. Fatigue associated with multiple sclerosis: diagnosis, impact and management. Mult Scler 2003; **9**:219-227

Balashov KE, Rottman JB, Weiner HL, Hancock WW. CCR5(+) and CXCR3(+) T cells are increased in multiple sclerosis and their ligands MIP-1alpha and IP-10 are expressed in demyelinating brain lesions. Proc Natl Acad Sci U S A 1999; **96**:6873-6878

Balcer LJ, Galetta SL, Calabresi PA, Confavreux C, Giovannoni G, Havrdova E, Hutchinson M, Kappos L, Lublin FD, Miller DH, O'Connor PW, Phillips JT, Polman CH, Radue EW, Rudick RA, Stuart WH, Wajgt A, Weinstock-Guttman B, Wynn DR, Lynn F, Panzara MA. Natalizumab reduces visual loss in patients with relapsing multiple sclerosis. Neurology 2007; **68**: 1299-1304.

Baltagi BH. Econometric Analysis of Panel Data. John Wiley and Sons, New York 1995

Bandopadhyay R, Orte C, Lawrenson JG, Reid AR, De SS, Allt G. Contractile proteins in pericytes at the blood-brain and blood-retinal barriers. J Neurocytol 2001; **30**: 35-44.

Baron JL, Madri JA, Ruddle NH, Hashim G, Janeway CA, Jr. Surface expression of alpha 4 integrin by CD4 T cells is required for their entry into brain parenchyma. J Exp Med 1993; **177**: 57-68.

Barkhof F, Scheltens P, Frequin ST, Nauta JJ, Tas MW, Valk J, Hommes OR. Relapsing-remitting multiple sclerosis: sequential enhanced MR imaging vs clinical findings in determining disease activity. AJR Am J Roentgenol 1992;**159**: 1041-1047.

Barkhof F, Filippi M, Miller DH, Scheltens P, Campi A, Polman CH, Comi G, Ader HJ, Losseff N, Valk J Comparison of MRI criteria at first presentation to predict conversion to clinically definite multiple sclerosis. Brain 1997; **120** (Pt 11):2059-2069

Barkhof F, Bruck W, De Groot CJ, Bergers E, Hulshof S, Guerts J, Polman CH, van der Valk P. Remyelinated lesions in multiple sclerosis: magnetic resonance image appearance. Arch Neurol. 2003; **60**:1073-8

Barkhof F, Held U, Simon JH, Daumer M, Fazekas F, Filippi M, Frank JA, Kappos L, Li D, Menzler S, Miller DH, Petkau J, Wolinsky J. Predicting gadolinium enhancement status in MS patients eligible for randomized clinical trials. Neurology ; **65**: 1447-1454

Bastianello S, Pozzilli C, Bernardi S, Bozzao L, Fantozzi LM, Buttinelli C, Fieschi C. Serial study of gadolinium-DTPA MRI enhancement in multiple sclerosis. Neurology 1990; **40**: 591-595.

Bauer HJ, Hanefeld F, Christen HJ. Multiple sclerosis in early childhood. Lancet 1990; **336**:1190

Bazzoni G, Dejana E. Endothelial cell-to-cell junctions: molecular organization and role in vascular homeostasis Physiol Rev 2004; **84**: 869-901.

Beck J, Rondot P, Catinot L, Falcoff E, Kirchner H, Wietzerbin J. Increased production of interferon gamma and tumor necrosis factor precedes clinical manifestation in multiple sclerosis: do cytokines trigger off exacerbations? Acta Neurol Scand 1998; **78**:318-323

Beck RW, Chandler DL, Cole SR, Simon JH, Jacobs LD, Kinkel RP, Selhorst JB, Rose JW, Cooper JA, Rice G, Murray TJ, Sandrock AW. Interferon beta-1a for early multiple sclerosis: CHAMPS trial subgroup analyses. Ann Neurol 2002; **51**:481-490

Berger JR, Koralnik IJ. Progressive multifocal leukoencephalopathy and natalizumab--unforeseen consequences. N Engl J Med. 2005; **353**:414-416

Bermel RA, Sharma J, Tjoa CW, Puli SR, Bakshi R. A semiautomated measure of whole-brain atrophy in multiple sclerosis. J Neurol Sci 2003; **208**:57-65

Berzin TM, Zipser BD, Rafii MS, Kuo-Leblanc V, Yancopoulos GD, Glass DJ, Fallon JR, Stopa EG. Agrin and microvascular damage in Alzheimer's disease. Neurobiol Aging 2000; **21**: 349-55.

Bitsch A, Schuchardt J, Bunkowski S, Kuhlmann T, Bruck W. Acute axonal injury in multiple sclerosis. Correlation with demyelination and inflammation. Brain 2000;

123:1174-1183

Bjartmar C, Trapp BD. Axonal and neuronal degeneration in multiple sclerosis: mechanisms and functional consequences. Curr Opin Neurol 2001; **14**:271-278

Bloch F. Nuclear induction. *Phys Rev* 1946; **70:** 460-474.

Bo L, Vedeler CA, Nyland H, Trapp BD, Mork SJ. Intracortical multiple sclerosis lesions are not associated with increased lymphocyte infiltration. Mult Scler 2003; **9**:323-331

Bochner BS, Luscinskas FW, Gimbrone MA Jr., Newman W, Sterbinsky SA, Derse-Anthony CP, Klunk D, Schleimer RP. Adhesion of human basophils, eosinophils, and neutrophils to interleukin 1-activated human vascular endothelial cells: contributions of endothelial cell adhesion molecules. J Exp Med 1991; **173**: 1553-1557.

Bondan EF, Lallo MA, Dagli ML, Pereira LA, Graca DL. Blood-brain barrier breakdown following gliotoxic drug injection in the brainstem of Wistar rats. Arq Neuropsiquiatr 2002; **60**: 582-9.

Brex PA, Jenkins R, Fox NC, Crum WR, O'Riordan JI, Plant GT, Miller DH. Detection of ventricular enlargement in patients at the earliest clinical stage of MS. Neurology 2000; **8**: 1689-1691.

Brex PA, Molyneux PD, Smiddy P, Barkhof F, Filippi M, Yousry TA, Hahn D, Rolland

Y, Salonen O, Pozzilli C, Polman CH, Thompson AJ, Kappos L, Miller DH. The effect of IFNbeta-1b on the evolution of enhancing lesions in secondary progressive MS. Neurology 2001; **57**: 2185-2190.

Brex PA, Ciccarelli O, O'Riordan JI, Sailer M, Thompson AJ, Miller DH. A longitudinal study of abnormalities on MRI and disability from multiple sclerosis. N Engl J Med 2002;**346**:158-64.

Brightman MW, Reese TS. Junctions between intimately apposed cell membranes in the vertebrate brain. J Cell Biol 1969;**40**: 648-677.

Brocke S, Piercy C, Steinman L, Weissman IL, Veromaa T. Antibodies to CD44 and integrin alpha4, but not L-selectin, prevent central nervous system inflammation and experimental encephalomyelitis by blocking secondary leukocyte recruitment Proc Natl Acad Sci U S A 1999; **96**:6896-901.

Broman T. Blood-brain barrier damage in multiple sclerosis supravital test-observations. Acta Neurol Scand 1964;**40**:SUPPL 10:21-4.

Bruck W, Bitsch A, Kolenda H, Bruck Y, Stiefel M, Lassmann H. Inflammatory central nervous system demyelination: correlation of magnetic resonance imaging findings with lesion pathology. Ann Neurol 1997; **42**:783-793.

Bruck W, Kuhlmann T, Stadelmann C. Remyelination in multiple sclerosis. J. Neurol Sci. 2003; **206**:181-5.

Brusaferri F, Candelise L. Steroids for multiple sclerosis and optic neuritis: a meta-analysis of randomized controlled clinical trials. J Neurol 2000; **247**: 435-442

Burkly LC, Jakubowski A, Newman BM, Rosa MD, Chi-Rosso G, Lobb RR. Signaling by vascular cell adhesion molecule-1 (VCAM-1) through VLA-4 promotes CD3-dependent T cell proliferation. Eur J Immunol 1991 Nov; **21**: 2871-2875.

Butt AM, Jones HC, Abbott NJ. Electrical resistance across the blood-brain barrier in anaesthetized rats: a developmental study. J Physiol 1990; **429**: 47-62.

Butcher EC. Leukocyte-endothelial cell recognition: three (or more) steps to specificity and diversity. Cell 1991; **67**: 1033-1036.

Cada DJ, Levien T, Baker DE. Natalizumab. Hospital Pharmacy 2005;**40**:336 –346

Carlos TM, Schwartz BR, Kovach NL, Yee E, Rosa M, Osborn L, Chi-Rosso G, Newman B, Lobb R. Harlan JM. Vascular cell adhesion molecule-1 mediates lymphocyte adherence to cytokine-activated cultured human endothelial cells. Blood.

1990; **76**: 965-970

Carman CV, Springer TA. A transmigratory cup in leukocyte diapedesis both through individual vascular endothelial cells and between them. J Cell Biol 2004; **167**: 377-88.

Carpenter J, Bithell J. Bootstrap confidence intervals: when, which, what? A practical guide for medical statisticians. Stat Med 2000; **19**:1141-1164

Carrithers MD, Visintin I, Kang SJ, Janeway CA, Jr. Differential adhesion molecule requirements for immune surveillance and inflammatory recruitment. Brain 2000; **123**: 1092-1101

Carvalho-Tavares J, Hickey MJ, Hutchison J, Michaud J, Sutcliffe IT, Kubes P. A role for platelets and endothelial selectins in tumor necrosis factor-alpha-induced leukocyte recruitment in the brain microvasculature. Circ Res 2000; **87**: 1141-1148.

Chabas D, Baranzini SE, Mitchell D, Bernard CC, Rittling SR, Denhardt DT, Sobel RA, Lock C, Karpuj M, Pedotti R, Heller R, Oksenberg JR, Steinman L. The influence of the proinflammatory cytokine, osteopontin, on autoimmune demyelinating disease. Science 2001; **294**: 1731-1735.

Chard DT, Griffin CM, Parker GJ, Kapoor R, Thompson AJ, Miller DH. Brain atrophy in clinically early relapsing-remitting multiple sclerosis. Brain 2002a;**125**:327-337.

Chard DT, Parker GJ, Griffin CM, Thompson AJ, Miller DH. The reproducibility and sensitivity of brain tissue volume measurements derived from an SPM-based segmentation methodology. J Magn Reson Imaging. 2002b;**15**: 259-267

Chard DT, Griffin CM, McLean MA, Kapeller P, Kapoor R, Thompson AJ, Miller DH. Brain metabolite changes in cortical grey and normal-appearing white matter in clinically early relapsing- remitting multiple sclerosis. Brain 2002c; **125**: 2342-2352

Chard DT, Brex PA, Ciccarelli O, Griffin CM, Parker GJ, Dalton C, Altmann DR, Thompson AJ, Miller DH. The longitudinal relation between brain lesion load and atrophy in multiple sclerosis: a 14 year follow up study. J Neurol Neurosurg Psychiatry 2003; **74**:1551-1554

Cipolla MJ, Crete R, Vitullo L, Rix RD. Transcellular transport as a mechanism of blood-brain barrier disruption during stroke. Front Biosci 2004; **9**: 777-785.

Claudio L, Raine CS, Brosnan CF. Evidence of persistent blood-brain barrier abnormalities in chronic-progressive multiple sclerosis. Acta Neuropathol (Berl) 1995;**90**: 228-238.

Clawson CC, Hartmann JF, Vernier RL. Electron microscopy of the effect of gram-negative endotoxin on the blood-brain barrier. J Comp Neurol 1966; **127**: 183-98.

Cohen Z, Molinatti G, Hamel E. Astroglial and vascular interactions of noradrenaline terminals in the rat cerebral cortex. J Cereb Blood Flow Metab 1997;**17**: 894-904.

Compston A. The 150th anniversary of the first depiction of the lesions of multiple sclerosis. J Neurol Neurosurg Psychiatry 1988; **51**:1249-1252

Compston A, Sadovnick AD. Epidemiology and genetics of multiple sclerosis. Curr Opin Neurol Neurosurg 1992; **5**:175-181

Compston A. The genetic epidemiology of multiple sclerosis. Philos Trans R Soc Lond B Biol Sci 1999; **354**:1623-1634

Compston A, Coles A. Multiple sclerosis. Lancet 2002; **359**:1221-1231

Compston A, Lassmann H, McDonald I. The story of multiple sclerosis. In: Compston A, Confavreux C, Lassmann H McDonald I, Miller D, Noseworthy J, Smith K, Wekerle H eds. *McAlpine's multiple sclerosis 4th Ed.* London: Churchill Livingstone; 2006a: 3-62

Compston A, Confavreux C. The distribution of multiple sclerosis. In: Compston A, Confavreux C, Lassmann H McDonald I, Miller D, Noseworthy J, Smith K, Wekerle H eds. *McAlpine's multiple sclerosis 4th Ed.* London: Churchill Livingstone; 2006b: 71-105

Compston A, Wekerle H, McDonald I. The origins of multiple sclerosis; a synthesis. In: Compston A, Confavreux C, Lassmann H McDonald I, Miller D, Noseworthy J, Smith K, Wekerle H eds. *McAlpine's multiple sclerosis 4th Ed.* London: Churchill Livingstone; 2006c: 273-284

Confavreux C, Aimard G, Devic M. Course and prognosis of multiple sclerosis assessed by the computerized data processing of 349 patients. Brain 1980; **103**: 281-300

Confavreux C, Vukusic S, Moreau T, Adeleine P. Relapses and progression of disability in multiple sclerosis. N Engl J Med 2000; **343**:1430-1438.

Confavreux C, Vukusic S, Adeleine P. Early clinical predictors and progression of irreversible disability in multiple sclerosis: an amnesic process. Brain 2003; **126**:770-782.

Confavreux C, Compston A. The natural history of multiple sclerosis. In: Compston A, Confavreux C, Lassmann H McDonald I, Miller D, Noseworthy J, Smith K, Wekerle H eds. *McAlpine's multiple sclerosis 4th Ed.* London: Churchill Livingstone; 2006: 183-269

Cook SD. Multiple sclerosis. Arch Neurol 1998; **55**:421-423

Coomber BL, Stewart PA. Morphometric analysis of CNS microvascular endothelium. Microvasc Res 1985; **30**: 99-115.

Cornford EM, Oldendorf WH. Epilepsy and the blood-brain barrier. Adv Neurol 1986;**44**: 787-812.

Cossins JA, Clements JM, Ford J, Miller KM, Pigott R, Vos W, van d, V, De Groot CJ. Enhanced expression of MMP-7 and MMP-9 in demyelinating multiple sclerosis lesions. Acta Neuropathol (Berl) 1997; **94**: 590-598.

Cottrell DA, Kremenchutzky M, Rice GP, Koopman WJ, Hader W, Baskerville J, Ebers GC. The natural history of multiple sclerosis: a geographically based study. 5. The clinical features and natural history of primary progressive multiple sclerosis. Brain 1999; **122**:625-639

Crone C, Christensen O. Electrical resistance of a capillary endothelium. J Gen Physiol 1981; **77**: 349-371.

Crone C, Olesen SP. Electrical resistance of brain microvascular endothelium. Brain Res 1982; **241**: 49-55.

Damle NK, Aruffo A. Vascular cell adhesion molecule 1 induces T-cell antigen receptor-dependent activation of CD4+T lymphocytes. Proc Natl Acad Sci U S A 1991; **88**: 6403-6407.

Dalton CM, Brex PA, Miszkiel KA, Hickman SJ, MacManus DG, Plant GT, Thompson AJ, Miller DH. Application of the new McDonald criteria to patients with clinically isolated syndromes suggestive of multiple sclerosis. Ann Neurol 2002a; **52**:47-53

Dalton CM, Brex PA, Jenkins R, Fox NC, Miszkiel KA, Crum WR, O'Riordan JI, Plant GT, Thompson AJ, Miller DH. Progressive ventricular enlargement in patients with clinically isolated syndromes is associated with the early development of multiple sclerosis. J Neurol Neurosurg Psychiatry 2002b;**73**:141-147.

Dalton CM, Miszkiel KA, Barker GJ, Macmanus DG, Pepple TI, Panzara M, Yang M, Hulme A, O'Connor P, Miller DH. Effect of natalizumab on conversion of gadolinium enhancing lesions to T1 hypointense lesions in relapsing multiple sclerosis. J Neurol 2004a; **251**: 407-413.

Dalton CM, Chard DT, Davies GR, Miszkiel KA, Altmann DR, Fernando K, Plant GT, Thompson AJ, Miller DH. Early development of multiple sclerosis is associated with progressive grey matter atrophy in patients presenting with clinically isolated syndromes. Brain 2004b; **127**: 1101-1107

Dalton CM, Miszkiel KA, O'Connor PW, Plant GT, Rice GP, Miller D. Ventricular enlargement in MS: one-year change at various stages of disease. Neurology. 2006; **66**:693-698

Davie CA, Barker GJ, Webb S, Tofts PS, Thompson AJ, Harding AE, McDonald WI, Miller DH. Persistent functional deficit in multiple sclerosis and autosomal dominant cerebellar ataxia is associated with axon loss. Brain 1995; **118**:1583-1592

Davies DC. Blood-brain barrier breakdown in septic encephalopathy and brain tumours. J Anat 2002; **200**: 639-46.

De Stefano N, Matthews PM, Fu L, Narayanan S, Stanley J, Francis GS, Antel JP, Arnold DL. Axonal damage correlates with disability in patients with relapsing-remitting multiple sclerosis. Results of a longitudinal magnetic resonance spectroscopy study. Brain 1998; **121**:1469-1477

De Stefano N, Narayanan S, Francis GS, Arnaoutelis R, Tartaglia MC, Antel JP, Matthews PM, Arnold DL. Evidence of axonal damage in the early stages of multiple sclerosis and its relevance to disability. Arch Neurol 2001; **58**: 65-70

De Stefano N, Matthews PM, Filippi M, Agosta F, De Luca M, Bartolozzi ML, Guidi L, Ghezzi A, Montanari E, Cifelli A, Federico A, Smith SM. Evidence of early cortical atrophy in MS: relevance to white matter changes and disability. Neurology 2003;**60**:1157-1162.

de Vries HE, Kuiper J, de Boer AG, Van Berkel TJ, Breimer DD. The blood-brain barrier in neuroinflammatory diseases. Pharmacol Rev 1997; **49**: 143-55.

Dean G, Kurtzke JF. On the risk of multiple sclerosis according to age at immigration to South Africa. Br Med J 1971; **3**:725-729

Dean G, Grimaldi G, Kelly R, Karhausen L. Multiple sclerosis in southern Europe. I: Prevalence in Sicily in 1975. J Epidemiol Community Health 1979; **33**: 107-110

Dean G, Elian M. Age at immigration to England of Asian and Caribbean immigrants and the risk of developing multiple sclerosis. J Neurol Neurosurg Psychiatry 1997; **63**:565-568

del Pilar Martin M, Cravens PD, Winger R, Frohman EM, Racke MK, Eagar TN, Zamvil SS, Weber MS, Hemmer B, Karandikar NJ, Kleinschmidt-DeMasters BK, Stüve O. Decrease in the numbers of dendritic cells and CD4+ T cells in cerebral perivascular spaces due to natalizumab. Arch Neurol. 2008; **65**: 1596-603

Deng X, Wang X, Andersson R. Endothelial barrier resistance in multiple organs after septic and nonseptic challenges in the rat. J Appl Physiol 1995; **78**: 2052-2061.

Department of Health. *Cost effective provision of disease modifying therapies for people with Multiple Sclerosis. Health Service Circular 2002;* ***HSC 2002/2004****;* www.dh.gov.uk/assetRoot/04/01/22/14/04012214.pdf

Dettke M, Scheidt P, Prange H, Kirchner H. Correlation between interferon production and clinical disease activity in patients with multiple sclerosis. J Clin Immunol 1997; **17**: 293-300

Dore-Duffy P, Washington R, Dragovic L. Expression of endothelial cell activation antigens in microvessels from patients with multiple sclerosis. Adv Exp Med Biol 1993;**331**:243-8.

Durelli L, Bongioanni MR, Cavallo R, Ferrero B, Ferri R, Ferrio MF, Bradac GB, Riva A, Vai S, Geuna M, . Chronic systemic high-dose recombinant interferon alfa-2a reduces exacerbation rate, MRI signs of disease activity, and lymphocyte interferon gamma production in relapsing-remitting multiple sclerosis. Neurology 1994; **44**:406-413.

Dustin ML, Rothlein R, Bhan AK, Dinarello CA, Springer TA. Induction by IL 1 and interferon-gamma: tissue distribution, biochemistry, and function of a natural adherence molecule (ICAM-1). J Immunol 1986; **137**: 245-254.

Edan G, Miller D, Clanet M, Confavreux C, Lyon-Caen O, Lubetzki C, Brochet B, Berry I, Rolland Y, Froment JC, Cabanis E, Iba-Zizen MT, Gandon JM, Lai HM, Moseley I, Sabouraud O. Therapeutic effect of mitoxantrone combined with methylprednisolone in multiple sclerosis: a randomised multicentre study of active disease using MRI and clinical criteria. J Neurol Neurosurg Psychiatry 1997;**62**: 112-

118.

Ehrlich P. Eine Farbenanalytische Studie. Hirschwald, Berlin; 1885.

Elices MJ, Osborn L, Takada Y, Crouse C, Luhowskyj S, Hemler ME, Lobb RR. VCAM-1 on activated endothelium interacts with the leukocyte integrin VLA-4 at a site distinct from the VLA-4/fibronectin binding site. Cell. 1990; **60**: 577-584

Elovaara I, Lalla M, Spare E, Lehtimaki T, Dastidar P. Methylprednisolone reduces adhesion molecules in blood and cerebrospinal fluid in patients with MS. Neurology 1998; **51**: 1703-8.

Engelhardt B, Ransohoff RM. The ins and outs of T-lymphocyte trafficking to the CNS: anatomical sites and molecular mechanisms Trends Immunol 2005; **26:** 485-495.

Enzinger C, Ropele S, Smith S, Strasser-Fuchs S, Poltrum B, Schmidt H, Matthews PM, Fazekas F. Accelerated evolution of brain atrophy and "black holes" in MS patients with APOE-epsilon 4. Ann Neurol 2004; **55**: 563-569

Evangelou N, Konz D, Esiri MM, Smith S, Palace J, Matthews PM. Regional axonal loss in the corpus callosum correlates with cerebral white matter lesion volume and distribution in multiple sclerosis. Brain 2000; **123**:1845-1849

European Study Group on interferon beta-1b in secondary progressive MS. Placebo-controlled multicentre randomised trial of interferon beta-1b in treatment of secondary progressive multiple sclerosis. Lancet 1998; **352**:1491-1497

Farquhar MG, Palade GE. Junctional complexes in various epithelia. J Cell Biol 1963; **17**: 375-412.

Fenstermacher J, Gross P, Sposito N, Acuff V, Pettersen S, Gruber K. Structural and functional variations in capillary systems within the brain. Ann N Y Acad Sci 1988; **529**: 21-30.

Ferguson B, Matysak MK, Esiri MM, Perry VH. Axonal damage in acute multiple sclerosis lesions. Brain 1997; **120**: 393-399.

Fernando KT, McLean MA, Chard DT, MacManus DG, Dalton CM, Miszkiel KA, Gordon RM, Plant GT, Thompson AJ, Miller DH. Elevated white matter myo-inositol in clinically isolated syndromes suggestive of multiple sclerosis. Brain 2004;**127**:1361-9

Filippi M, Yousry T, Campi A, Kandziora C, Colombo B, Voltz R, Martinelli V, Spuler S, Bressi S, Scotti G, Comi G. Comparison of triple dose versus standard dose gadolinium-DTPA for detection of MRI enhancing lesions in patients with MS. Neurology 1996;**46(2)**:379-84.

Filippi M, Rovaris M, Rocca MA, Sormani MP, Wolinsky JS, Comi G. Glatiramer acetate reduces the proportion of new MS lesions evolving into "black holes".

Neurology 2001;**57**:731-3.

Filippi M, Bozzali M, Rovaris M, Gonen O, Kesavadas C, Ghezzi A, Martinelli V, Grossman RI, Scotti G, Comi G, Falini A. Evidence for widespread axonal damage at the earliest clinical stage of multiple sclerosis. Brain 2003; **126**:433-437

Filippi M, Rovaris M, Inglese M, Barkhof F, De Stefano N, Smith S, Comi G. Interferon beta-1a for brain tissue loss in patients at presentation with syndromes suggestive of multiple sclerosis: a randomised, double-blind, placebo-controlled trial. Lancet 2004; **364**:1489-1496

Firth D. The Case of Augustus D'Este (1794-1848): The first account of Disseminated Sclerosis. Proc R Soc Med 1941; **34**: 381-384

Fischer JS, Rudick RA, Cutter GR, Reingold SC. The Multiple Sclerosis Functional Composite Measure (MSFC): an integrated approach to MS clinical outcome assessment. National MS Society Clinical Outcomes Assessment Task Force. Mult Scler. 1999; **5**: 244-250

Fischer S, Wobben M, Kleinstuck J, Renz D, Schaper W. Effect of astroglial cells on hypoxia-induced permeability in PBMEC cells. Am J Physiol Cell Physiol 2000; **279**: C935-C944.

Fischer S, Wobben M, Marti HH, Renz D, Schaper W. Hypoxia-induced hyperpermeability in brain microvessel endothelial cells involves VEGF-mediated changes in the expression of zonula occludens-1. Microvasc Res 2002; **63**: 70-80.

Fisher E, Rudick RA, Simon JH, Cutter G, Baier M, Lee JC, Miller D, Weinstock-Guttman B, Mass MK, Dougherty DS, Simonian NA. Eight-year follow-up study of brain atrophy in patients with MS. Neurology 2002; **59**:1412-20.

Fisher E, Lee JC, Nakamura K, Rudick RA. Gray matter atrophy in multiple sclerosis: a longitudinal study. Ann Neurol. 2008; **64**:255-65.

Fisniku LK, Brex PA, Altmann DR, Miszkiel KA, Benton CE, Lanyon R, Thompson AJ, Miller DH. Disability and T2 MRI lesions: a 20-year follow-up of patients with relapse onset of multiple sclerosis. Brain. 2008a; **131**:808-17.

Fisniku LK, Chard DT, Jackson JS, Anderson VM, Altmann DR, Miszkiel KA, Thompson AJ, Miller DH. Gray matter atrophy is related to long-term disability in multiple sclerosis. Ann Neurol. 2008b; **64**:247-54.

Food and Drug Administration. Tysabri Prescribing Information. 2008; 7

Fox NC, Freeborough PA. Brain atrophy progression measured from registered serial MRI: validation and application to Alzheimer's disease. J Magn Reson Imaging 1997; **7**:1069-1075

Freeborough PA, Fox NC. The boundary shift integral: an accurate and robust measure of cerebral volume changes from registered repeat MRI. IEEE Trans Med Imaging 1997; **16**:623-629.

Freeman JA, Langdon DW, Hobart JC, Thompson AJ. The impact of inpatient rehabilitation on progressive multiple sclerosis. Ann Neurol 1997; **42**: 236-244

Fu L, Wolfson C, Worsley KJ, De Stefano N, Collins DL, Narayanan S, Arnold DL. Statistics for investigation of multimodal MR imaging data and an application to multiple sclerosis patients. NMR Biomed 1996; **9**: 339-346

Fu L, Matthews PM, De SN, Worsley KJ, Narayanan S, Francis GS, Antel JP, Wolfson C, Arnold DL. Imaging axonal damage of normal-appearing white matter in multiple sclerosis. Brain 1998; **121**: 103-113

Gallagher HL, MacManus DG, Webb SL, Miller DH. A reproducible repositioning method for serial magnetic resonance imaging studies of the brain in treatment trials for multiple sclerosis. J Magn Reson Imaging 1997; **7**:439-441

Gasperini C, Paolillo A, Giugni E, Galgani S, Bagnato F, Mainero C, Onesti E, Bastianello S, Pozzilli C. MRI brain volume changes in relapsing-remitting multiple sclerosis patients treated with interferon beta-1a. Mult Scler 2002;**8**:119-23.

Gawne-Cain ML, O'Riordan JI, Coles A, Newell B, Thompson AJ, Miller DH. MRI lesion volume measurement in multiple sclerosis and its correlation with disability: a comparison of fast fluid attenuated inversion recovery (fFLAIR) and spin echo sequences. J Neurol Neurosurg Psychiatry 1998;**64**:197-203.

Gay D, Esiri M. Blood-brain barrier damage in acute multiple sclerosis plaques. An immunocytological study. Brain 1991; **114**: 557-572

Ge Y, Law M, Johnson G, Herbert J, Babb JS, Mannon LJ, Grossman RI. Dynamic susceptibility contrast perfusion MR imaging of multiple sclerosis lesions: characterizing hemodynamic impairment and inflammatory activity. AJNR Am J Neuroradiol 2005;**26**:1539-47.

Ghosh S, Goldin E, Gordon FH, Malchow HA, Rask-Madsen J, Rutgeerts P, Vyhnalek P, Zadorova Z, Palmer T, Donoghue S. Natalizumab for active Crohn's disease. N Engl J Med 2003; **348**: 24-32.

Giovannoni G, Lai M, Thorpe J, Kidd D, Chamoun V, Thompson AJ, Miller DH, Feldmann M, Thompson EJ. Longitudinal study of soluble adhesion molecules in multiple sclerosis: correlation with gadolinium enhanced magnetic resonance imaging. Neurology 1997; **48**: 1557-1565.

Gold R, Jawad A, Miller DH, Henderson DC, Fassas A, Fierz W, Hartung HP. Expert opinion: guidelines for the use of natalizumab in multiple sclerosis patients previously treated with immunomodulating therapies. J Neuroimmunol. 2007; **187**: 156-158.

Goldmann EE. Vitalfarbung am Zentralnervensystem. Abhandl Konigl preuss Akad Wiss 1914; **1**: 1-60.

Goldstein H. Multilevel Statistical Models (Kendall's Library of Statistics Series 3). Hodder Arnold,1995

Goodman AD, Rossman H, Bar-Or A, Miller A, Miller DH, Schmierer K, Lublin F, Khan O, Bormann NM, Yang M, Panzara MA, Sandrock AW; Glance Investigators. GLANCE: results of a phase 2, randomized, double-blind, placebo-controlled study. Neurology 2009; **72**: 806-812

Gordon FH, Lai CW, Hamilton MI, Allison MC, Srivastava ED, Fouweather MG, Donoghue S, Greenlees C, Subhani J, Amlot PL, Pounder RE. A randomized placebo-controlled trial of a humanized monoclonal antibody to alpha4 integrin in active Crohn's disease. Gastroenterology 2001; **121**: 268-74.

Griffin CM, Dehmeshki J, Chard DT, Parker GJ, Barker GJ, Thompson AJ, Miller DH. T1 histograms of normal-appearing brain tissue are abnormal in early relapsing-remitting multiple sclerosis Mult Scler 2002; **8**: 211-216

Grimaud J, Lai M, Thorpe J, Adeleine P, Wang L, Barker GJ, Plummer DL, Tofts PS, McDonald WI, Miller DH. Quantification of MRI lesion load in multiple sclerosis: a comparison of three computer-assisted techniques. Magn Reson Imaging. 1996; **14**: 495-505.

Grossman RI, Gonzalez-Scarano F, Atlas SW, Galetta S, Silberberg DH. Multiple sclerosis: gadolinium enhancement in MR imaging. Radiology 1986; **161**:721-725

Guan JL, Hynes RO. Lymphoid cells recognize an alternatively spliced segment of fibronectin via the integrin receptor alpha 4 beta 1. Cell 1990; **60(1)**: 53-61.

Geurts JJ, Bo L, Pouwels PJ, Castelijns JA, Polman CH, Barkhof F. Cortical lesions in multiple sclerosis: combined postmortem MR imaging and histopathology. AJNR Am J Neuroradiol 2005; **26**:572-577

Hammond SR, English D, de WC, Maxwell IC, Millingen KS, Stewart-Wynne EG, McLeod JG, McCall MG. The clinical profile of MS in Australia: a comparison between medium- and high-frequency prevalence zones. Neurology 1988; **38**:980-986

Hammond SR, English DR, McLeod JG. The age-range of risk of developing multiple sclerosis: evidence from a migrant population in Australia. Brain 2000; **123**:968-974

Harris JO, Frank JA, Patronas N, McFarlin DE, McFarland HF. Serial gadolinium-enhanced magnetic resonance imaging scans in patients with early, relapsing-remitting multiple sclerosis: implications for clinical trials and natural history. Ann Neurol 1991;**29**: 548-555.

Harris NG, Gauden V, Fraser PA, Williams SR, Parker GJ. MRI measurement of blood-brain barrier permeability following spontaneous reperfusion in the starch microsphere model of ischemia. Magn Reson Imaging 2002; **20**: 221-30.

Hartung HP, Reiners K, Archelos JJ, Michels M, Seeldrayers P, Heidenreich F, Pflughaupt KW, Toyka KV. Circulating adhesion molecules and tumor necrosis factor receptor in multiple sclerosis: correlation with magnetic resonance imaging Ann Neurol 1995; **38**: 186-93.

Hartung HP. New cases of progressive multifocal leukoencephalopathy after treatment with natalizumab. Lancet Neurol. 2009; **8**: 28-31

Haselhorst R, Kappos L, Bilecen D, Scheffler K, Mori D, Radu EW, Seelig J. Dynamic susceptibility contrast MR imaging of plaque development in multiple sclerosis: application of an extended blood-brain barrier leakage correction. J Magn Reson

Imaging 2000; **11**:495-505

Hawkins BT, Davis TP. The blood-brain barrier/neurovascular unit in health and disease. Pharmacol Rev 2005; **57(2)**: 173-85.

Hawkins CP, Munro PM, MacKenzie F, Kesselring J, Tofts PS, du Boulay EP, Landon DN, McDonald WI. Duration and selectivity of blood-brain barrier breakdown in chronic relapsing experimental allergic encephalomyelitis studied by gadolinium-DTPA and protein markers. Brain 1990;**113**:365-378.

Hayashi K, Nakao S, Nakaoke R, Nakagawa S, Kitagawa N, Niwa M. Effects of hypoxia on endothelial/pericytic co-culture model of the blood-brain barrier. Regul Pept 2004; **123**: 77-83.

Hickman SJ, Brex PA, Brierley CM, Silver NC, Barker GJ, Scolding NJ, Compston DA, Moseley IF, Plant GT, Miller DH. Detection of optic nerve atrophy following a single episode of unilateral optic neuritis by MRI using a fat-saturated short-echo fast FLAIR sequence. Neuroradiology 2001; **43**: 123-128.

Hickman SJ, Toosy AT, Miszkiel KA, Jones SJ, Altmann DR, MacManus DG, Plant GT, Thompson AJ, Miller DH. Visual recovery following acute optic neuritis--a clinical, electrophysiological and magnetic resonance imaging study. J Neurol. 2004; **251**: 996-1005

Hiehle JF, Jr., Grossman RI, Ramer KN, Gonzalez-Scarano F, Cohen JA. Magnetization transfer effects in MR-detected multiple sclerosis lesions: comparison with gadolinium-enhanced spin-echo images and nonenhanced T1-weighted images. AJNR Am J Neuroradiol 1995;**16**:69-77.

Hohol MJ, Guttmann CR, Orav J, Mackin GA, Kikinis R, Khoury SJ, Jolesz FA, Weiner HL. Serial neuropsychological assessment and magnetic resonance imaging analysis in multiple sclerosis. Arch Neurol 1997; **54:**1018-1025

Hori S, Ohtsuki S, Hosoya K, Nakashima E, Terasaki T. A pericyte-derived angiopoietin-1 multimeric complex induces occludin gene expression in brain capillary endothelial cells through Tie-2 activation in vitro. J Neurochem 2004; **89**:503-13.

IFNB Multiple Sclerosis Study Group. Interferon beta-1b is effective in relapsing-remitting multiple sclerosis. I. Clinical results of a multicenter, randomized, double-blind, placebo-controlled trial. Neurology 1993; **43**:655-661

IFNB Multiple Sclerosis Study Group and University of British Columbia MS/MRI

Analysis Group. Interferon beta-1b in the treatment of multiple sclerosis: final outcome of the randomized controlled trial. Neurology 1995; **45**:1277-1285i

Ingle GT, Stevenson VL, Miller DH, Thompson AJ. Primary progressive multiple sclerosis: a 5-year clinical and MR study. Brain 2003;**126**: 2528-2536.

International Multiple Sclerosis Genetics Consortium, Hafler DA, Compston A, Sawcer S, Lander ES, Daly MJ, De Jager PL, de Bakker PI, Gabriel SB, Mirel DB, Ivinson AJ, Pericak-Vance MA, Gregory SG, Rioux JD, McCauley JL, Haines JL, Barcellos LF, Cree B, Oksenberg JR, Hauser SL. Risk alleles for multiple sclerosis identified by a genomewide study. N Engl J Med. 2007; **357**:851-62.

Jacobs LD, Cookfair DL, Rudick RA, Herndon RM, Richert JR, Salazar AM, Fischer JS, Goodkin DE, Granger CV, Simon JH, Alam JJ, Bartoszak DM, Bourdette DN, Braiman J, Brownscheidle CM, Coats ME, Cohan SL, Dougherty DS, Kinkel RP, Mass MK, Munschauer FE, III, Priore RL, Pullicino PM, Scherokman BJ, Whitham RH. The Multiple Sclerosis Collaborative Research Group (MSCRG). Intramuscular interferon beta-1a for disease progression in relapsing multiple sclerosis. Ann Neurol 1996; **39:** 285-294

Jimenez J, Jy W, Mauro LM, Horstman LL, Ahn ER, Ahn YS, Minagar A. Elevated endothelial microparticle-monocyte complexes induced by multiple sclerosis plasma and the inhibitory effects of interferon-beta 1b on release of endothelial microparticles, formation and transendothelial migration of monocyte-endothelial microparticle complexes. Mult Scler. 2005; **11**: 310-5

Johnson KP, Brooks BR, Cohen JA, Ford CC, Goldstein J, Lisak RP, Myers LW, Panitch HS, Rose JW, Schiffer RB. The Copolymer 1 Multiple Sclerosis Study Group. Copolymer 1 reduces relapse rate and improves disability in relapsing-remitting multiple sclerosis: results of a phase III multicenter, double-blind placebo-controlled trial. Neurology 1995; **45**:1268-1276

Kalkers NF, Bergers E, Castelijns JA, van Walderveen MA, Bot JC, Ader HJ, Polman CH, Barkhof F. Optimizing the association between disability and biological markers in MS. Neurology 2001; **57**: 1253-1258.

Kalkers NF, Ameziane N, Bot JC, Minneboo A, Polman CH, Barkhof F. Longitudinal brain volume measurement in multiple sclerosis: rate of brain atrophy is independent of the disease subtype. Arch Neurol 2002; **59**:1572-1576

Kantarci OH, De Andrade M, Weinshenker BG Identifying disease modifying genes in multiple sclerosis. J Neuroimmunol 2002; **123**:144-159

Kappos L, Moeri D, Radue EW, Schoetzau A, Schweikert K, Barkhof F, Miller D, Guttmann CR, Weiner HL, Gasperini C, Filippi M. Predictive value of gadolinium-enhanced magnetic resonance imaging for relapse rate and changes in disability or impairment in multiple sclerosis: a meta-analysis. Gadolinium MRI Meta-analysis Group. Lancet 1999; **353**: 964-969.

Kappos L, Bates D, Hartung HP, Havrdova E, Miller D, Polman CH, Ravnborg M, Hauser SL, Rudick RA, Weiner HL, O'Connor PW, King J, Radue EW, Yousry T, Major EO, Clifford DB. Natalizumab treatment for multiple sclerosis: recommendations for patient selection and monitoring. Lancet Neurol. 2007; **6**: 431-441.

Karussis DM, Meiner Z, Lehmann D, Gomori JM, Schwarz A, Linde A, Abramsky O. Treatment of secondary progressive multiple sclerosis with the immunomodulator linomide: a double-blind, placebo-controlled pilot study with monthly magnetic resonance imaging evaluation. Neurology 1996;**47**:341-6.

Katz D, Taubenberger JK, Cannella B, McFarlin DE, Raine CS, McFarland HF. Correlation between magnetic resonance imaging findings and lesion development in chronic, active multiple sclerosis. Ann Neurol 1993; **34**:661-669.

Keeley KA, Rivey MP, Allington DR. Natalizumab for the treatment of multiple sclerosis and Crohn's disease. Ann Pharmacother 2005; **39**:1833-1843.

Kempski O. Cerebral edema. Semin Nephrol 2001; **21**: 303-7.

Kent SJ, Karlik SJ, Rice GP, Horner HC. A monoclonal antibody to alpha 4-integrin reverses the MR-detectable signs of experimental allergic encephalomyelitis in the guinea pig. J Magn Reson Imaging. 1995a; **5**: 535-40.

Kent SJ, Karlik SJ, Cannon C, Hines DK, Yednock TA, Fritz LC, Horner HC. A monoclonal antibody to alpha 4 integrin suppresses and reverses active experimental allergic encephalomyelitis. J Neuroimmunol 1995b; **58**: 1-10.

Kerfoot SM, Kubes P. Overlapping roles of P-selectin and alpha 4 integrin to recruit leukocytes to the central nervous system in experimental autoimmune encephalomyelitis. J Immunol 2002; **169:** 1000-1006.

Kermode AG, Thompson AJ, Tofts P, MacManus DG, Kendall BE, Kingsley DP, Moseley IF, Rudge P, McDonald WI. Breakdown of the blood-brain barrier precedes symptoms and other MRI signs of new lesions in multiple sclerosis. Pathogenetic and clinical implications. Brain 1990; **113**: 1477-1489

Khatri BO, Man S, Giovannoni G, Koo AP, Lee JC, Tucky B, Lynn F, Jurgensen S, Woodworth J, Goelz S, Duda PW, Panzara MA, Ransohoff RM, Fox RJ. Effect of plasma exchange in accelerating natalizumab clearance and restoring leukocyte function. Neurology. 2009; **72**: 402-409.

Kidd D, Thorpe JW, Thompson AJ, Kendall BE, Moseley IF, Macmanus DG, McDonald WI, Miller DH. Spinal cord MRI using multi-array coils and fast spin echo. II. Findings in multiple sclerosis. Neurology 1993;**43**:2632-7.

Kidd D, Barker GJ, Tofts PS, Gass A, Thompson AJ, McDonald WI, Miller DH. The transverse magnetisation decay characteristics of longstanding lesions and normal-appearing white matter in multiple sclerosis. J Neurol 1997; **244**:125-130

Kidd D, Barkhof F, McConnell R, Algra PR, Allen IV, Revesz T. Cortical lesions in multiple sclerosis. Brain 1999; **122**:17-26

Kira J. Multiple sclerosis in the Japanese population. Lancet Neurol 2003; **2**:117-127

Kirk J, Plumb J, Mirakhur M, McQuaid S. Tight junctional abnormality in multiple sclerosis white matter affects all calibres of vessel and is associated with blood-brain barrier leakage and active demyelination J Pathol 2003; 201:319-327

Kleinschmidt-DeMasters BK, Tyler KL. Progressive multifocal leukoencephalopathy complicating treatment with natalizumab and interferon beta-1a for multiple sclerosis. N

Engl J Med. 2005; **353**: 369-374.

Kornek B, Storch MK, Weissert R, Wallstroem E, Stefferl A, Olsson T, Linington C, Schmidbauer M, Lassmann H. Multiple sclerosis and chronic autoimmune encephalomyelitis: a comparative quantitative study of axonal injury in active, inactive, and remyelinated lesions. Am J Pathol 2000; **157**:267-276

Krumbholz M, Meinl I, Kümpfel T, Hohlfeld R, Meinl E. Natalizumab disproportionately increases circulating pre-B and B cells in multiple sclerosis. Neurology. 2008; **71**: 1350-1354

Kuhlmann T, Lingfeld G, Bitsch A, Schuchardt J, Bruck W. Acute axonal damage in multiple sclerosis is most extensive in early disease stages and decreases over time. Brain 2002; **125**:2202-2212

Kuroiwa T, Shibutani M, Okeda R. Blood-brain barrier disruption and exacerbation of ischemic brain edema after restoration of blood flow in experimental focal cerebral ischemia. Acta Neuropathol (Berl) 1988; **76**: 62-70.

Kurtzke JF. A new scale for evaluating disability in multiple sclerosis. Neurology 1955; **5**: 580-583.

Kurtzke JF. A reassessment of the distribution of multiple sclerosis. Acta Neurol Scand

1975; **51**:137-157

Kurtzke JF, Beebe GW, Norman JE, Jr. Epidemiology of multiple sclerosis in U.S. veterans: 1. Race, sex, and geographic distribution. Neurology 1979; **29**:1228-1235

Kurtzke JF. Rating neurologic impairment in multiple sclerosis: An expanded disability status scale (EDSS). Neurology 1983; 33: 1444- 1452.

Kurtzke JF. Multiple sclerosis in time and space--geographic clues to cause. J Neurovirol 2000; **6**: S134-S140

Kurtzke JF. Origin of DSS: to present the plan. Mult Scler 2007; **13**: 120-123

Kutzelnigg A, Lucchinetti CF, Stadelmann C, Bruck W, Rauschka H, Bergmann M, Schmidbauer M, Parisi JE, Lassmann H. Cortical demyelination and diffuse white matter injury in multiple sclerosis. Brain 2005; **128**: 2705-2712

Kwon EE, Prineas JW. Blood-brain barrier abnormalities in longstanding multiple sclerosis lesions. An immunohistochemical study. J Neuropathol Exp Neurol 1994; **53**:625-36.

Lai M, Hodgson T, Gawne-Cain M, Webb S, MacManus D, McDonald WI, Thompson AJ, Miller DH. A preliminary study into the sensitivity of disease activity detection by serial weekly magnetic resonance imaging in multiple sclerosis. J Neurol Neurosurg Psychiatry. 1996; **60**: 339-341

Lai M, Hodgson T, Gawne-Cain M, Webb S, MacManus D, McDonald WI, Thompson AJ, Lassman H. Hypoxia-like tissue injury as a component of multiple sclerosis lesions. J Neurol Sci 2003**; 206**: 187-191

Langer-Gould A, Atlas SW, Green AJ, Bollen AW, Pelletier D. Progressive multifocal leukoencephalopathy in a patient treated with natalizumab. N Engl J Med. 2005; **353**: 375-81

Laschinger M, Vajkoczy P, Engelhardt B. Encephalitogenic T cells use LFA-1 for transendothelial migration but not during capture and initial adhesion strengthening in healthy spinal cord microvessels in vivo. Eur J Immunol 2002; **32**: 3598-3606.

Lauer K. Diet and multiple sclerosis. Neurology 1997; **49**: S55-S61

Leary SM, Miller DH, Stevenson VL, Brex PA, Chard DT, Thompson AJ. Interferon beta-1a in primary progressive MS: an exploratory, randomized, controlled trial. Neurology 2003; **60**: 44-51

Lee SJ, Benveniste EN. Adhesion molecule expression and regulation on cells of the central nervous system. J Neuroimmunol 1999; **98**: 77-88.

Leech S, Kirk J, Plumb J, McQuaid S. Persistent endothelial abnormalities and blood-brain barrier leak in primary and secondary progressive multiple sclerosis. Neuropathol

Appl Neurobiol. 2007; **33**: 86-98

Leger OJ, Yednock TA, Tanner L, Horner HC, Hines DK, Keen S, Saldanha J, Jones ST, Fritz LC, Bendig MM. Humanization of a mouse antibody against human alpha-4 integrin: a potential therapeutic for the treatment of multiple sclerosis. Hum Antibodies 1997; **8**: 3-16.

Leussink VI, Zettl UK, Jander S, Pepinsky RB, Lobb RR, Stoll G, Toyka KV, Gold R. Blockade of signaling via the very late antigen (VLA-4) and its counterligand vascular cell adhesion molecule-1 (VCAM-1) causes increased T cell apoptosis in experimental autoimmune neuritis. Acta Neuropathol (Berl) 2002; **103**: 131-136.

Lewandowsky M. Zur Lehre von der Cerebrospinalflussigkeit. Z Klin Med 1900; **40**: 480-94.

Lin X, Blumhardt LD, Constantinescu CS. The relationship of brain and cervical cord volume to disability in clinical subtypes of multiple sclerosis: a three-dimensional MRI study. Acta Neurol Scand 2003a; **108**: 401-406

Lin X, Tench CR, Turner B, Blumhardt LD, Constantinescu CS. Spinal cord atrophy and disability in multiple sclerosis over four years: application of a reproducible automated technique in monitoring disease progression in a cohort of the interferon beta-1a (Rebif) treatment trial. J Neurol Neurosurg Psychiatry 2003b;**74**:1090-4.

Liu C, Blumhardt LD. Assessing relapses in treatment trials of relapsing and remitting multiple sclerosis: can we do better? Mult Scler. 1999; **5**: 22-28

Long DM. Capillary ultrastructure in human metastatic brain tumors. J Neurosurg 1979; **51**: 53-8.

Losseff NA, Wang L, Lai HM, Yoo DS, Gawne-Cain ML, McDonald WI, Miller DH, Thompson AJ. Progressive cerebral atrophy in multiple sclerosis. A serial MRI study. Brain 1996; **119**: 2009-19.

Lublin FD, Reingold SC. Defining the clinical course of multiple sclerosis: results of an international survey. National Multiple Sclerosis Society (USA) Advisory Committee on Clinical Trials of New Agents in Multiple Sclerosis. Neurology 1996; **46**:907-911

Lucchinetti C, Bruck W, Parisi J, Scheithauer B, Rodriguez M, Lassmann H. A quantitative analysis of oligodendrocytes in multiple sclerosis lesions. A study of 113 cases. Brain 1999; **122**: 2279-95

Lucchinetti C, Bruck W, Parisi J, Scheithauer B, Rodriguez M, Lassmann H. Heterogeneity of multiple sclerosis lesions: implications for the pathogenesis of demyelination. Ann Neurol 2000; **47**:707-17.

Madri JA, Graesser D, Haas T. The roles of adhesion molecules and proteinases in lymphocyte transendothelial migration. Biochem Cell Biol 1996; **74**: 749-57.

Maeda A, Sobel RA. Matrix metalloproteinases in the normal human central nervous system, microglial nodules, and multiple sclerosis lesions. J Neuropathol Exp Neurol 1996; **55**: 300-309.

Mammi S, Filippi M, Martinelli V, Campi A, Colombo B, Scotti G, Canal N, Comi G. Correlation between brain MRI lesion volume and disability in patients with multiple sclerosis. Acta Neurol Scand 1996; **94(2)**: 93-6.

Mancardi GL, Sardanelli F, Parodi RC, Melani E, Capello E, Inglese M, Ferrari A, Sormani MP, Ottonello C, Levrero F, Uccelli A, Bruzzi P. Effect of copolymer-1 on serial gadolinium-enhanced MRI in relapsing remitting multiple sclerosis. Neurology 1998;**50(4)**:1127-33.

Mark KS, Davis TP. Cerebral microvascular changes in permeability and tight junctions induced by hypoxia-reoxygenation. Am J Physiol Heart Circ Physiol 2002; **282**: H1485-H1494.

Mark KS, Burroughs AR, Brown RC, Huber JD, Davis TP. Nitric oxide mediates hypoxia-induced changes in paracellular permeability of cerebral microvasculature. Am J Physiol Heart Circ Physiol 2004; **286**: H174-H180.

Marrosu MG, Murru MR, Costa G, Cucca F, Sotgiu S, Rosati G, Muntoni F. Multiple sclerosis in Sardinia is associated and in linkage disequilibrium with HLA-DR3 and -DR4 alleles Am J. Hum. Genet. 1997; **61**: 454–457.

Martyn CN. Infection in childhood and neurological diseases in adult life. Br Med Bull 1997; **53**: 24-39

Maxwell K, Berliner JA, Cancilla PA. Induction of gamma-glutamyl transpeptidase in cultured cerebral endothelial cells by a product released by astrocytes. Brain Res 1987; **410**: 309-14.

McDonald WI, Compston A, Edan G, Goodkin D, Hartung HP, Lublin FD, McFarland HF, Paty DW, Polman CH, Reingold SC, Sandberg-Wollheim M, Sibley W, Thompson A, van den NS, Weinshenker BY, Wolinsky JS. Recommended diagnostic criteria for multiple sclerosis: guidelines from the International Panel on the diagnosis of multiple sclerosis. Ann Neurol 2001; **50**:121-127

McFarland HF, Frank JA, Albert PS, Smith ME, Martin R, Harris JO, Patronas N, Maloni H, McFarlin DE. Using gadolinium-enhanced magnetic resonance imaging lesions to monitor disease activity in multiple sclerosis. Ann Neurol. 1992; **32**: 758-766.

McFarland HF, Barkhof F, Antel J, Miller DH. The role of MRI as a surrogate outcome measure in multiple sclerosis. 2002; Mult Scler **8**: 40-51

Medana I, Martinic MA, Wekerle H, Neumann H. Transection of major histocompatibility complex class I-induced neurites by cytotoxic T lymphocytes.Am J Pathol 2001; **159**:809-15

Miller DH, Rudge P, Johnson G, Kendall BE, MacManus DG, Moseley IF, Barnes D, McDonald WI. Serial gadolinium enhanced magnetic resonance imaging in multiple sclerosis. Brain 1988; **111**:927-939

Miller DH. A preliminary study into the sensitivity of disease activity detection by serial weekly magnetic resonance imaging in multiple sclerosis. J Neurol Neurosurg Psychiatry 1996; 60: 339-341.

Miller DH, Khan OA, Sheremata WA, Blumhardt LD, Rice GP, Libonati MA, Willmer-Hulme AJ, Dalton CM, Miszkiel KA, O'Connor PW. A controlled trial of natalizumab for relapsing multiple sclerosis. N Engl J Med 2003; **348**: 15-23.

Miller DH. Biomarkers and surrogate outcomes in neurodegenerative disease: lessons from multiple sclerosis. NeuroRx 2004; **1**: 284-94.

Miller DH, Soon D, Fernando KT, MacManus DG, Barker GJ, Yousry TA, Fisher E, O'Connor PW, Phillips JT, Polman CH, Kappos L, Hutchinson M, Havrdova E, Lublin FD, Giovannoni G, Wajgt A, Rudick R, Lynn F, Panzara MA, Sandrock AW; AFFIRM Investigators. MRI outcomes in a placebo-controlled trial of natalizumab in relapsing MS. Neurology. 2007; **68**: 1390-401

Miller DM, Weinstock-Guttman B, Bethoux F, Lee JC, Beck G, Block V, Durelli L, LaMantia L, Barnes D, Sellebjerg F, Rudick RA. A meta-analysis of methylprednisolone in recovery from multiple sclerosis exacerbations. Mult Scler 2000; **6**:267-273

Minagar A, Alexander JS. Blood-brain barrier disruption in multiple sclerosis. Mult Scler 2003; **9**:540-549

Minagar A, Long A, Ma T, Jackson TH, Kelley RE, Ostanin DV, Sasaki M, Warren AC, Jawahar A, Cappell B, Alexander JS. Interferon (IFN)-beta 1a and IFN-beta 1b block IFN-gamma-induced disintegration of endothelial junction integrity and barrier. Endothelium 2003;10(6):299-307.

Minn A, Ghersi-Egea JF, Perrin R, Leininger B, Siest G. Drug metabolizing enzymes in the brain and cerebral microvessels. Brain Res Brain Res Rev 1991; **16**: 65-82.

Mitchell DG. MR imaging contrast agents--what's in a name? J Magn Reson Imaging 1997 ;**7**:1-4.

Molyneux PD, Filippi M, Barkhof F, Gasperini C, Yousry TA, Truyen L, Lai HM, Rocca MA, Moseley IF, Miller DH. Correlations between monthly enhanced MRI lesion rate and changes in T2 lesion volume in multiple sclerosis. Ann Neurol 1998; **43**: 332-339.

Molyneux PD, Miller DH, Filippi M, Yousry TA, Radu EW, Ader HJ, Barkhof F. Visual analysis of serial T2-weighted MRI in multiple sclerosis: intra- and interobserver reproducibility. Neuroradiology 1999; **41**: 882-888

Molyneux PD, Kappos L, Polman C, Pozzilli C, Barkhof F, Filippi M, Yousry T, Hahn D, Wagner K, Ghazi M, Beckmann K, Dahlke F, Losseff N, Barker GJ, Thompson AJ, Miller DH. The effect of interferon beta-1b treatment on MRI measures of cerebral atrophy in secondary progressive multiple sclerosis. European Study Group on Interferon beta-1b in secondary progressive multiple sclerosis. Brain 2000; **123**: 2256-2263

Mooradian AD. Central nervous system complications of diabetes mellitus--a perspective from the blood-brain barrier. Brain Res Rev 1997; **23**: 210-8.

Moreau T, Thorpe J, Miller D, Moseley I, Hale G, Waldmann H, Clayton D, Wing M, Scolding N, Compston A. Preliminary evidence from magnetic resonance imaging for reduction in disease activity after lymphocyte depletion in multiple sclerosis. Lancet 1994;**344**:298-301.

Moreau T, Coles A, Wing M, Isaacs J, Hale G, Waldmann H, Compston A. Transient increase in symptoms associated with cytokine release in patients with multiple sclerosis. Brain 1996; **119**: 225-237

Munger KL, Zhang SM, O'Reilly E, Hernan MA, Olek MJ, Willett WC, Ascherio A. Vitamin D intake and incidence of multiple sclerosis. Neurology 2004; **62**:60-65

National Collaborating Centre for Chronic Condtions (NCC-CC) at the Royal College of Physicians. Multiple Sclerosis: National Clinical Guideline for diagnosis and management in primary and secondary care. 2004: 1-7

Neuhaus J, Risau W, Wolburg H. Induction of blood-brain barrier characteristics in bovine brain endothelial cells by rat astroglial cells in transfilter coculture. Ann N Y Acad Sci 1991; **633**: 578-80.

Neumann H, Medana IM, Bauer J, Lassmann H. Cytotoxic T lymphocytes in autoimmune and degenerative CNS diseases. Trends Neurosci 2002; **25**: 313-319

O'Connor PW, Goodman A, Willmer-Hulme AJ, Libonati MA, Metz L, Murray RS, Sheremata WA, Vollmer TL, Stone LA. Randomized multicenter trial of natalizumab in acute MS relapses: clinical and MRI effects. Neurology 2004; **62:** 2038-43.

O'Connor P, Miller D, Riester K, Yang M, Panzara M, Dalton C, Miszkiel K, Khan O, Rice G, Sheremata W; International Natalizumab Trial Group. Relapse rates and enhancing lesions in a phase II trial of natalizumab in multiple sclerosis. Mult Scler. 2005;**11**: 568-572

Oldendorf WH, Brown WJ. Greater number of capillary endothelial cell mitochondria in brain than in muscle. Proc Soc Exp Biol Med 1975; **149**: 736-738.

Oldendorf WH, Cornford ME, Brown WJ. The large apparent work capability of the blood-brain barrier: a study of the mitochondrial content of capillary endothelial cells in brain and other tissues of the rat. Ann Neurol 1977; **1**: 409-417.

Olerup O, Hillert J. HLA class II-associated genetic susceptibility in multiple sclerosis: a critical evaluation. Tissue Antigens 1991; **38**:1-15

O'Riordan JI, Gawne CM, Coles A, Wang L, Compston DA, Tofts P, Miller DH. T1 hypointense lesion load in secondary progressive multiple sclerosis: a comparison of pre versus post contrast loads and of manual versus semi automated threshold techniques for lesion segmentation. Mult Scler 1998;**4(5)**:408-412.

Oshima T, Laroux FS, Coe LL, Morise Z, Kawachi S, Bauer P, Grisham MB, Specian RD, Carter P, Jennings S, Granger DN, Joh T, Alexander JS. Interferon-gamma and interleukin-10 reciprocally regulate endothelial junction integrity and barrier function. Microvasc Res 2001; **61**: 130-43

Page WF, Kurtzke JF, Murphy FM, Norman JE, Jr. Epidemiology of multiple sclerosis in U.S. veterans: V. Ancestry and the risk of multiple sclerosis. Ann Neurol 1993; **33**:632-639

Panitch H, Miller A, Paty D, Weinshenker B; North American Study Group on Interferon beta-1b in Secondary Progressive MS. Interferon beta-1b in secondary progressive MS: results from a 3-year controlled study. Neurology 2004; **63**: 1788 – 1795.

Pankov R, Yamada KM. Fibronectin at a glance. J Cell Sci. 2002; **115**: 3861-3863

Paolillo A, Coles AJ, Molyneux PD, Gawne-Cain M, MacManus D, Barker GJ, Compston DA, Miller DH. Quantitative MRI in patients with secondary progressive MS treated with monoclonal antibody Campath 1H. Neurology 1999;**53**:751-7.

Paolillo A, Pozzilli C, Gasperini C, Giugni E, Mainero C, Giuliani S, Tomassini V, Millefiorini E, Bastianello S. Brain atrophy in relapsing-remitting multiple sclerosis: relationship with black holes, disease duration and clinical disability. J Neurol Sci 2000; **2**: 85-91

Paolillo A, Pozzilli C, Giugni E, Tomassini V, Gasperini C, Fiorelli M, Mainero C, Horsfield M, Galgani S, Bastianello S, Buttinelli C. A 6-year clinical and MRI follow-up study of patients with relapsing-remitting multiple sclerosis treated with Interferon-beta. Eur J Neurol 2002; **9**: 645-655

Paolillo A, Piattella MC, Pantano P, et al. The relationship between inflammation and atrophy in clinically isolated syndromes suggestive of multiple sclerosis. A monthly MRI study after triple-dose gadolinium-DTPA. J Neurol 2004; **4**: 432-439.

Papadopoulos MC, Lamb FJ, Moss RF, Davies DC, Tighe D, Bennett ED. Faecal peritonitis causes oedema and neuronal injury in pig cerebral cortex. Clin Sci (Lond) 1999; **96**: 461-6.

Parker GJ, Barker GJ, Tofts PS. Accurate multislice gradient echo T(1) measurement in the presence of non-ideal RF pulse shape and RF field nonuniformity. Magn Reson Med 2001 May;**45**:838-845.

Parker GJ, Padhani AR. T_1-w DCE-MRI: T_1-weighted Dynamic Contrast Enhanced MRI. In: Tofts P *ed.* Quantitative MRI of the Brain. Measuring Changes Caused by Disease. Chichester; John Wiley; 2003: 341-364

Parry A, Clare S, Jenkinson M, Smith S, Palace J, Matthews PM. White matter and lesion T1 relaxation times increase in parallel and correlate with disability in multiple sclerosis. J Neurol. 2002; **249**: 1279-1286.

Paty DW, Li DK. Interferon beta-1b is effective in relapsing-remitting multiple sclerosis. II. MRI analysis results of a multicenter, randomized, double-blind, placebo-controlled trial. UBC MS/MRI Study Group and the IFNB Multiple Sclerosis Study Group. Neurology 1993; **43**:662-7.

Paty DW, Ebers GC. Clinical features. In: Paty DW, Ebers GC, eds. *Multiple sclerosis.* Philadelphia: FA Davis; 1997: 135-191.

Peterson JW, Bo L, Mork S, Chang A, Trapp BD. Transected neurites, apoptotic neurons, and reduced inflammation in cortical multiple sclerosis lesions. Ann Neurol 2001; **50**:389-400

Piccio L, Rossi B, Scarpini E, Laudanna C, Giagulli C, Issekutz AC, Vestweber D, Butcher EC, Constantin G. Molecular mechanisms involved in lymphocyte recruitment in inflamed brain microvessels: critical roles for P-selectin glycoprotein ligand-1 and heterotrimeric G(i)-linked receptors. J Immunol 2002; **168**: 1940-1949.

Piras MR, Magnano I, Canu ED, Paulus KS, Satta WM, Soddu A, Conti M, Achene A, Solinas G, Aiello I. Longitudinal study of cognitive dysfunction in multiple sclerosis: neuropsychological, neuroradiological, and neurophysiological findings. J Neurol

Neurosurg Psychiatry 2003; **74**:878-885

Pirko I, Luchinetti CF, Sriram S, Bakshi R. Gray matter involvement in multiple sclerosis. Neurology 2007; **68**: 634-642

Plateel M, Teissier E, Cecchelli R. Hypoxia dramatically increases the nonspecific transport of blood-borne proteins to the brain. J Neurochem 1997; **68**: 874-877.

Plumb J, McQuaid S, Mirakhur M, Kirk J. Abnormal endothelial tight junctions in active lesions and normal-appearing white matter in multiple sclerosis. Brain Pathol 2002; **12**: 154-169.

Plummer DL. Dispimage: a display and analysis tool for medical images. Rivista di Neuroradiologia 1992;**5**:489-495.

Pober JS, Gimbrone MA, Jr., Lapierre LA, Mendrick DL, Fiers W, Rothlein R, Springer TA. Overlapping patterns of activation of human endothelial cells by interleukin 1, tumor necrosis factor, and immune interferon. J Immunol 1986; **137(6)**: 1893-6.

Podolsky DK, Lobb R, King N, Benjamin CD, Pepinsky B, Sehgal P, de Beaumont M. Attenuation of colitis in the cotton-top tamarin by anti-alpha 4 integrin monoclonal antibody. J Clin Invest 1993; **92**: 372-80.

Polman CH, Reingold SC, Edan G, Filippi M, Hartung HP, Kappos L, Lublin FD, Metz LM, McFarland HF, O'Connor PW, Sandberg-Wollheim M, Thompson AJ, Weinshenker BG, Wolinsky JS. Diagnostic criteria for multiple sclerosis: 2005 revisions to the "McDonald Criteria".Ann Neurol. 2005;**58**:840-846.

Polman CH, O'Connor PW, Havrdova E, Hutchinson M, Kappos L, Miller DH, Phillips JT, Lublin FD, Giovannoni G, Wajgt A, Toal M, Lynn F, Panzara MA, Sandrock AW; AFFIRM Investigators. A randomized, placebo-controlled trial of natalizumab for relapsing multiple sclerosis. Engl J Med. 2006; **354**: 899-910.

Poser CM, Paty DW, Scheinberg L, McDonald WI, Davis FA, Ebers GC, Johnson KP, Sibley WA, Silberberg DH, Tourtellotte WW. New diagnostic criteria for multiple sclerosis: guidelines for research protocols. Ann Neurol 1983; **13**: 227-231

Povlishock JT, Becker DP, Sullivan HG, Miller JD. Vascular permeability alterations to horseradish peroxidase in experimental brain injury. Brain Res 1978;**153**: 223-39.

Pozzilli C, Bastianello S, Koudriavtseva T, Gasperini C, Bozzao A, Millefiorini E, Galgani S, Buttinelli C, Perciaccante G, Piazza G, Bozzao L, Fieschi C. Magnetic resonance imaging changes with recombinant human interferon-beta-1a: a short term study in relapsing-remitting multiple sclerosis. J Neurol Neurosurg Psychiatry 1996;**61**: 251-258.

Prat A, Biernacki K, Becher B, Antel JP. B7 expression and antigen presentation by human brain endothelial cells: requirement for proinflammatory cytokines. J Neuropathol Exp Neurol 2000; **59**:129-136

Prentice RL. Surrogate endpoints in clinical trials: definition and operational criteria. Stat Med 1989; **8**: 431-440

Prineas JW, Barnard RO, Kwon EE, Sharer LR, Cho ES. Multiple Sclerosis: Remyelination of Nascent Lesions. Ann Neurol. 1993; **33**:137-151

PRISMS (Prevention of Relapses and Disability by Interferon beta-1a Subcutaneously in Multiple Sclerosis) Study Group. Randomised double-blind placebo-controlled study of interferon beta-1a in relapsing/remitting multiple sclerosis. Lancet 1998; **352**:1498-1504

Proescholdt MA, Jacobson S, Tresser N, Oldfield EH, Merrill MJ. Vascular endothelial growth factor is expressed in multiple sclerosis plaques and can induce inflammatory lesions in experimental allergic encephalomyelitis rats. J Neuropathol Exp Neurol 2002; **61**: 914-925.

Ramsauer M, Krause D, Dermietzel R. Angiogenesis of the blood-brain barrier in vitro and the function of cerebral pericytes. FASEB J 2002;**16**:1274-6.

Ransohoff RM. Natalizumab and PML. Nat Neurosci. 2005; **8**: 1275.

Rashid W, Parkes LM, Ingle GT, Chard DT, Toosy AT, Altmann DR, Symms MR, Tofts PS, Thompson AJ, Miller DH. Abnormalities of cerebral perfusion in multiple sclerosis. J Neurol Neurosurg Psychiatry 2004;**75**: 1288-93.

Riahi F, Zijdenbos A, Narayanan S, Arnold D, Francis G, Antel J, Evans AC. Improved correlation between scores on the expanded disability status scale and cerebral lesion load in relapsing-remitting multiple sclerosis. Results of the application of new imaging methods. Brain 1998; **121**:1305-12.

Rice GP, Hartung HP, Calabresi PA. Anti-alpha4 integrin therapy for multiple sclerosis: mechanisms and rationale. Neurology 2005; **64**: 1336-42.

Rieckmann P, Martin S, Weichselbraun I, Albrecht M, Kitze B, Weber T, Tumani H, Broocks A, Luer W, Helwig A, . Serial analysis of circulating adhesion molecules and TNF receptor in serum from patients with multiple sclerosis: cICAM-1 is an indicator for relapse. Neurology 1994; **44**: 2367-2372.

Romero IA, Radewicz K, Jubin E, Michel CC, Greenwood J, Couraud PO, Adamson P. Changes in cytoskeletal and tight junctional proteins correlate with decreased permeability induced by dexamethasone in cultured rat brain endothelial cells. Neurosci Lett 2003; **344(2)**: 112-6.

Rosati G. The prevalence of multiple sclerosis in the world: an update. Neurol Sci 2001; **22**:117-139

Rosenman SJ, Shrikant P, Dubb L, Benveniste EN, Ransohoff RM. Cytokine-induced expression of vascular cell adhesion molecule-1 (VCAM-1) by astrocytes and astrocytoma cell lines. J Immunol 1995; **154**: 1888-1899.

Rovaris M, Comi G, Rocca MA, Wolinsky JS, Filippi M. Short-term brain volume change in relapsing-remitting multiple sclerosis: effect of glatiramer acetate and implications. Brain 2001; **124**:1803-1812.

Rudick R, Antel J, Confavreux C, Cutter G, Ellison G, Fischer J, Lublin F, Miller A, Petkau J, Rao S, Reingold S, Syndulko K, Thompson A, Wallenberg J, Weinshenker B, Willoughby E. Recommendations from the National Multiple Sclerosis Society Clinical Outcomes Assessment Task Force. Ann Neurol 1997; **42:** 379-8 .

Rudick RA, Fisher E, Lee JC, Simon J, Jacobs L. Use of the brain parenchymal fraction to measure whole brain atrophy in relapsing-remitting MS. Multiple Sclerosis Collaborative Research Group. Neurology 1999;**53**:1698-704.

Rudick RA, Fisher E, Lee JC, Duda JT, Simon J. Brain atrophy in relapsing multiple sclerosis: relationship to relapses, EDSS, and treatment with interferon beta-1a. Mult Scler 2000; **6**: 365-372

Rudick RA, Stuart WH, Calabresi PA, Confavreux C, Galetta SL, Radue EW, Lublin FD, Weinstock-Guttman B, Wynn DR, Lynn F, Panzara MA, Sandrock AW; SENTINEL Investigators. Natalizumab plus interferon beta-1a for relapsing multiple sclerosis. N Engl J Med. 2006; **354:** 911-923.

Runmarker B, Andersen O. Prognostic factors in a multiple sclerosis incidence cohort with twenty-five years of follow-up. Brain 1993; **116**:117-134

Sailer M, Losseff NA, Wang L, Gawne-Cain ML, Thompson AJ, Miller DH. T1 lesion load and cerebral atrophy as a marker for clinical progression in patients with multiple sclerosis. A prospective 18 months follow-up study. Eur J Neurol 2001; **8**:37-42.

Sandborn WJ, Colombel JF, Enns R, Feagan BG, Hanauer SB, Lawrance IC, Panaccione R, Sanders M, Schreiber S, Targan S, van DS, Goldblum R, Despain D, Hogge GS, Rutgeerts P. Natalizumab induction and maintenance therapy for Crohn's disease. N Engl J Med 2005 Nov;**353**:1912-25.

Savettieri G, Di L, I, Catania C, Licata L, Pitarresi GL, D'Agostino S, Schiera G, De C, V, Giandalia G, Giannola LI, Cestelli A. Neurons and ECM regulate occludin localization in brain endothelial cells. Neuroreport 2000; **11**: 1081-4.

Schinkel AH, Smit JJ, van Tellingen O, Beijnen JH, Wagenaar E, van Deemter L, Mol CA, van der Valk MA, Robanus-Maandag EC, te Riele HP, *et al*. Disruption of the mouse mdr1a P-glycoprotein gene leads to a deficiency in the blood-brain barrier and to increased sensitivity to drugs. Cell 1994; **77**: 491-502.

Schmierer K, Scaravilli F, Altmann DR, Barker GJ, Miller DH. Magnetization transfer ratio and myelin in postmortem multiple sclerosis brain. Ann Neurol. 2004; **56**:407-15

Schneeberger EE, Karnovsky MJ. Substructure of intercellular junctions in freeze-fractured alveolar-capillary membranes of mouse lung. Circ Res 1976; **38**: 404-411.

Sedlakova R, Shivers RR, Del Maestro RF. Ultrastructure of the blood-brain barrier in the rabbit. J Submicrosc Cytol Pathol 1999; **31**: 149-61.

Schumacher GA, Beebe G, Kibler RF, Kurland LT, Kurtzke JF, McDowell F, Nagler B, Sibley WA, Tourtellotte WW, Willmon TL. Problems of Experimental Trials of therapy in Multiple Sclerosis: Report by the panel on the evaluation of experimental trials of therapy in multiple sclerosis. Ann NY Acad Sci. 1965; **122**:552-568.

Sharma J, Sanfilipo MP, Benedict RH, Weinstock-Guttman B, Munschauer FE III, Bakshi R. Whole-brain atrophy in multiple sclerosis measured by automated versus semiautomated MR imaging segmentation. AJNR Am J Neuroradiol 2004; **25**: 985-996

Sharrack B, Hughes RA. Clinical scales for multiple sclerosis. J Neurol Sci. 1996; **135**:1-9

Shimizu Y, van Seventer GA, Horgan KJ, Shaw S. Costimulation of proliferative responses of resting CD4+ T cells by the interaction of VLA-4 and VLA-5 with fibronectin or VLA-6 with laminin. J Immunol 1990; **145**: 59-67.

Siger-Zajdel M, Selmaj KW. Proton magnetic resonance spectroscopy of normal appearing white matter in familial and sporadic multiple sclerosis. J Neurol. 2005; **252**: 830-832

Silver NC, Good CD, Barker GJ, Macmanus DG, Thompson AJ, Moseley IF, McDonald WI, Miller DH. Sensitivity of contrast enhanced MRI in multiple sclerosis. Effects of gadolinium dose, magnetization transfer contrast and delayed imaging. Brain 1997; **120**:1149-61.

Silver NC, Good CD, Sormani MP, Macmanus DG, Thompson AJ, Filippi M, Miller DH. A modified protocol to improve the detection of enhancing brain and spinal cord lesions in multiple sclerosis. J Neurol 2001a; **248**:215-24.

Silver NC, Tofts PS, Symms MR, Barker GJ, Thompson AJ, Miller DH. Quantitative contrast-enhanced magnetic resonance imaging to evaluate blood-brain barrier integrity in multiple sclerosis: a preliminary study. Mult Scler 2001b; **7**: 75-82.

Simon JH, Jacobs LD, Campion MK, Rudick RA, Cookfair DL, Herndon RM, Richert JR, Salazar AM, Fischer JS, Goodkin DE, Simonian N, Lajaunie M, Miller DE, Wende K, Martens-Davidson A, Kinkel RP, Munschauer FE III, Brownscheidle CM et al. A longitudinal study of brain atrophy in relapsing multiple sclerosis. The Multiple Sclerosis Collaborative Research Group (MSCRG). *Neurology* 1999; **53**: 139-148

Sipe JC, Romine JS, Koziol JA, McMillan R, Zyroff J, Beutler E. Cladribine in treatment of chronic progressive multiple sclerosis. Lancet 1994 Jul; **344**:9-13.

Skegg DC, Corwin PA, Craven RS, Malloch JA, Pollock M. Occurrence of multiple sclerosis in the north and south of New Zealand. J Neurol Neurosurg Psychiatry 1987;

50:134-139

Smith KJ, Kapoor R, Hall SM, Davies M. Electrically active axons degenerate when exposed to nitric oxide. Ann Neurol 2001; **49**: 470-476

Smith ME, Stone LA, Albert PS, Frank JA, Martin R, Armstrong M, Maloni H, McFarlin DE, McFarland HF. Clinical worsening in multiple sclerosis is associated with increased frequency and area of gadopentetate dimeglumine-enhancing magnetic resonance imaging lesions. Ann Neurol 1993;**33**:480-9.

Smith SM, Zhang Y, Jenkinson M, Chen J, Matthews PM, Federico A, De Stefano N. Accurate, robust, and automated longitudinal and cross-sectional brain change analysis. *Neuroimage* 2002; **17**: 479-489.

Soilu-Hanninen M, Roytta M, Salmi A, Salonen R. Therapy with antibody against leukocyte integrin VLA-4 (CD49d) is effective and safe in virus-facilitated experimental allergic encephalomyelitis. J Neuroimmunol 1997; **72**: 95-105.

Solari A, Filippini G, Gasco P, Colla L, Salmaggi A, La ML, Farinotti M, Eoli M, Mendozzi L. Physical rehabilitation has a positive effect on disability in multiple sclerosis patients. Neurology 1999; **52**:57-62

Secondary Progressive Efficacy Clinical Trial of Recombinant Interferon-beta-1a in MS (SPECTRIMS) Study Group. Randomized controlled trial of interferon-beta-1a in secondary progressive MS: clinical results. Neurology 2001; **56**: 1496 –1504.

Stevenson VL, Leary SM, Losseff NA, Parker GJ, Barker GJ, Husmani Y, Miller DH, Thompson AJ. Spinal cord atrophy and disability in MS: a longitudinal study. Neurology 1998;**51**:234-8.

Stevenson VL, Parker GJ, Barker GJ, Birnie K, Tofts PS, Miller DH, Thompson AJ. Variations in T1 and T2 relaxation times of normal appearing white matter and lesions in multiple sclerosis. J Neurol Sci 2000;**178**:81-7.

Stewart PA, Wiley MJ. Developing nervous tissue induces formation of blood-brain barrier characteristics in invading endothelial cells: a study using quail--chick transplantation chimeras. Dev Biol 1981; **84**: 183-192.

Stone LA, Frank JA, Albert PS, Bash CN, Calabresi PA, Maloni H, McFarland HF. Characterization of MRI response to treatment with interferon beta-1b: contrast-enhancing MRI lesion frequency as a primary outcome measure. Neurology. 1997;**49**:862-869

Studholme C, Hill DLG, Hawkes DJ. An overlap invariant entropy measure of 3D medical image alignment. Pattern Recognition 1999; **32**:71-86

Stüve O, Marra CM, Jerome KR, Cook L, Cravens PD, Cepok S, Frohman EM, Phillips JT, Arendt G, Hemmer B, Monson NL, Racke MK. Immune surveillance in multiple sclerosis patients treated with natalizumab. Ann Neurol. 2006; **59**:743-747

Stüve O, Cravens PD, Frohman EM, Phillips JT, Remington GM, von Geldern G, Cepok S, Singh MP, Cohen Tervaert JW, De Baets M, MacManus D, Miller DH, Radü EW, Cameron EM, Monson NL, Zhang S, Kim R, Hemmer B, Racke MK. Immunologic, clinical, and radiologic status 14 months after cessation of natalizumab therapy. Neurology. 2009; **72**: 396-340

Sudlow CL, Counsell CE. Problems with UK government's risk sharing scheme for assessing drugs for multiple sclerosis. BMJ 2003; **326**: 388-392

Sundstrom P, Juto P, Wadell G, Hallmans G, Svenningsson A, Nystrom L, Dillner J, Forsgren L. An altered immune response to Epstein-Barr virus in multiple sclerosis: a prospective study. Neurology 2004; **62**:2277-2282

Swanton JK, Fernando K, Dalton CM, Miszkiel KA, Thompson AJ, Plant GT, Miller DH. Modification of MRI criteria for multiple sclerosis in patients with clinically isolated syndromes. J Neurol Neurosurg Psychiatry. 2006; **77**:830-833

Swanton JK, Rovira A, Tintore M, Altmann DR, Barkhof F, Filippi M, Huerga E, Miszkiel KA, Plant GT, Polman C, Rovaris M, Thompson AJ, Montalban X, Miller DH. MRI criteria for multiple sclerosis in patients presenting with clinically isolated syndromes: a multicentre retrospective study.Lancet Neurol. 2007; **6**: 677-686

Tao-Cheng JH, Nagy Z, Brightman MW. Tight junctions of brain endothelium in vitro are enhanced by astroglia. J Neurosci 1987; **7**: 3293-9.

Tan IL, van Schijndel RA, Pouwels PJ, van Walderveen MA, Reichenbach JR, Manoliu RA, Barkhof F. MR venography of multiple sclerosis. AJNR Am J Neuroradiol 2000; **21**:1039-42.

Tchilian EZ, Owen JJ, Jenkinson EJ. Anti-alpha 4 integrin antibody induces apoptosis in murine thymocytes and staphylococcal enterotoxin B-activated lymph node T cells. Immunology 1997; **92**:321-327.

Theien BE, Vanderlugt CL, Eagar TN, Nickerson-Nutter C, Nazareno R, Kuchroo VK, Miller SD. Discordant effects of anti-VLA-4 treatment before and after onset of relapsing experimental autoimmune encephalomyelitis. J Clin Invest 2001; **107**: 995–1006.

Thompson AJ, Kermode AG, Wicks D, Macmanus DG, Kendall BE, Kingsley DP, McDonald WI. Major differences in the dynamics of primary and secondary progressive multiple sclerosis. Ann Neurol 1991; **29(1)**:53-62.

Thompson AJ, Miller D, Youl B, MacManus D, Moore S, Kingsley D, Kendall B, Feinstein A, McDonald WI. Serial gadolinium-enhanced MRI in relapsing/remitting multiple sclerosis of varying disease duration. Neurology 1992;**42**:60-3.

Thompson AJ, Montalban X, Barkhof F, Brochet B, Filippi M, Miller DH, Polman CH, Stevenson VL, McDonald WI. Diagnostic criteria for primary progressive multiple sclerosis: a position paper. Ann Neurol 2000; **47**:831-835

Thorpe JW, Kidd D, Moseley IF, Kenndall BE, Thompson AJ, Macmanus DG, McDonald WI, Miller DH. Serial gadolinium-enhanced MRI of the brain and spinal cord in early relapsing-remitting multiple sclerosis. Neurology 1996;**46**:373-8.

Tiberio M, Chard DT, Altmann DR, Davies G, Griffin CM, Rashid W, Sastre-Garriga J, Thompson AJ, Miller DH. Gray and white matter volume changes in early RRMS: a 2-year longitudinal study. Neurology 2005; **64**:1001-1007

Tilling T, Korte D, Hoheisel D, Galla HJ. Basement membrane proteins influence brain capillary endothelial barrier function in vitro. J Neurochem 1998; **71**: 1151-7.

Tintore M, Rovira A, Martinez MJ, Rio J, az-Villoslada P, Brieva L, Borras C, Grive E, Capellades J, Montalban X. Isolated demyelinating syndromes: comparison of different MR imaging criteria to predict conversion to clinically definite multiple sclerosis. Am J Neuroradiol 2000; **21**:702-706

Tintore M, Rovira A, Rio J, Nos C, Grive E, Sastre-Garriga J, Pericot I, Sanchez E, Comabella M, Montalban X. New diagnostic criteria for multiple sclerosis: application in first demyelinating episode. Neurology 2003; **60**: 27-30

Tofts PS, Kermode AG. Measurement of the blood-brain barrier permeability and leakage space using dynamic MR imaging. 1. Fundamental concepts. Magn Reson Med 1991; **17(2)**: 357-67.

Tofts PS, Berkowitz BA. Measurement of capillary permeability from the Gd enhancement curve: a comparison of bolus and constant infusion injection methods. Magn Reson Imaging 1994; **12**:81-91

Tofts PS, Brix G, Buckley DL, Evelhoch JL, Henderson E, Knopp MV, Larsson HB, Lee TY, Mayr NA, Parker GJ, Port RE, Taylor J, Weisskoff RM. Estimating kinetic parameters from dynamic contrast-enhanced T(1)-weighted MRI of a diffusable tracer: standardized quantities and symbols. J Magn Reson Imaging 1999;**10**: 223-232.

Tong XK, Hamel E. Basal forebrain nitric oxide synthase (NOS)-containing neurons project to microvessels and NOS neurons in the rat neocortex: cellular basis for cortical blood flow regulation. Eur J Neurosci 2000; **12**: 2769-80.

Tortorella C, Codella M, Rocca MA, Gasperini C, Capra R, Bastianello S, Filippi M. Disease activity in multiple sclerosis studied by weekly triple-dose magnetic resonance imaging. J Neurol 1999; **246**:689-92.

Trapp BD, Peterson J, Ransohoff RM, Rudick R, Mork S, Bo L. Axonal transection in the lesions of multiple sclerosis. N Engl J Med 1998; **338**:278-285

Trebst C, Ransohoff RM, Windhagen A, Stangel M. Chemokine--possible new options for the treatment of multiple sclerosis. Nervenarzt 2003;**74:** 850-7.

Trojano M, Avolio C, Liuzzi GM, Ruggieri M, Defazio G, Liguori M, Santacroce MP, Paolicelli D, Giuliani F, Riccio P, Livrea P. Changes of serum sICAM-1 and MMP-9 induced by rIFNbeta-1b treatment in relapsing-remitting MS. Neurology 1999; **53**: 1402-1408.

Truyen L, van Waesberghe JH, van Walderveen MA, van Oosten BW, Polman CH, Hommes OR, Ader HJ, Barkhof F. Accumulation of hypointense lesions ("black holes") on T1 spin-echo MRI correlates with disease progression in multiple sclerosis. Neurology 1996; **47(6)**: 1469-76.

Tsukada N, Matsuda M, Miyagi K, Yanagisawa N. Increased levels of intercellular adhesion molecule-1 (ICAM-1) and tumor necrosis factor receptor in the cerebrospinal fluid of patients with multiple sclerosis. Neurology 1993; **43**: 2679-2682.

Tubridy N, Ader HJ, Barkhof F, Thompson AJ, Miller DH. Exploratory treatment trials in multiple sclerosis using MRI: sample size calculations for relapsing-remitting and secondary progressive subgroups using placebo controlled parallel groups. J Neurol Neurosurg Psychiatry 1998a;**64(1)**:50-5.

Tubridy N, Coles AJ, Molyneux P, Compston DA, Barkhof F, Thompson AJ, McDonald WI, Miller DH. Secondary progressive multiple sclerosis: the relationship between short-term MRI activity and clinical features. Brain 1998b;**121**:225-31.

Tubridy N, Behan PO, Capildeo R, Chaudhuri A, Forbes R, Hawkins CP, Hughes RA, Palace J, Sharrack B, Swingler R, Young C, Moseley IF, Macmanus DG, Donoghue S, Miller DH. The effect of anti-alpha4 integrin antibody on brain lesion activity in MS. The UK Antegren Study Group. Neurology 1999; **53**: 466-472.

Turner B, Ramli N, Blumhardt LD, Jaspan T. Ventricular enlargement in multiple sclerosis: a comparison of three-dimensional and linear MRI estimates. *Neuroradiology* 2001; **8**: 608-614

Vajkoczy P, Laschinger M, Engelhardt B. Alpha4-integrin-VCAM-1 binding mediates G protein-independent capture of encephalitogenic T cell blasts to CNS white matter microvessels. J Clin Invest 2001;**108**: 557-565.

Van Assche G, Van Ranst M, Sciot R, Dubois B, Vermeire S, Noman M, Verbeeck J, Geboes K, Robberecht W, Rutgeerts P. Progressive multifocal leukoencephalopathy after natalizumab therapy for Crohn's disease. N Engl J Med. 2005; **353(4)**: 362-8

Van Au Duong M, Audoin B, Le Fur Y, Confort-Gouny S, Malikova I, Soulier E, Viout P, Ali-Cherif A, Pelletier J, Cozzone PJ, Ranjeva JP. Relationships between gray matter metabolic abnormalities and white matter inflammation in patients at the very early stage of MS : a MRSI study. J Neurol. 2007; **254**:914- 923.

van der Laan LJ, van der GA, Wauben MH, Ruuls SR, Dopp EA, De Groot CJ, Kuijpers TW, Elices MJ, Dijkstra CD. Beneficial effect of modified peptide inhibitor of alpha4 integrins on experimental allergic encephalomyelitis in Lewis rats. J Neurosci Res 2002; **67**: 191-199.

van der Maesen K, Hinojoza JR, Sobel RA. Endothelial cell class II major histocompatibility complex molecule expression in stereotactic brain biopsies of patients with acute inflammatory/demyelinating conditions. J Neuropathol Exp Neurol 1999; **58**: 346-358.

van der Mei IA, Ponsonby AL, Dwyer T, Blizzard L, Simmons R, Taylor BV, Butzkueven H, Kilpatrick T. Past exposure to sun, skin phenotype, and risk of multiple sclerosis: case-control study. BMJ 2003; **327**:316

van Waesberghe JH, van Walderveen MA, Castelijns JA, Scheltens P, Lycklama à Nijeholt GJ, Polman CH, Barkhof F. Patterns of lesion development in multiple sclerosis: longitudinal observations with T1-weighted spin-echo and magnetization transfer MR. Am J Neuroradiol. 1998; **19(4)**:675-683.

van Waesberghe JH, Kamphorst W, De Groot CJ, van Walderveen MA, Castelijns JA, Ravid R, Nijeholt GJ, van d, V, Polman CH, Thompson AJ, Barkhof F. Axonal loss in multiple sclerosis lesions: magnetic resonance imaging insights into substrates of disability. Ann Neurol 1999; **46**:747-754 van Walderveen MA, Kamphorst W, Scheltens P, van Waesberghe JH, Ravid R, Valk J, Polman CH, Barkhof F Histopathologic correlate of hypointense lesions on T1-weighted spin-echo MRI in multiple sclerosis. Neurology. 1998; **50**: 1282-1288

van Walderveen MA, Barkhof F, Pouwels PJ, van Schijndel RA, Polman CH, Castelijns JA. Neuronal damage in T1-hypointense multiple sclerosis lesions demonstrated in vivo using proton magnetic resonance spectroscopy. Ann Neurol 1999; **46:** 79-87.

van Walderveen MA, Lycklama ANG, Ader HJ, Jongen PJ, Polman CH, Castelijns JA, Barkhof F. Hypointense lesions on T1-weighted spin-echo magnetic resonance imaging: relation to clinical characteristics in subgroups of patients with multiple sclerosis. Arch Neurol 2001; **58**:76-81.

Vassallo L, Elian M, Dean G. Multiple sclerosis in southern Europe. II: Prevalence in Malta in 1978. J Epidemiol Community Health 1979; **33**:111-113

Vaucher E, Linville D, Hamel E. Cholinergic basal forebrain projections to nitric oxide synthase-containing neurons in the rat cerebral cortex. Neuroscience 1997; **79**: 827-36.

Waubant E, Goodkin DE, Gee L, Bacchetti P, Sloan R, Stewart T, Andersson PB, Stabler G, Miller K. Serum MMP-9 and TIMP-1 levels are related to MRI activity in relapsing multiple sclerosis. Neurology 1999; **53**: 1397-401.

Weinshenker BG, Ebers GC. The natural history of multiple sclerosis. Can J Neurol Sci 1987; **14**:255-261

Weinshenker BG, Bass B, Rice GP, Noseworthy J, Carriere W, Baskerville J, Ebers GC. The natural history of multiple sclerosis: a geographically based study. 2. Predictive value of the early clinical course. Brain 1989; **112**: 1419-1428

Weiss JM, Downie SA, Lyman WD, Berman JW. Astrocyte-derived monocyte-chemoattractant protein-1 directs the transmigration of leukocytes across a model of the human blood-brain barrier. J Immunol 1998; **161**: 6896-903.

Werring DJ, Clark CA, Barker GJ, Thompson AJ, Miller DH. Diffusion tensor imaging of lesions and normal-appearing white matter in multiple sclerosis. Neurology 1999;**52**:1626-32.

Willoughby EW, Paty DW. Scales for rating impairment in multiple sclerosis: a critique. Neurology 1988; **38**:1793-1798.

Witt KA, Mark KS, Hom S, Davis TP. Effects of hypoxia-reoxygenation on rat blood-brain barrier permeability and tight junctional protein expression. Am J Physiol Heart Circ Physiol 2003; **285**: H2820-H2831.

Wolinsky JS, Narayana PA, O'Connor P, Coyle PK, Ford C, Johnson K, Miller A, Pardo L, Kadosh S, Ladkani D; PROMiSe Trial Study Group. Glatiramer acetate in primary progressive multiple sclerosis: results of a multinational, multicenter, double-blind, placebo-controlled trial. Ann Neurol. 2007;**61**: 14-24.

Woods RP, Cherry SR, Mazziotta JC. Rapid automated algorithm for aligning and reslicing PET images. J Comput Assist Tomogr 1992; **16**:620-633

Wuerfel J, Bellmann-Strobl J, Brunecker P, Aktas O, McFarland H, Villringer A, Zipp F. Changes in cerebral perfusion precede plaque formation in multiple sclerosis: a longitudinal perfusion MRI study. Brain 2004; **127**: 111-119

Wujek JR, Bjartmar C, Richer E, Ransohoff RM, Yu M, Tuohy VK, Trapp BD. Axon loss in the spinal cord determines permanent neurological disability in an animal model of multiple sclerosis. J Neuropathol Exp Neurol 2002; **61**:23-32

Yednock TA, Cannon C, Fritz LC, Sanchez-Madrid F, Steinman L, Karin N. Prevention of experimental autoimmune encephalomyelitis by antibodies against alpha 4 beta 1 integrin. Nature 1992;**356**:63-6.

Youl BD, Turano G, Miller DH, Towell AD, MacManus DG, Moore SG, Jones SJ, Barrett G, Kendall BE, Moseley IF, Tofts PS, Halliday AM, McDonald WI. The pathophysiology of acute optic neuritis. An association of gadolinium leakage with clinical and electrophysiological deficits. Brain. 1991;**114**:2437-2450

Yousry TA, Major EO, Ryschkewitsch C, Fahle G, Fischer S, Hou J, Curfman B, Miszkiel K, Mueller-Lenke N, Sanchez E, Barkhof F, Radue EW, Jäger HR, Clifford DB. Evaluation of patients treated with natalizumab for progressive multifocal leukoencephalopathy. N Engl J Med. 2006; **354**: 924-33.

Zhu XP, Li KL, Kamaly-Asl ID, Checkley DR, Tessier JJ, Waterton JC, Jackson A. Quantification of endothelial permeability, leakage space, and blood volume in brain tumors using combined T1 and T2* contrast-enhanced dynamic MR imaging. J Magn Reson Imaging 2000; **11**: 575-585.